Experimental determination of the reactivity of basalts as a function of their degree of alteration

Sylvain Delerce, Matylda Heřmanská, Pascale Bénézeth, Jacques Schott, Eric Oelkers

Geochimica et Cosmochimica Acta

Experimental determination of the reactivity of basalts as a function of their degree of alteration

--Manuscript Draft--

Manuscript Number:	GCA-D-22-00877R2
Article Type:	Article
Keywords:	basalt; alteration; mineralization; CO2 storage; weathering
Corresponding Author:	Sylvain Delerce National Centre for Scientific Research Geosciences Environment Laboratory Toulouse Toulouse, Occitanie FRANCE
Corresponding Author's Institution:	National Centre for Scientific Research Geosciences Environment Laboratory Toulouse
First Author:	Sylvain Delerce
Order of Authors:	Sylvain Delerce
	Matylda Heřmanská
	Pascale Bénézeth
	Jacques Schott
	Eric H. Oelkers
Abstract:	The element release rates of naturally altered basalts were measured in batch experiments at 27°C, and mixed-flow experiments at 25 °C in reactive fluids initially consisting of pH 3 or 4 aqueous solutions. The basalts reacted in this study consist of 1) surface altered basalts ranging in age up to 13 million years, and 2) hydrothermally altered basalts having experienced from zeolite to actinolite facies alteration. The in-situ pH in the batch experiments increased over time with the final pH of the fluids ranging from to 4 to 8. All experiments exhibited a preferential release of Ca and Mg compared to Si from the dissolving basalt both initially and over the long-term. This behavior is attributed to the combination of an initial rapid cation-proton exchange reaction and the relatively fast dissolution rate of Ca-bearing minerals. The BET surface area normalized Si release rates for all of the altered basalts are within 1 order of magnitude from each other, and from 1 to 2 orders of magnitude lower than corresponding rates from fresh basaltic glass and fresh crystalline basalts. This is interpreted to stem from 1) the fast removal of reactive basaltic glass and olivine from fresh basalts during the natural alteration of the rocks, 2) the similarity of the dissolution rates of the remaining albitic plagioclase, pyroxenes, epidote, and zeolites, and 3) the high surface areas of certain less reactive secondary mineral such as clays. Overall the results indicate that all altered basalts will be effective in consuming CO2 during both natural and engineered processes, though at a somewhat slower rate than unaltered basalt.

Experimental determination of the reactivity of basalts as a function of their degree of alteration

Sylvain Delerce[a*], Matylda Heřmanská[a], Pascale Bénézeth[a], Jacques Schott[a], Eric H. Oelkers[b]

[a]*Géosciences Environnement Toulouse, GET – CNRS – CNES – IRD – OMP – Université de Toulouse, 14 Avenue Edouard Belin, 31400 Toulouse, France*

[b] *Institute of Earth Sciences, University of Iceland, Sæmundargata 2, 102 Reykjavík, Iceland*

Abstract

The element release rates from naturally altered basalts were measured in batch experiments at 27 °C, and in mixed-flow experiments at 25 °C in reactive fluids initially consisting of pH 3 or 4 aqueous solutions. The basalts reacted in this study consist of 1) surface weathered basalts ranging in age up to 13 million years, and 2) hydrothermally altered basalts from zeolite to actinolite alteration zones (temperatures of ~ 50 to 300 °C). The *in situ* pH in the batch experiments increased over time with the final pH of the fluids ranging from to 4 to 8. Most experiments exhibited a preferential release of Ca and Mg compared to Si from the dissolving basalts, both initially and over the long-term. This behavior is attributed to the combination of an initial rapid cation-proton exchange reaction and the relatively fast dissolution rates of Ca-bearing minerals. The BET surface area normalized Si release rates for all of the altered basalts are within one order of magnitude of each other, and from one to two orders of magnitude lower than corresponding rates from fresh basaltic glass and fresh crystalline basalts. This is interpreted to stem from 1) the fast removal of reactive basaltic glass and olivine from fresh basalts during the natural alteration of the rocks, 2) the similarity of the dissolution rates of the remaining albitic plagioclase, pyroxenes, epidote, and zeolites, and 3) the high surface areas of some less reactive secondary minerals such as clays. Overall, the results suggest that altered basalts will be effective in consuming CO_2 during both natural and engineered processes, though at a somewhat slower rate than unaltered basalts.

Keywords: basalt, alteration, mineralization, CO_2 storage, weathering

1. Introduction

The weathering of basalts on the Earth's surface and the ocean floor plays a critical role in the global carbon cycle. It proceeds through the dissolution of atmospheric CO_2 into aqueous solutions forming a weak acid. This slightly acidic solution dissolves basalts, which both increases the pH and releases divalent cations, notably Ca^{2+} and Mg^{2+}, to the fluid phase (Walker et al., 1981; Berner, 1999; Dessert et al., 2003). The released divalent metal cations combine with bicarbonate ions to form stable carbonate minerals. The weathering rate of basalts is temperature and runoff dependent (Brady and Carroll, 1994; Stefánsson and Gíslason, 2001; Gislason et al., 2009; Li et al., 2016; Deng et al., 2022). This creates a feedback between atmospheric CO_2, global temperature and the CO_2 drawdown capacity caused by silicate weathering. This feedback has constrained Earth's temperature variations over geologic timescales (Brady, 1991; Falkowski et al., 2000; Colbourn et al., 2015; Penman et al., 2020). Numerous studies have shown that fresh basalts are particularly efficient at lowering atmospheric CO_2 concentrations through Earth surface weathering right after major volcanic events (Louvat and Allègre, 1997, 1998; Rad et al., 2013; Li et al., 2016; Galeczka et al., 2018; Liu et al., 2019). It has also been suggested that the weathering rates of silicate rocks decrease as they are altered (Colman, 1981; Taylor and Blum, 1995; White et al., 1996; Kennedy et al., 1998; Chadwick et al., 1999; Hodson and Langan, 1999; White and Brantley, 2003), lowering their CO_2 drawdown potential over time (Börker et al., 2019).

Similar processes have been observed in the subsurface, notably in geothermal systems where basalt (Alt and Teagle, 1999; Rogers et al., 2006) and peridotite dissolution (Kelemen et al., 2011, 2018; Peuble et al., 2018) can provoke the CO_2 mineralization. This process has attracted interest as a means to store CO_2 in the subsurface (Matter and Kelemen, 2009; Matter et al., 2016; McGrail et al., 2017; Kelemen et al., 2019; Snæbjörnsdóttir et al., 2020). Efforts are currently under development to optimize this process, either at Earth surface conditions by enhanced weathering (Harrison et al., 2013; Renforth et al., 2015; Power et al., 2020; Chukwuma et al., 2021; Lewis et al., 2021; Rinder and von Hagke, 2021; Knapp and Tipper, 2022; Stubbs et al., 2022) or in the subsurface (Oelkers et al., 2018, 2022; Xiong et al., 2018; Gadikota et al., 2020; White et al., 2020; Gadikota, 2021; Campbell et al., 2022; Maesano et al., 2022) by injecting CO_2 captured from

either industrial sites or directly from the atmosphere. The results obtained by the CarbFix project in Iceland and the Wallula project in the USA demonstrated that it is possible to fix CO_2 through its mineralization in subsurface reservoirs containing fresh or mildly altered basalts in a matter of years (Matter et al., 2016; McGrail et al., 2017; Clark et al., 2020; Ratouis et al., 2022). The degree to which CO_2 mineralization can be efficient in more altered basaltic rocks is currently unclear. Nevertheless, altered basalts are more available on Earth's surface than fresh basalts or other young mafic rocks, which are primarily limited to active volcanic systems and rift zones (Courtillot and Renne, 2003; Seton et al., 2020). It is therefore necessary to investigate in detail the degree to which mineral carbon storage may be possible and effective in altered basaltic rocks.

To date there has been relatively few studies of the reactivity of altered basaltic rocks and their ability to mineralize CO_2. Marieni and Oelkers (2018) compared the dissolution rates of primary and secondary basaltic minerals and concluded that the carbonation rates of altered basalts are likely 0.5 to 3 orders of magnitude slower than that of fresh basaltic glass. Xiong et al. (2017) exposed fractured cores of Columbia River Basalt and of serpentinized basalt to CO_2 charged water at 100 and 150 °C and found significant differences in the resulting carbonation products after 40 weeks of reaction. Taking account of these results, Liu et al. (2019) suggested that the slower dissolution rates of altered basalts compared to fresh basalts could be advantageous to better maintain fluid circulation in the subsurface reservoirs.

The objective of this study is to quantify the reactivity of altered basalts. Towards this goal we have measured the element release rates of 22 different basalts representing both surface-weathered and hydrothermally altered basalts, as a function of their age and degree of alteration in batch reactors at 27 °C. An additional four mixed-flow experiments were performed to validate the batch experiment results. From the results obtained in this study we can (i) assess the potential for the subsurface carbonation of altered basalts, and (ii) illuminate the degree to which chemical weathering rates slow as basaltic rocks alter over time.

2. Material and methods

2.1. Sample preparation and characterization

Two suites of altered basalts have been collected and studied; one consisting of Earth surface weathered basalts of various ages and the other of hydrothermally altered basalts collected from the subsurface. These samples were selected to span the likely compositions to be targeted for Earth surface and subsurface mineral carbon storage.

2.1.1. Surface weathered basalts as a function of age

Surface basalt samples were collected from Eastern Iceland and have ages ranging from 9 to 13 Myr. The samples were collected from the Grjótá olivine basalt group (GOB), the Vindháls porphyritic group (VP), the Grænavatn porphyritic group (GRVP) and the Heiðarvatn olivine basalt group. The age, formation and composition of these basalts have been previously described by Óskarsson and Riishuus (2013), Walker (1958), Óskarsson et al. (2017), and Walker (1963) respectively. Younger basalt samples were originally collected by Eiriksdottir et al. (2008). These latter samples consist of suspended basaltic material collected from Eastern Iceland rivers. The ages of these suspended material samples, estimated from the average age of the bedrock in the river catchment areas, range from 0.2 to 2.1 Myr (Eiriksdottir et al., 2008). Finally, volcanic ash collected during the 2011 Grímsvötn's volcanic eruption was also used to represent youngest basalt (Olsson et al., 2013).

2.1.2. Basalt hydrothermal alteration as a function of depth/temperature

Ten basalt samples were selected from a core originally retrieved in Eastern Iceland during the Iceland Research Drilling Project (IRDP). The two kilometer long core, drilled near Reyðarfjörður during the summer of 1978 (Fridleifsson et al., 1982; Robinson et al., 1982a) crossed a succession of lava flows with their corresponding flow tops and breccias (Mehegan et al., 1982; Robinson et al., 1982b). We selected samples from the brecciated flow tops, where the alteration is more pronounced (McGrail et al., 2006), rather than from the thick dense lava flows. Three additional samples were provided by CarbFix and taken from well HE-65 near the Hellisheiði powerplant (southeast Iceland). A summary of the samples is provided in Table 1 and the sampling locations are shown in Figure 1.

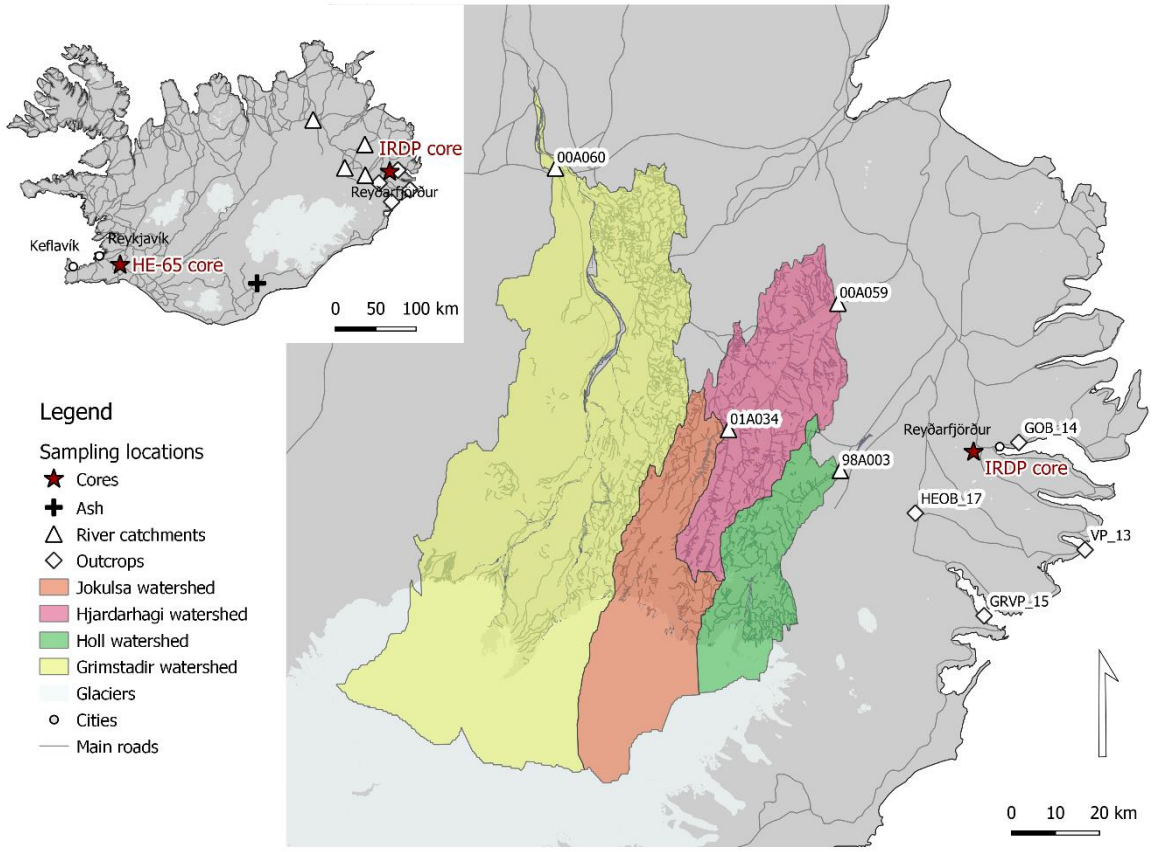

Figure 1 : Map showing the sampling locations of each altered basalt considered in this study. The colored areas represent the catchment area covered by each of the sampling points from which suspended material was collected.

2.2. Preparation of the solids

Core and outcrop samples were first cleaned to remove any evident foreign material. In cases where outer parts of the samples exhibited distinct differences from the bulk rock sample, they were removed using a diamond saw. The samples were cut and a representative part of each rock was selected to prepare 30 µm thick thin sections for microprobe analysis. The remaining rock sample was then crushed by hammer and subsequently ground using an agate vibrating-disc mill. The resulting powders were dry sieved to obtain the 40-150 µm size fraction with the exception of sample HE65_22 for which the 40-125 µm size fraction was collected. This final sample had a slightly different size fraction as it was originally prepared for a different study. To ensure that the results of our experiments are consistent with previously reported rates, the prepared size fractions were first cleaned to remove fine particles by gravitational settling using ultrapure deionized

water (DIW) and then further cleaned using an ultrasonic bath with DIW and then ethanol. Depending on the sample, 5 to 20 cleaning cycles using DIW and gravitational setting and 5 to 10 cleaning cycles using the ultrasonic bath with DIW and ethanol were required to clean the collected basalt powders. The grains were considered clean when the fluid phase was clear to the eye after an ultrasonic cleaning cycle. The cleaned powders were finally oven dried at 50 °C for two days. The suspended material samples collected from rivers and the volcanic ash were dry sieved to remove particles larger than 630 µm, then used directly in the experiments. SEM images of representative prepared powders before the experiments are depicted in Figure 2a and b. Grains appear clean with no fine particles present. The size of the grains corresponds to the selected size fraction.

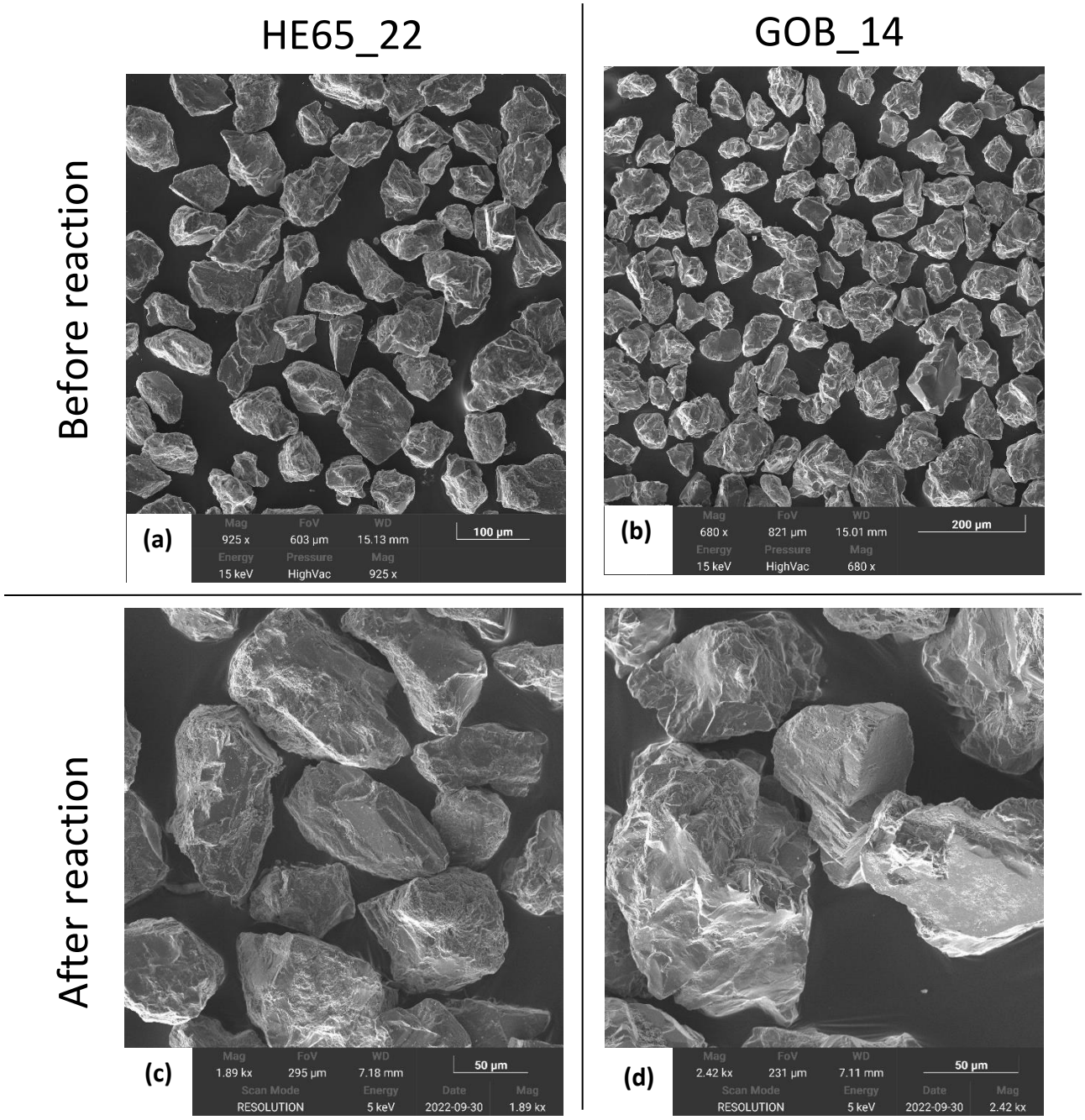

Figure 2 : SEM images of the prepared powders before experiment of (a) sample HE65_22 and (b) GOB_14, and after batch experiments of (c) sample HE65_22 and (d) GOB_14. Images of powders before the experiment are shown at a smaller scale to show the homogeneity of the grains and the quality of the preparation. Images of powders after reactions have a larger scale to make it possible to see potential precipitated phases.

2.3. Characterization of the prepared rock powders

The specific surface areas of the prepared rock powders before their use in the experiments were measured using the Brunauer-Emmet-Teller (BET) method with 11 adsorption points. The measurements were performed using the Quantachrome Autosorb-

1MP gas sorption system at Géosciences Environment Toulouse. The geometric surface areas of the prepared powders were also calculated using:

$$A_{geo} = \frac{6}{\rho * d_{eff}} \quad (1)$$

where ρ refers to the density of the rock and d_{eff} corresponds to the effective particle diameter (Tester et al., 1994). The density of the basalts considered in this study were not measured directly. Instead, we used the average density of basalt of 2.9 g cm^{-3} (Philpotts and Ague, 2009). The variation of sample mineral and elemental composition suggests the density of our solids should vary by no more than 10% from this value. The effective particle diameter, d_{eff} was calculated using (Tester et al., 1994):

$$d_{eff} = \frac{d_{max} - d_{min}}{\ln(\frac{d_{max}}{d_{min}})} \quad (2)$$

where d_{max} and d_{min} refer to the maximum and minimum diameter of the sieves used to prepare the powders. The geometric surface area could not be calculated for the volcanic ash or the river-suspended materials as these samples were naturally ground and the available mass of these samples was too low to measure their grain size distribution.

The bulk chemical compositions of the prepared rock powders were measured using X-Ray Fluorescence spectrometry (XRF) using a S2 Ranger Bruker spectrometer (GET, Toulouse, France). The measured compositions are reported in Table S1. The mineralogy of all solid samples was determined at Activation laboratories (Canada) using a Bruker D8 Endeavour diffractometer equipped with Cu X-ray source measuring at 40 kV and 40 mA on a range of 4 – 70° with a step size of 0.02°. The PDF4/Minerals ICDD database was used for mineral identification. The quantities of the crystalline mineral phases were determined by Rietveld refinement. The amounts of the crystalline minerals were recalculated based on the addition of a known percentage of corundum to the sample. The mass of amorphous and poorly crystalline material was estimated from the difference between the sum of the volume fractions of the identified crystalline phases and 100%. To further characterize the mineralogy of the samples, the composition of selected minerals was determined by microprobe analyses on a CAMECA SXFive electronic microprobe located at the Raimond Castaing micro characterization center in Toulouse.

2.4. Experimental methods

Dissolution experiments with all the prepared rock samples were performed in batch reactors. They were complemented with four mixed-flow experiments at pH 4, as described below.

2.4.1. Batch experiments

Batch dissolution experiments were run in parallel in closed 750 ml High-Density Polyethylene (HDPE) reactors immersed in a GFL 1083 thermoregulated shaking bath (Baker et al., 2009; Zhen-Wu et al., 2016). The temperature of the bath was maintained at 27±1 °C throughout all batch experiments. Before each experiment, three grams of the selected rock powder was placed into the reactor together with 300 ml of the initial reactive fluid. This water to rock ratio was chosen to allow sufficient reaction to characterize rates and sufficient fluid for sampling over two months while ensuring measurable elemental concentrations. The initial reactive fluid was made from Merck reagent grade HCl and NaCl diluted into ultrapure distilled water to obtain a pH 3 solution with an ionic strength of 0.01 mol kg^{-1}. This pH was chosen to be close to that of the CO_2 charged waters that are injected during subsurface mineral carbonation efforts (Gislason et al., 2010). The ionic strength was chosen to mimic the salinity observed in the CarbFix injection site (Snæbjörnsdóttir et al., 2017; Clark et al., 2018), and to facilitate the comparison of the results with previously reported experimental data. A schematic illustration of the experimental reactor system is shown in Figure 3.

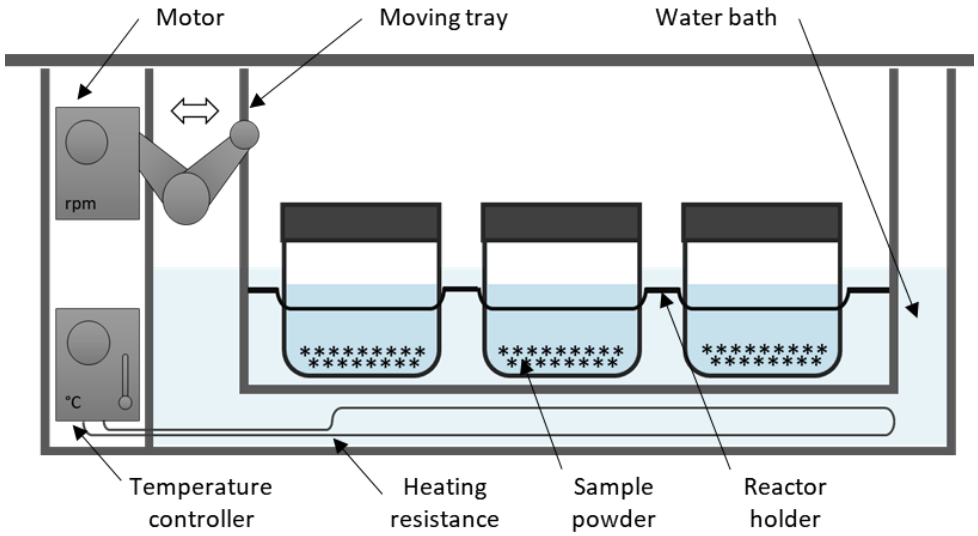

Figure 3 : Schematic illustration of the batch reactor system used in this study

Reactive fluids samples were collected regularly using syringes equipped with 0.45 µm Polytetrafluoroethylene (PTFE) filters to track the temporal evolution of the chemical composition of the fluids. The fluid samples for element concentration analysis were immediately acidified with Suprapur HNO_3 prior to storage in a refrigerator and further analysis.

2.4.2. Mixed flow reactor experiments

Four mixed-flow reactors experiments were run in closed 120 ml Savillex reactors. Each reactor had an inlet and an outlet port. The inlet port injected fluid into the bottom of the reactor, while the outlet port removed fluid from the top. Each reactor was equipped with a Teflon suspended stirring bar, allowing fluid-solid mixing and avoiding rock powder grinding. The reactors were positioned on a multi magnetic stirring plate so that all had identical stirring rates. A Gilson manifold pump was used to inject the inlet fluid into the reactors at approximately 0.15 ml min^{-1}. The inlet fluids were stored in polypropylene compressible bags before their injection into the reactors. The reactor outlets were equipped with 0.45 µm cellulose ester filters to prevent the powder from escaping the reactor. The complete reactor system was placed in a thermoregulated chamber set at 25±1 °C. A schematic illustration of the experimental reactor system is provided in Figure 4.

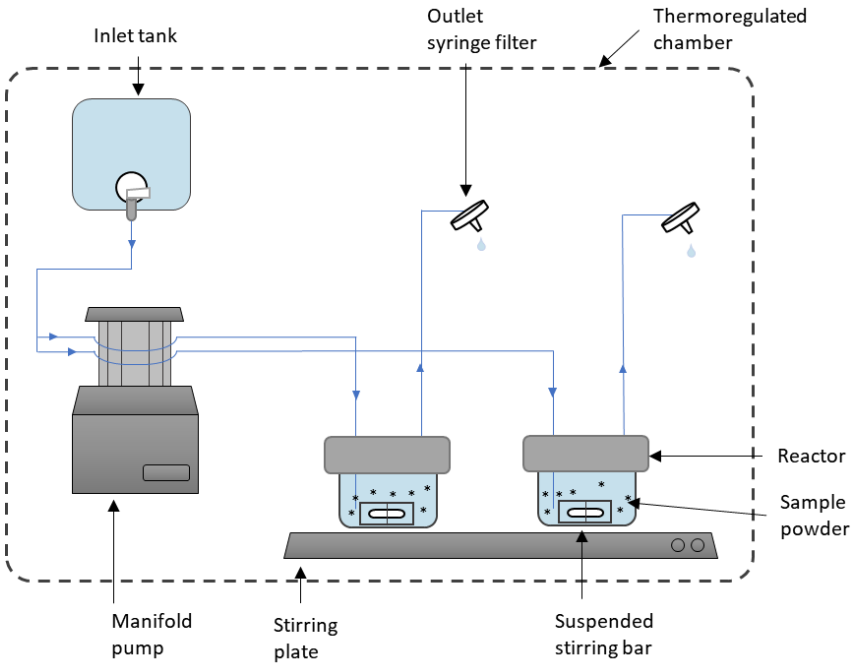

Figure 4 :Schematic illustration of the mixed-flow reactor system used in this study

Two to three grams of rock powder were initially placed in the reactors together with sufficient inlet fluid to fill the reactors. This leads to fluid-rock ratio of 40 to 60; the lower fluid to rock ratio was selected for sample B316S3 due to its lower surface area. The inlet fluid was made from Merck reagent grade HCl and NaCl diluted into DIW to obtain a pH 4 solution with an ionic strength of 0.01 mol kg^{-1}. This fluid composition was selected to match the conditions of the batch experiments. Once filled, the reactors were sealed and placed in the thermostatically controlled chamber and the experiment started. The outlet fluids were regularly sampled to measure pH and major elements. Some gas bubbles formed in some of the reactors over time. These were removed manually to avoid their potential blocking of the fluid outlet port.

At the end of the batch and mixed-flow experiments, the solids were recovered by filtering the reactor's content using a 0.45 µm PTFE filter. The post-experimental powders were air-dried for several days and stored for further analyses.

2.5. Chemical Analyses

The pH evolution of all sampled batch experiment reactive fluids was measured *in situ* using an extended pH probe connected to a MetrOhm pH meter. The pH in the mixed-flow experiments was measured immediately after sampling in non-acidified outlet fluid samples. The electrodes were calibrated using NIST pH 4.01, 7.00 and 10.01 buffer solutions, and replicate analyses of buffers and samples showed analytical accuracy of 0.03 pH units and precision of ±0.02 pH units at room temperature.

Fluid samples were analyzed for Al, Ca, Fe, Mg, and Si concentrations using a Horiba Ultima Expert Inductively Coupled Plasma Optical Emission Spectrometer (ICP-OES), with an analytical accuracy of 3% and quantification limits of 10 ppb for Al and Fe, and 20 ppb for Ca, Mg and Si. Potassium was not measured due to its low concentrations in the initial rock samples and Na was not measured since it was present in the initial solution at 0.01 mol kg^{-1} concentration.

2.6. Calculation of fluid saturation index and elemental release rates

Geochemical calculations in the present study were performed using PHREEQC V 3.6.2 (Parkhurst and Appelo, 2013) together with the CarbFix.dat V1.1 database (Voigt et al.,

2018). The saturation index of the reactive fluids with respect to primary and potential secondary phases were calculated based on the measured pH and element concentrations.

Element release rates from the batch experiments were calculated using two methods. The first consists of calculating the slope, dn_i/dt, of a least squares fit of the total mass of the i^{th} element released by the rock sample to the fluid as a function of time, as described in Marieni et al. (2021). The mass of each element released was calculated by multiplying the concentration of the element by the reactor fluid mass, taking into account the mass of fluid removed due to sampling over time. Because of large changes in reactive fluid pH and Si release rates, only concentrations measured in fluids collected after 12 days of the start of each experiment were used for calculating dn_i/dt. This allowed retrieval of approximately constant element release rates that were calculated using:

$$r_{i.j} = \frac{(\frac{dn_i}{dt})}{A_j\, m} \quad (3)$$

where (dn_i/dt) refers to the slope of the least square fit of the mass of the i^{th} element released from the rock as a function of time, A_j refers to the initial specific surface area of the solid before the experiment, j represents either BET or geometric surface area, and m designates the initial mass of the solid placed into the reactor. Initial surface areas were used for this calculation to be consistent with previously published rates and to avoid ambiguities associated with the contributions to surface areas of secondary minerals that might have formed during the experiments. The pH was not buffered during the batch experiments. Consequently, the rates obtained using equation (3) correspond to the reactive fluid pH from which the slope was obtained.

A second method used to quantify rates from the batch experiments took account of the change in pH over time following an approach proposed by Blum and Lasaga (1988), Guidry and Mackenzie (2003) Harouiya et al. (2007), and Zhen-Wu et al. (2016). In this approach the pH is first fit using:

$$pH = \alpha\, t^{1/\beta} + \gamma \quad (4)$$

where t designates the elapsed time since the beginning of the experiment and α, β and γ designate fit parameters. The proton activity generated using equation (4) and the measured Si concentrations in each reactor were then fit by numerical integration using:

$$r_{i,j} = dn_i/dt = (k_s/A_j\, m)\ a_{H^+}{}^{\varepsilon} \qquad (5)$$

where k_S refers to a rate constant, a_{H^+} denotes the proton activity and ε represents a reaction order. A_j refers to the initial specific surface area of the solid, j represents either BET or geometric surface area, and m designates the initial mass of the solid placed into the reactor. The parameters k_S and ε were estimated using a numerical solver so that the calculated rates best fit the measured reactor fluid compositions during the experiments. The resulting parameters can then be used together with equation (5) to estimate the element release rates at a chosen constant pH.

Steady-state elemental release rates in mixed-flow experiments were calculated using:

$$r_{i,j} = \frac{C_i\, Q}{A_j\, m} \qquad (6)$$

where $r_{i,j}$ refers to the release rate of the i^{th} element normalized to the surface area A_j, where j represents either BET or geometric surface area. C_i denotes the concentration of the i^{th} element in the outlet fluid, at steady state and Q designates the flow rate.

3. RESULTS

3.1. Mineral and chemical composition of the altered basalts

The mineralogical compositions of the collected surface weathered basalts are summarized in Figure 5 and further details are provided in Table S2. The mineralogy of these samples is dominated by primary phases. More than 88% of the mineral content of each of these rocks consists of plagioclase, pyroxenes, and an amorphous phase.

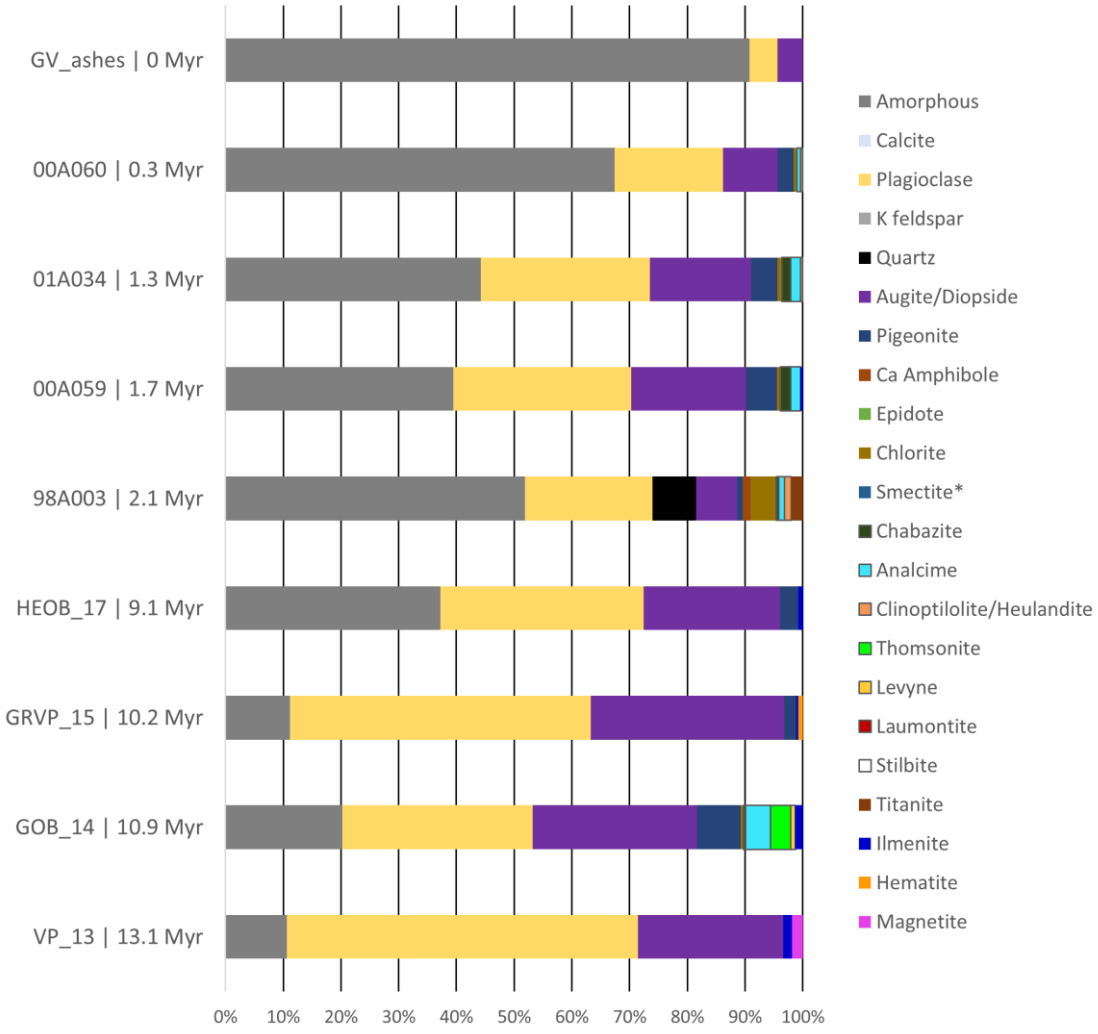

Figure 5 : Mineralogy of the surface samples as determined by XRD Rietveld refinement, in weight percent ordered based on the age of the samples.

Microprobe analyses revealed that the plagioclase in these rocks is mostly labradorite, with minor andesine and bytownite detected, and that the pyroxenes were of augitic composition. The secondary phases observed were primarily minor chlorites and zeolites. These secondary minerals may have been formed during the initial cooling of the molten basalts.

Two notable trends are evident in the composition of these rocks as a function of their age. First, as shown in Figure S1, the amorphous phase content of these rocks decreases substantially with age. The rocks less than 2.2 Myr old have amorphous contents ranging between 40 to 90%, while the older rocks have amorphous contents of less than 40%.

Second, the chemical composition of the amorphous phase contained in these samples exhibits distinct trends with rock age. These compositions, obtained from microprobe analyses, are listed in Table S3. The amorphous phase in the older rocks have lower Ca, Al, Na and K contents, but are relatively enriched in Fe compared to younger rocks and fresh basaltic glass. These observations suggest the continuous alteration of the original glass through palagonitization as described by Stroncik and Schmincke (2002) and Parruzot et al. (2015), where basaltic glass is replaced by a heterogeneous microcrystalline solid composed of different clays, zeolites, and oxides, or mixtures of these (Jercinovic et al., 1990; Zhou et al., 1992).

The mineralogical compositions of the collected hydrothermally altered basalt samples are depicted schematically in Figure 6.

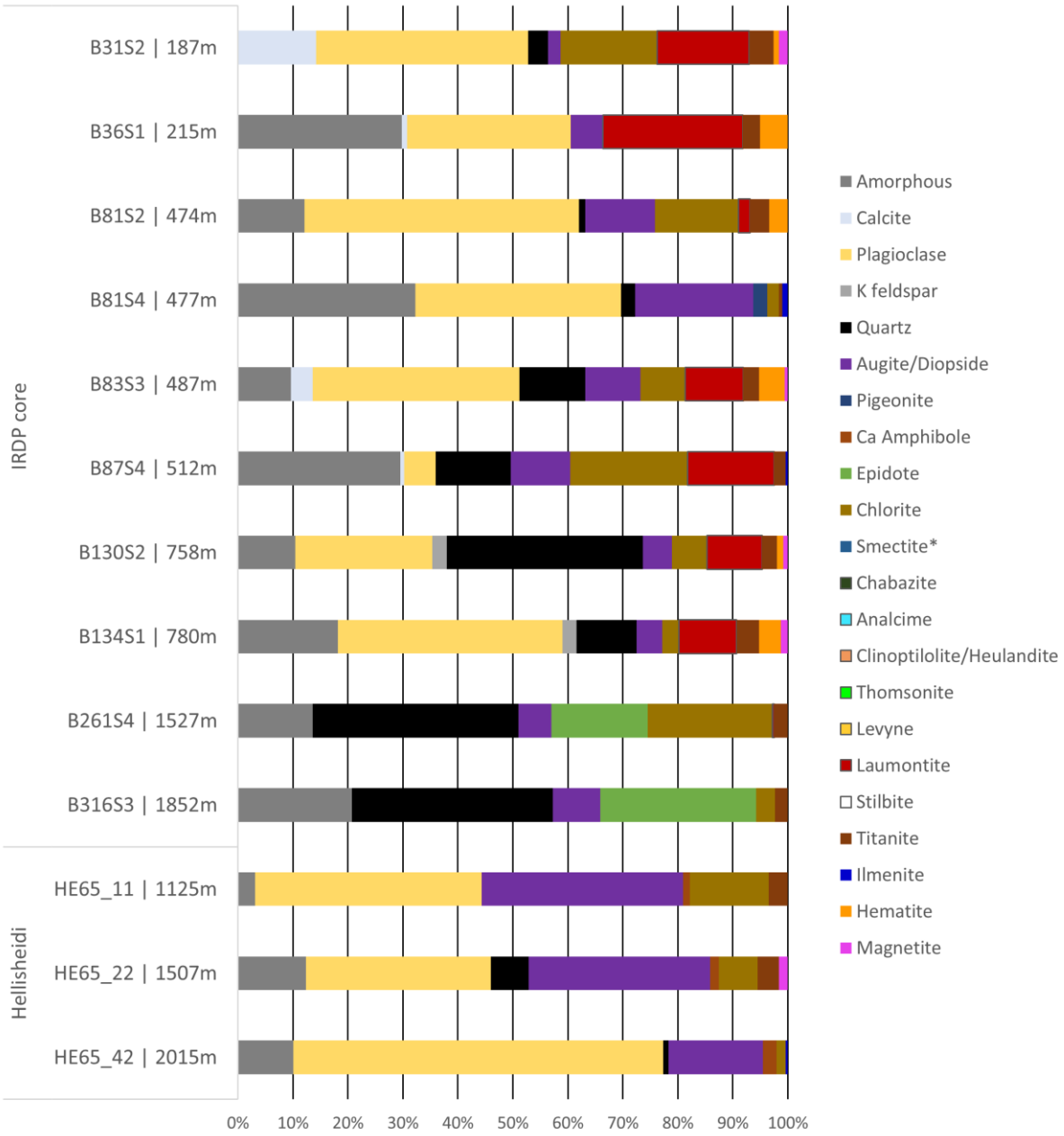

Figure 6: Mineralogy of the hydrothermally altered basalts considered in this study as determined by XRD Rietveld refinement, in weight percent. Samples are ordered by sample origin and increasing depth.

The alteration of samples collected from the IRDP core corresponds to the zeolite's facies with variable amounts of laumontite and chlorite. Only the two deepest samples from this core, B261S4 and B316S3, contain epidote. These deepest samples contain no plagioclase, but a significant amount of quartz. The plagioclases in the IRDP core samples were all of albitic composition and the pyroxenes had an augite composition. The alteration of the rocks sampled from the Hellisheiði core was less extensive, with primary phases better preserved. Plagioclase and pyroxenes are present in significant amounts in the

Hellisheiði samples, where andesine, labradorite, oligoclase, and albite were detected by microprobe. Pyroxenes were of augitic composition and some Ca-amphiboles were also present in small amounts. The amorphous phase content of all of the hydrothermally altered basalts varies between 0 and 30% with no consistent trend. Four samples from the shallower part of the IRDP core contain from 0.7 to 14.2 wt% calcite.

The chemical compositions of the amorphous phase of some of the hydrothermally altered basalts are shown in Table S3. The compositions of these amorphous phases are depleted in Ca, lower in Al and Si, and enriched in Fe compared to basaltic glass, possibly due to the palagonitization of the original basaltic glass (Stroncik and Schmincke, 2002; Parruzot et al., 2015).

The measured BET surface areas of all samples are reported in

Table 1 together with the corresponding calculated geometric surface areas. The BET specific surface areas of the rock powders used in the experiments varied from 0.3 to 28 $m^2 g^{-1}$. Part of this variation can be explained by sample preparation. Most rock samples were prepared at the CNRS laboratory in Toulouse in an identical manner, with the exception of the volcanic ash sample (GV_ash) and the four river suspended material samples (00A060, 01A034, 00A059, 98A003). These natural rock powders exhibited BET surface areas among the highest considered in this study (see

376 Table 1).

377

Table 1: BET and geometric surface areas of all the samples. NA stands for not available

		Sample	*Age (MYr) / **Depth (m)***	*Size fraction (µm)*	*BET surface area (m^2 g^{-1})*	*Geometric surface area (m^2 g^{-1})*
Surface weathered basalts	*Volcanic ash*	GV_ash	0	Raw <630	0.4	NA
	River suspended material	00A060	0.3	Raw <630	7.7	NA
		01A034	1.3	Raw <630	23.6	NA
		00A059	1.7	Raw <630	28.1	NA
		98A003	2.1	Raw <630	11.5	NA
	Surface outcrops	HEOB_17	9.1	40-150	0.4	0.0248
		GRVP_15	10.2	40-150	4.7	0.0248
		GOB_14	10.9	40-150	1.6	0.0248
		VP_13	13.1	40-150	5.0	0.0248
Hydrothermally altered basalts	*IRDP core*	B31S2	**187.3**	40-150	9.0	0.0248
		B36S1	**214.6**	40-150	4.5	0.0248
		B81S2	**473.9**	40-150	3.6	0.0248
		B81S4	**476.8**	40-150	2.7	0.0248
		B83S3	**487.1**	40-150	2.5	0.0248
		B87S4	**512.3**	40-150	4.2	0.0248
		B130S2	**758.4**	40-150	1.7	0.0248
		B134S1	**780.4**	40-150	2.3	0.0248
		B261S4	**1526.6**	40-150	1.5	0.0248
		B316S3	**1851.7**	40-150	0.4	0.0248
	Hellisheiði	HE65_11	**1125.3**	40-150	1.0	0.0248
		HE65_22	**1506.7**	40-125	2.0	0.0277
		HE65_42	**2014.6**	40-150	0.3	0.0248

3.2. Temporal evolution of the reactive fluid pH, elemental concentrations, and mineral saturation states

3.2.1. pH and elemental concentrations

The temporal evolution of the composition of reactive fluids in all batch experiments is provided in Table S4. The reactive fluid pH evolution of three representative experiments is provided in Figure 7.

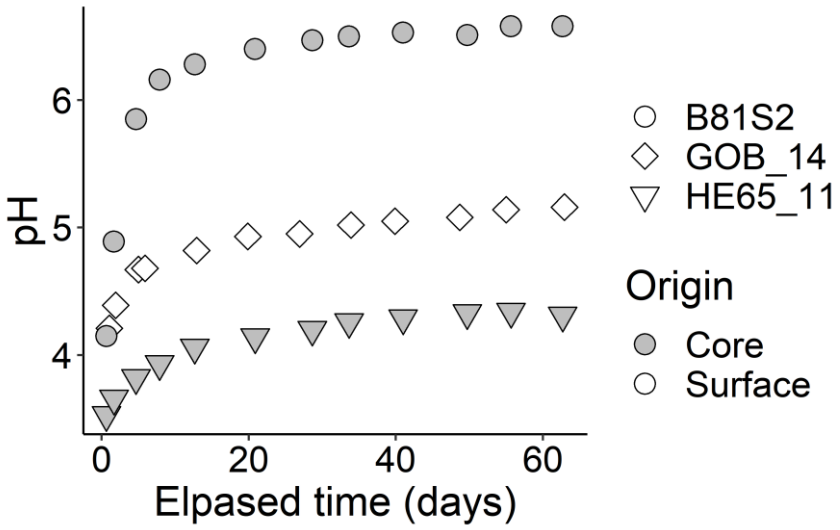

386

387 *Figure 7: Temporal evolution of the reactive fluid pH during three representative batch*
388 *experiments. The size of the uncertainties is smaller than the symbol size.*

389 The reactive fluid pH in all batch reactor experiments increases rapidly during the first
390 10 days. The highest final pH values, close to 8, were observed in experiments performed on
391 samples containing significant amounts of calcite in their original composition (see Table S4).

392 The temporal evolution of the dissolved Si, Ca, Mg, Al, and Fe concentrations during
393 three representative batch experiments are shown in Figure 8. The concentrations of Ca, Mg,
394 and Si increased in the fluids of all batch experiments over time. Al and Fe showed a distinct
395 behavior: Al concentrations decreased over time during most of the experiments and Fe
396 concentrations were below the detection limit in all experiments where the pH exceeded pH
397 5. These observations suggest the precipitation of Al and Fe-rich phases such as Al and Fe
398 oxy-hydroxides during the experiments.

399

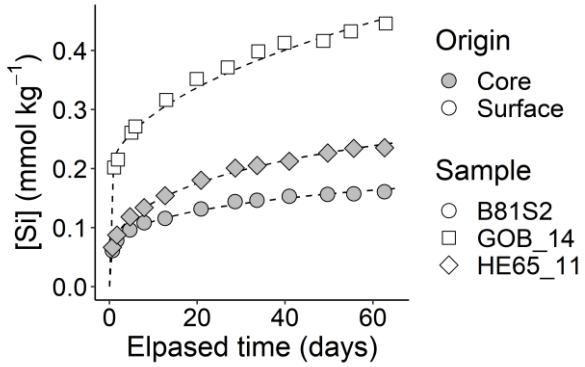

400

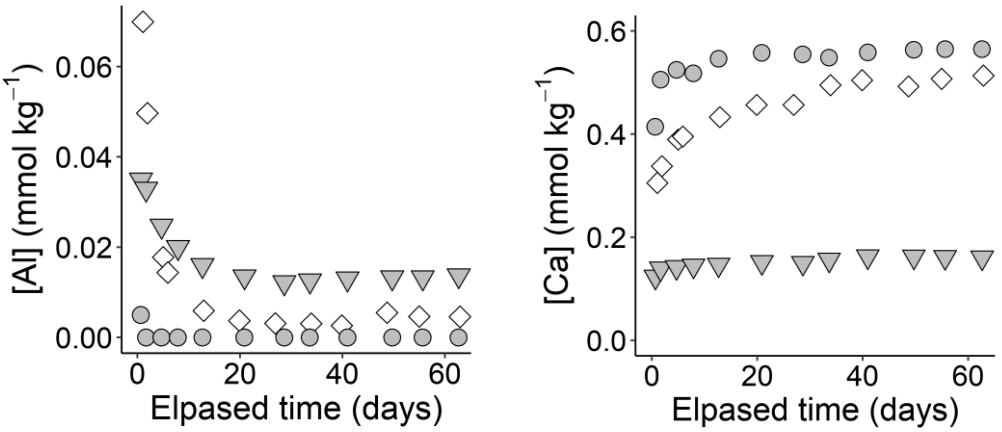

401

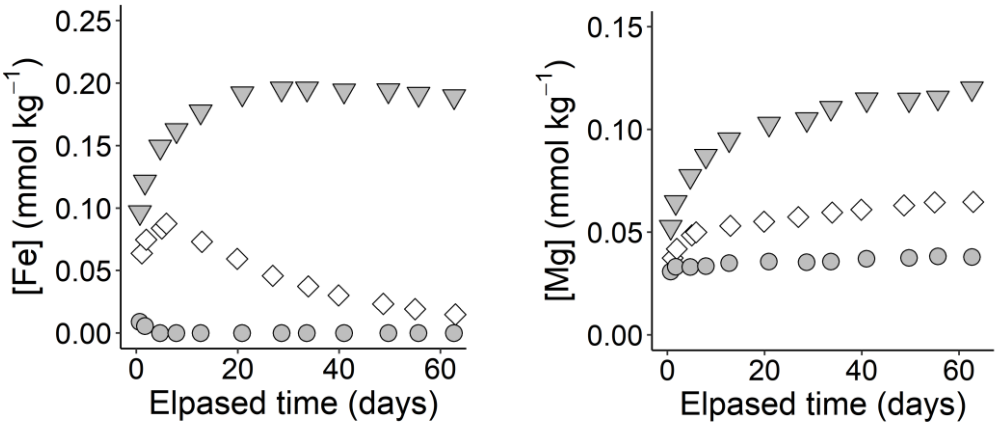

402

403 *Figure 8: Temporal evolution of Si, Al, Ca, Fe, and Mg concentrations of three representative*
404 *batch experiments. The dashed lines in the Si graph represent Si concentrations obtained*
405 *from equation (5) together with the fit parameters corresponding to each experiment. The*
406 *size of the uncertainties is smaller than the symbol size.*

407

3.2.2. Saturation state of the reactive fluids

The saturation indices of the reactive fluids with respect to the phases present in the initial solids and potential secondary phases were estimated using measured fluid chemistry and pH with PHREEQC. A complete list of these saturation indices is provided in Table S5. Numerous phases are found to be supersaturated during the experiments including smectites, aluminum and iron oxyhydroxides, and quartz. None of these phases, however, were identified in post experimental XRD analyses or the SEM observations (Figure 2). The precipitation of Al and Fe oxyhydroxides, however, is likely as the fluid concentrations of these elements decreased over time during most batch experiments. For some samples, scattered nanocrystals were observed on the reacted grains. These nanocrystals were too small to determine their composition with energy dispersive spectrometry.

3.3. Element release rates

3.3.1. Batch reactor experiments

Silicon release rates are often used as a proxy for the dissolution rates of silicate minerals because Si-O bonds maintain the structure of most of these minerals (Oelkers et al., 1994; Oelkers, 2001; Brantley, 2008; Schott et al., 2009). Silicon release rates from all experiments obtained using equation (3), together with the measured slopes of Si mass versus time are shown as a function of the *in situ* pH in Figure 9, and provided in Table S6. Also shown in this figure are Si release rates obtained from the mixed-flow experiments, as described below. Two observations are evident in this plot. First, the measured Si release rates obtained from the temporal evolution of the reactive fluid composition tend to be consistent with the steady-state rates obtained from the mixed flow reactors. Second, the Si release rates appear to plot as a single function of pH. This latter observation suggests that there is little effect of the degree of basalt alteration on these Si release rates.

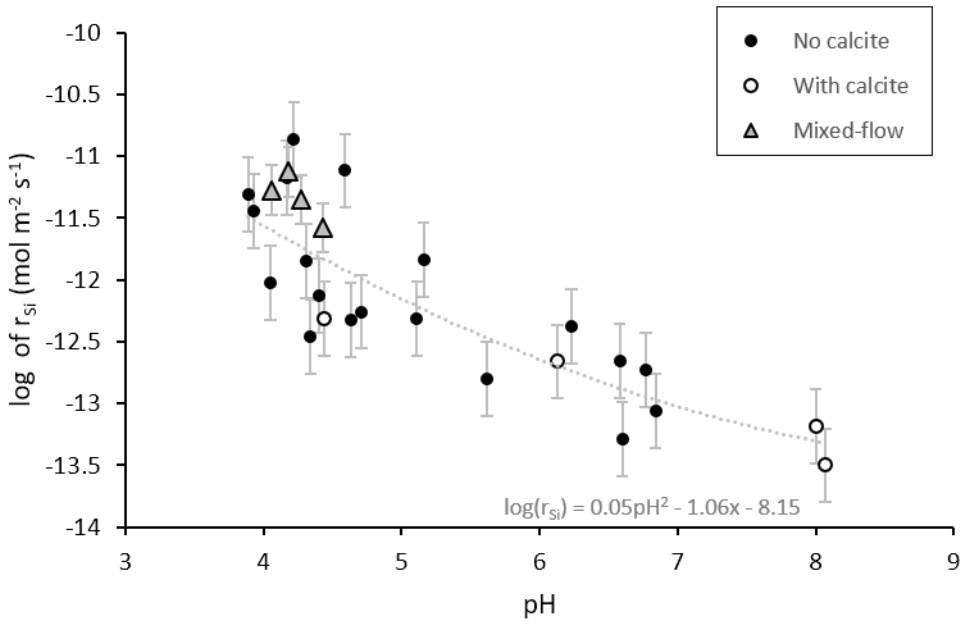

Figure 9: Logarithm of BET surface area normalized Si release rates as a function of the corresponding reactive fluid pH. The grey dashed line shows the result of a polynomial regression of these rates. Error bars indicate a ±0.3 log units uncertainty on the Si release rates. Uncertainties on the measured pH are smaller than the symbol size.

Si release rates generated for pH 4 using equations (4) and (5) are presented together with corresponding rates for individual silicate minerals in Figure Figure 60. All calculated rates are reported in Table S7. Silicon release rates at pH 4 are similar for most of the altered basalts, and many are identical to each other considering the associated uncertainty. Surface area normalized Si release rates range from $10^{-10.6}$ to $10^{-11.8}$ mol m^{-2} s^{-1}, except for sample B261S4, which had a release rate of $10^{-12.4}$ mol m^{-2} s^{-1}. These rates are substantially lower than either those of Ca-rich plagioclase or fresh basaltic glass, but substantially faster than those of common clay minerals. Although the least altered basalts considered in this study (based on the relative volume of primary phases present in the rocks) exhibit rates that are among the fastest rates measured, the Si release rates of surface and core samples are evenly distributed and no clear trends are evident.

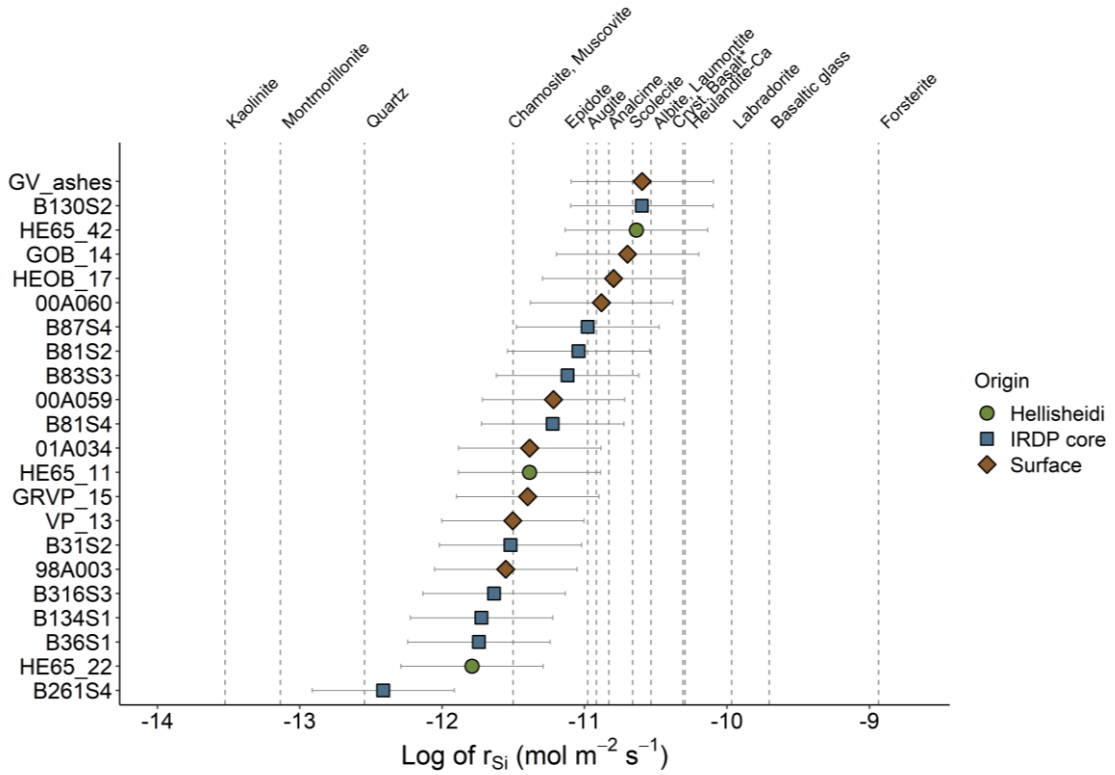

448

449 *Figure 60: Logarithm of estimated BET surface area normalized Si release rates at pH 4 for all*
450 *studied rock samples. Rates for individual minerals are represented with dashed lines and*
451 *were obtained using equations and parameters reported by Heřmanská et al. (2022). The*
452 *rate for crystalline basalt was taken from Gudbrandsson et al. (2011).*

453 **3.3.2. Mixed flow reactor experiments**

454 The rock samples used in the mixed-flow reactor experiments were selected to span
455 a diversity of mineralogy observed in the samples. An example of the temporal fluid
456 evolution of a mixed-flow reactor experiment is shown in Figure 71; a complete table of the
457 temporal fluid concentrations in the samples collected from the mixed-flow experiments is
458 provided in Table S8.

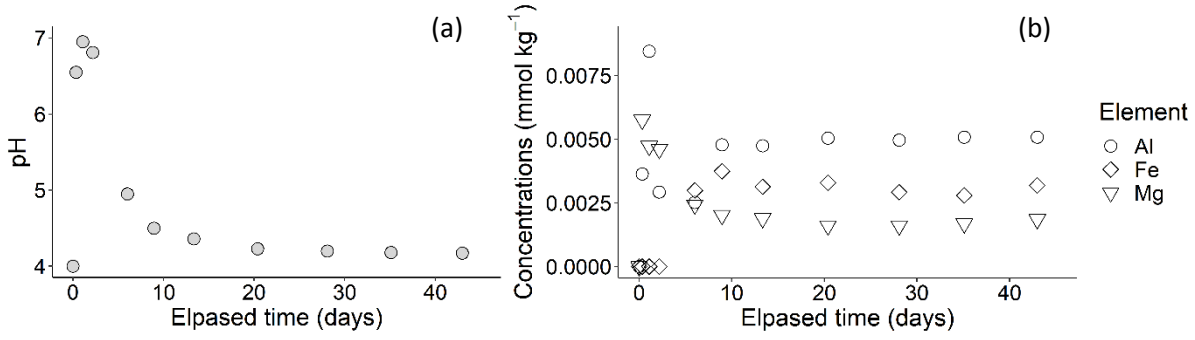

459

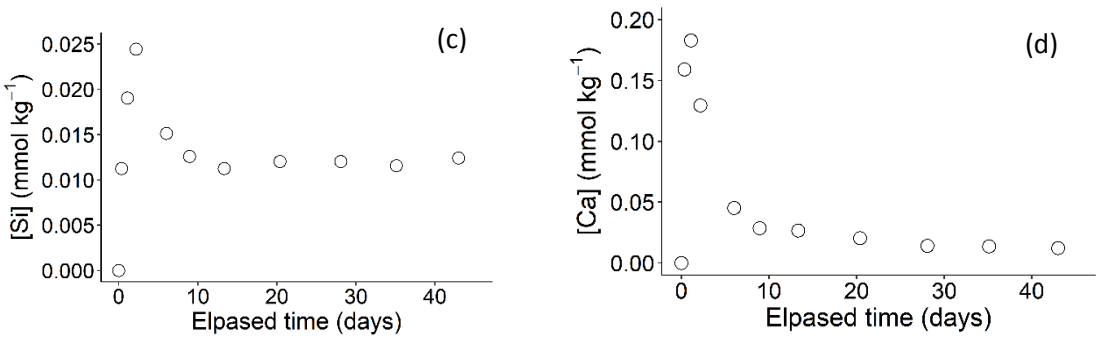

Figure 71: Temporal evolution of the (a) pH, (b) Al, Fe and Mg, (c) Si and (d) Ca concentrations of the outlet fluids for the B130S2 mixed-flow experiment. The size of the uncertainties is smaller than the symbol size.

In all the mixed-flow experiments, the pH, Si, Ca and Mg concentrations peaked during the first few days before decreasing towards a stable steady state value. During the early part of the B130S2 mixed-flow experiment, the pH reached values close to 7 before decreasing to 4. This high initial pH explains why Fe concentrations were below the quantification limit at the beginning of the experiment; likely due to Fe oxidation and precipitation (Singer and Stumm, 1970; Morgan and Lahav, 2007). Concentrations of Al did not exhibit consistent trends across all the experiments. Element release rates were obtained from the steady-state outlet fluid concentrations using equation (6). Resulting steady state reaction rates obtained from these experiments are summarized in Table 2. These rates are also plotted as a function of pH, together with corresponding batch experiment rates in Figure 9. The steady-state rates obtained from the mixed-flow experiments are largely consistent with corresponding rates obtained from batch reactors. One exception is the Si release rate of sample HE65_22, which is close to an order of magnitude faster than that of the corresponding rate estimated from the batch experiments.

Table 2: Summary of the results of the mixed-flow experiments. Steady state element release rates are given as logarithms values in units mol m^{-2} s^{-1}. The Log values of Si release rates from batch experiments were calculated using equation (5) at the final pH value of the corresponding mixed-flow experiment.

Sample	*B83S3*	*B130S2*	*B316S3*	*HE65_22*
Final pH	4.3	4.2	4.1	4.4
final fluid molar Ca/Si ratio	1.91	1.11	1.33	1.71
Molar Ca/Si of the rock sample	0.16	0.09	0.23	0.24
final fluid molar Mg/Si ratio	0.23	0.14	0.82	1.35

Molar Mg/Si ratio of the rock sample	0.12	0.05	0.11	0.17
Log of Ca release rate	-11.1	-11.1	-11.1	-11.3
Log of Mg release rate	-12.0	-12.0	-11.4	-11.4
Log of Si release rate	-11.3	-11.1	-11.3	-11.6
Log of Si release rate from corresponding batch experiment	-11.3	-10.7	-11.7	-12.5

3.4 Experimental uncertainties

The uncertainties associated with the reported surface area normalized Si release rates obtained from the batch experiments were estimated by summing the different sources of uncertainty. These sources include those associated with the BET surface area measurements, the measurement of reactive fluid compositions, and the linear regression of fluid Si masses over time. The combination of these uncertainties suggests that the rates generated using equation (3) and shown in Figure 9 have uncertainties on the order of 0.3 log units. Rates generated at a constant pH of 4 using equation (5) and summarized in Figure 10 have higher uncertainties due to the extrapolation of measured rates to this constant pH. The total uncertainty on these latter rates is estimated to be on the order of 0.5 log units. In contrast, Si release rates obtained from the mixed-flow experiments do not require a linear regression of fluid Si mass nor were extrapolated to a constant pH of 4. This results in lower uncertainty in the Si release rates from these experiments, which is estimated to be 0.2 log units.

4. Discussion

4.1. Surface areas

The BET surface areas of the laboratory prepared basalt powders range from 0.3 to 9 m^2 g^{-1}. The origin of these differences is challenging to determine, but sample mineralogy can have an influence. Minerals including the chlorites (Malmström et al., 1996), zeolites (Yates, 1968; Valdés et al., 2006), and clays (Murray and Quirk, 1990) have been reported to have relatively high BET surface areas. To illuminate the degree to which the presence of these minerals influences the surface areas of the laboratory prepared samples, the BET surface areas of all laboratory-prepared rock powders are plotted as a function of their combined chlorite and zeolite contents in Figure 82.

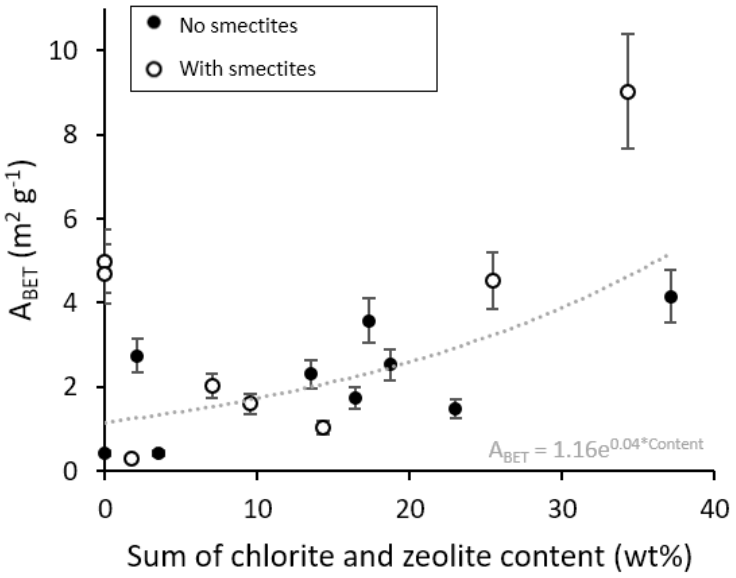

Figure 82: Plot of the BET surface area of the laboratory prepared rock powders used in this study as a function of the sum of their zeolite and chlorite contents. Open circles indicate samples observed to contain clay minerals. Error bars represent the uncertainty on BET measurements. The grey dashed line shows the result of an exponential regression of these surface areas.

Measured BET surface areas are observed to increase with chlorite and zeolite content. Note that the mass of clay minerals, such as smectite, was not quantified by Rietveld analysis. Only their presence or absence was reported. This may likely be the reason for the high surface areas of the two chlorite and zeolite-free samples that plot on the left side of Figure 82 as they do contain clays minerals.

4.2. Reactivity of altered basalts

Several significant observations can be made concerning the measured Si release rates determined in the present study. First the Si release rates from all altered basalts are similar, regardless of their degree of alteration. The differences in rates measured from batch experiments are largely explained by the pH differences, as seen in Figure 9. When these rates are recalculated to pH 4, as in Figure 10, the differences between these Si release rates are low compared to the associated uncertainty. The results from the mixed-flow experiments performed in this study confirm this observation, with rates measured from basalts with contrasting alteration profiles falling within 0.5 log units of one another.

528 The similarity in these rates likely stems from the mineralogy of these altered basalt
529 samples. The alteration of basalt rapidly removes basaltic glass and olivine due to their low
530 thermodynamic stability and high reactivity. After the removal of these phases the most
531 reactive minerals present in the altered basalts are plagioclase, augite, zeolites and epidote.
532 Collectively these minerals represent from 25 to 85 wt% of the mass of the studied samples.
533 The logarithm of Si release rates for these minerals at pH 4 and 25 °C range over a relatively
534 small range, from $10^{-10.0}$ to $10^{-11.5}$mol m^{-2} s^{-1}. Other minerals in these altered rocks, such as
535 chlorite, quartz and clay minerals are significantly less reactive than these phases (Brantley,
536 2008), and likely contribute little to the release of Si to the fluids during the experiments
537 performed in this study.

538 A second significant observation is that the BET surface area normalized Si release rates
539 measured in this study on altered basalts are one to two orders of magnitude slower than
540 that of basaltic glass, and somewhat slower than those of fresh crystalline basalt. This
541 observation confirms the impact of alteration on rock dissolution rates. Alteration
542 preferentially removes most reactive phases decreasing the average dissolution rate of the
543 overall rock. The slowing of weathering rates of rocks over time due to rock alteration has
544 been previously explored in a number of studies (e.g. Colman, 1981; White et al., 1996;
545 White and Brantley, 2003; Reeves and Rothman, 2013).

546 A third observation is that the measured surface area normalized rates of altered
547 basalts determined in this study tend to be lower than those of the individual minerals, such
548 as plagioclase, present in the altered rock samples. The lower surface area normalized Si
549 release rates determined in this study can be attributed to the formation of high surface
550 area but slowly reacting minerals during the natural alteration process. The formation of clay
551 minerals, chlorite, and nanocrystalline Fe and Al-oxides increases the surface area of altered
552 basalts without changing significantly the rate of Si release. As a consequence, the presence
553 of such phases lowers the measured surface area normalized Si release rates of altered
554 basalts.

555 **4.3. Relative release rates of the elements**

556 The temporal evolution of the Ca/Si molar release ratios normalized to the
557 corresponding ratio of the original rock for some representative experiments is shown in

Figure 93. The reactive fluid Ca concentration was significantly higher than that of Si at the beginning of each batch experiment. The Ca/Si molar ratio of the reactive fluids decreased sharply after the first days of each experiment and tended to stabilize over time. Marieni et al. (2020) observed a similar behavior reacting altered oceanic basalts in batch reactors. The initial rapid Ca release could result either from rapid initial cation for proton exchange reactions (Oelkers et al., 2009; Zhang et al., 2013), consistent with the observation that the intensity of the observed preferential release of divalent cations is correlated to increased surface areas of the altered basalt samples, or from the presence of a rapidly dissolving Ca bearing, Si-free mineral such as calcite, in the original rock samples. Note that although calcite was not observed to be present with XRD analyses in the solids considered in Figure 13, minor quantities of calcite could have gone undetected as the detection limit for XRD is on the order of 1%.

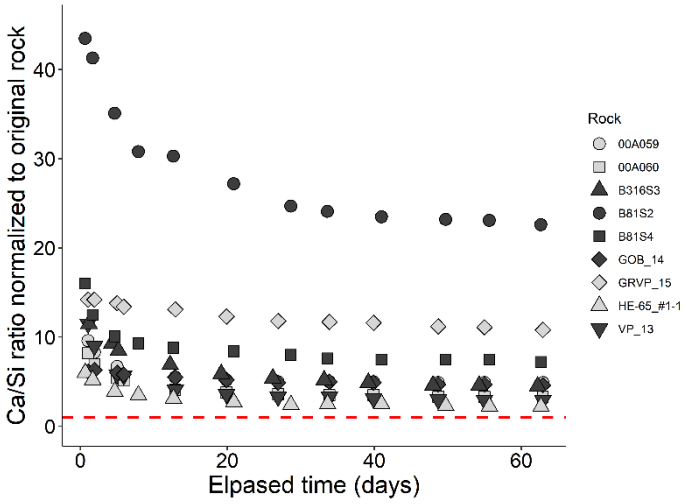

Figure 93: Temporal evolution of the Ca/Si molar ratio of the reactive fluids normalized to that of the original rock for selected representative batch experiments. The red dashed line represents the Ca/Si ratio of stoichiometric dissolution.

In some cases, the preferential release of both Mg and Ca persists until the end of the experiments. To further explore this preferential release, the Ca and Mg to Si release rate ratios were calculated from a linear regression of the fluid masses during the latter part of each batch experiment using equation (3). The resulting release rate ratios are provided in Table 3. Most hydrothermally altered basalt samples exhibited a preferential release of Ca and Mg, relative to Si over the whole experiment, whereas surface altered samples tended to approach stoichiometric element release rates over time. This behavior may stem from

581 the alteration process itself. The hydrothermal alteration of basalts leads to the formation of
582 minerals such as zeolites and epidote (Humphris and Thompson, 1978; Kristmannsdottir,
583 1979). These minerals contain abundant Ca and react relatively fast compared to Ca poor
584 alteration phases. The alteration of basalts at the Earth's surface tends to preferentially
585 remove Ca and to a lesser degree Mg, without the precipitation of divalent metal-rich
586 secondary phases (e.g.Eggleton et al., 1987). This process does tend to result in relatively
587 lower quantities of Ca and Mg bearing secondary minerals. The long-term preferential
588 release of Mg can be explained by the faster dissolution rate of augite/diopside relative to
589 the whole rock, or by the exchange of Mg from chlorites and smectites.

590 *Table 3: Ratios of the molar Ca and Mg release rates to Si release rates during the final part*
591 *of all batch experiments. Values in bold correspond to experiments where the Ca and Mg*
592 *release rates were significantly higher than the corresponding original altered basalt*
593 *stoichiometry.*

Origin	*Sample*	*Ca/Si release rate*	*Rock Ca/Si*	*Mg/Si Release rate*	*Rock Mg/Si*	*Rock Normalized Ca/Si ratio*	*Rock Normalized Mg/Si ratio*
IRDP core	B31S2*	**9.97**	0.19	**0.34**	0.16	**51.8**	**2.1**
	B36S1*	**0.32**	0.18	0.10	0.16	**1.7**	0.7
	B81S2	**0.41**	0.16	0.08	0.15	**2.6**	0.6
	B81S4	**0.78**	0.22	**0.31**	0.15	**3.6**	**2.1**
	B83S3*	**27.51**	0.16	**0.25**	0.12	**168.9**	**2.2**
	B87S4*	NA	0.14	**0.21**	0.20	**NA**	**1.0**
	B130S2	**1.98**	0.09	0.07	0.05	**21.8**	**1.3**
	B134S1	**0.82**	0.12	**0.24**	0.08	**6.6**	**3.1**
	B261S4	**0.35**	0.21	**0.58**	0.19	**1.7**	**3.0**
	B316S3	**0.44**	0.23	**1.38**	0.11	**1.9**	**13.1**
Hellisheiði	HE65_11	0.21	0.31	**0.29**	0.26	0.7	**1.1**
	HE65_22	0.19	0.24	**0.58**	0.17	0.8	**3.4**
	HE65_42	0.14	0.30	0.15	0.23	0.5	0.7
River suspended material	00A059	**0.55**	0.23	0.16	0.18	**2.4**	0.9
	00A060	0.13	0.22	0.15	0.16	0.6	0.9
	01A034	**0.81**	0.21	**0.35**	0.17	**3.9**	**2.0**
	98A003	0.14	0.15	0.08	0.19	0.9	0.4
Surface outcrops	GOB_14	**0.64**	0.25	0.10	0.22	**2.6**	0.5
	GRVP_15	**0.74**	0.26	**0.29**	0.18	**2.9**	**1.6**
	VP_13	0.15	0.23	**0.24**	0.15	0.6	**1.6**
	HEOB_17	0.14	0.23	**0.22**	0.18	0.6	**1.2**
Volcanic ash	GV_ash	0.21	0.21	0.15	0.17	1.0	0.9

594 *Sample marked with * contained calcite*

The preferential release of Ca and Mg was also observed during the mixed-flow experiments. The measured elemental release ratios of elements are shown in Table 2. All four mixed-flow experiments exhibited a preferential Ca and Mg release at steady state, even after more than 40 days of reaction. In these experiments, an initial maximum of molar Ca/Si and Mg/Si release ratios was also observed, again consistent with a rapid initial metal for proton exchange reaction. Similar results were reported by Marieni et al. (2020), who observed a strong preferential initial and long-term release of Ca compared to Si from altered mid-ocean ridge basalts collected from the Juan de Fuca Plate and the Mid-Atlantic ridge.

4.4 Insight into the slowing of basalt weathering rates as a function of age and alteration

The ages of the surface altered samples investigated in this study ranged from 0.3 to 13 Myr. All samples were void of olivine, and their original basaltic glass variably altered. The Si release rates from all surface weathered basalt samples are similar considering uncertainties. This suggests that after a rapid palagonitization of basaltic glass and the removal of any olivine present, the reactivity of surface altered basalts becomes largely insensitive to the age or degree of alteration of the rock. Nesbitt and Wilson (1992) came to similar conclusion in their study of the reactivity of altered basalts from Baytown, Australia, and so did Gislason et al. (1996) in their study of the weathering of basalt in Iceland.

All the surface altered basalt samples contained a substantial quantity of primary phases, notably plagioclase and pyroxene. These are among the most reactive minerals after basaltic glass and olivine. It is likely, therefore, that the Si release rates of altered basalts are controlled by the presence of plagioclase and pyroxene in these rocks. As these phases persist in all of the studied Earth surface altered samples, their measured Si release rates are similar to each other.

Based on such observations, it seems likely that the slowing of basalt weathering rates in nature is a non-linear function of time. Rates decrease rapidly as the reactive olivine and basaltic glass are selectively removed. Once these are depleted from the basalts, a slower longer term but near constant Si release rate is observed due to the persistence of plagioclase and pyroxene in these rocks. Similar results were suggested by Gislason et al.

625 (1996) and are consistent with observations reported by Kennedy et al. (1998) and Chadwick
626 et al. (1999).

627 The slowing of element release rates, as a result of the surface alteration of basalts, and
628 the non-linear slowing of these rates has implications for the drawdown of CO_2 following
629 large volcanic events. Although volcanic eruptions emit large masses of CO_2, they also emit
630 large quantities of fresh volcanic rock, which can drawdown CO_2 due to weathering. A
631 number of past studies noted that fresh basalts may have a large contribution to drawing
632 down CO_2 from the atmosphere after major eruptions (Parnell et al., 2014; Cox et al., 2016;
633 Shen et al., 2022). The results of the present study suggest this enhanced drawdown due to
634 the presence of fresh basalts on the Earth's surface is short lived and will persist only as long
635 as fresh basaltic glass and olivine in present in these basalts.

636 **4.5. Application to subsurface carbon mineralization**

637 The experiments in the present study were performed at acidic conditions and at
638 atmospheric CO_2 concentrations. The direct carbonation of the altered basalts at these
639 conditions is not observed. The results presented in this study, nevertheless, suggest that
640 altered basalts could be favorable for subsurface carbon storage by mineralization. The
641 ability of altered basalts to promote CO_2 carbonation is favored by the preferential release of
642 the divalent metal Ca and Mg to the fluid phase and the ability of altered basalt dissolution
643 to increase fluid pH. Both processes, observed in our experiments, favor the formation of
644 carbonate minerals in the presence of water dissolved CO_2.

645 The surface area normalized Si release rates of the altered basalts considered in this
646 study are one to two orders of magnitude slower than the corresponding fresh basalts. Part
647 of this gap is most probably associated to the increased surface area due to the presence of
648 alteration minerals with high surface area and low reactivity. The lower Si release rates of
649 the altered basalts is somewhat compensated by the preferential release rates of Ca and Mg
650 from these rocks even after the initial phase due to exchange reactions. This was particularly
651 true for hydrothermally altered basalts and related to the presence of reactive secondary
652 phases such as zeolites and epidote.

653 The observation that altered basalts are less reactive than corresponding fresh basalts
654 agree with the results obtained from mixed-flow reactor experiments at 120 °C in Delerce et

al., (2023). In this previous study, Si release rates from altered basalts were also found to be similar to each other and mostly independent of the extent of basalt alteration. Although basalt alteration slows reactivity, the effect of this slower rate in terms of carbon storage through mineralization can be overcome by increasing temperature. This is confirmed by the comparison of the results obtained in this study with those from Delerce et al., (2023) and by the observations made during the CarbFix project. During CarbFix1, 95% of the CO_2 injected into fresh basalt at ~30 °C and 400 to 800 m depth mineralized in less than two years (Matter et al., 2016). During the CarbFix2 project, more than half of the CO_2 injected into hydrothermally altered basalts at ~250 °C and 750 m depth was mineralized within 4 months (Clark et al., 2020). This illustrates how increased temperature can compensate for the slower reactivity of altered basalts for mineral carbon storage.

5. Conclusions

This study measured and reported the element release rates of a wide variety of altered basalts of various ages. The major conclusions of this study include:

- Alteration of basalt at the Earth's surface tends to rapidly remove reactive basaltic glass and olivine. This alteration slows the BET surface area-normalized Si release rates from the rocks by one to two orders of magnitude. Although some of this decrease in rates can be attributed to the formation of less reactive high-surface-area minerals during alteration, the slowing of these rates is also evident in natural systems (c.f. Gislason et al., 1996).
- Once the rapidly reactive phases are removed from the fresh basalt, surface area normalized Si release rates remain close to constant.
- A preferential release of Ca and Mg is observed during the first days of reaction for all the altered basalts. A long-term preferential release of these elements is observed for the studied hydrothermally altered basalts containing secondary phases such as zeolites and epidote. This preferential release of divalent cations, and the associated increase in fluid pH could favor the carbonation of altered basaltic rocks.

6. Acknowledgments

The authors are particularly grateful to Iwona Galeczka for her help in sampling during COVID lockdowns with the valuable advice of Birgir Vilhelm Óskarsson. They also thank Sigurdur R. Gislason for coordinating access to the IRDP core. The authors acknowledge the valuable insights and support from Chiara Marieni, Giuseppe Saldi, Carole Causserand, Alain Castillo, and Pascal Gisquet. This work has been carried out within the European projects CarbFix2 and GECO that have received funding from the European Union's Horizon 2020 research and innovation program under grant agreements # 764760 and # 818169, respectively.

7. Appendix A: Supplementary material

The supplementary material to this article contains: the chemical composition of all the rock samples used in this study, the mineralogy of all the samples used in the study, the chemical composition of the amorphous phase in selected samples, the temporal evolution of the pH, the fluid volume present in the reactor, the elemental concentrations for Al, Ca, Fe, Mg, and Si in batch experiments, the calculated saturation indices for all possible mineral phases based on fluid chemistry at the end of the experiment, the BET and geometric surface areas normalized release rates calculated using equation (3), the calculated Si release rates at pH 4 using the fitting method, the temporal evolution of the pH, the elemental concentrations for Al, Ca, Fe, Mg, and Si in mixed flow experiments, the last measured Ca/Si and Mg/Si values for all the rocks, compared to the initial Ca/Si and Mg/Si ratios of the rocks, and the evolution of the amorphous phase content of the surface basalt samples as a function of age.

8. References

Alt J. C. and Teagle D. A. H. (1999) The uptake of carbon during alteration of ocean crust. *Geochim. Cosmochim. Acta* **63**, 1527–1535.

Baker H. M., Massadeh A. M. and Younes H. A. (2009) Natural Jordanian zeolite: Removal of heavy metal ions from water samples using column and batch methods. *Environ. Monit. Assess.* **157**, 319–330.

Berner, R.A., (1999) A new look at the long-term carbon cycle, *GSA Today* **9**, 11, 1-6.

Blum A. and Lasaga A. (1988) Role of surface speciation in the low-temperature dissolution of minerals. *Nature* **331**, 431–433.

Börker J., Hartmann J., Romero-Mujalli G. and Li G. (2019) Aging of basalt volcanic systems and decreasing CO_2 consumption by weathering. *Earth Surf. Dyn.* **7**, 191–197.

Brady P. V. (1991) The effect of silicate weathering on global temperature and atmospheric CO_2. *J. Geophys. Res.* **96**, 18,101-18,106.

Brady P. V. and Carroll S. A. (1994) Direct effects of CO_2 and temperature on silicate weathering: Possible implications for climate control. *Geochim. Cosmochim. Acta* **58**, 1853–1856.

Brantley S. L. (2008) Kinetics of Mineral Dissolution. In *Kinetics of Water-Rock Interaction* Springer New York, pp. 151–210.

Campbell J. S., Foteinis S., Furey V., Hawrot O., Pike D., Aeschlimann S., Maesano C. N., Reginato P. L., Goodwin D. R., Looger L. L., Boyden E. S. and Renforth P. (2022) Geochemical Negative Emissions Technologies : Part I . Front Clim. **4**:879133.

Chadwick O. A., Derry L. A., Vitousek P. M., Huebert B. J. and Hedin L. O. (1999) Changing sources of nutrients during four million years of ecosystem development. *Nature* **397**, 491–497.

Chukwuma J. S., Pullin H. and Renforth P. (2021) Assessing the carbon capture capacity of South Wales' legacy iron and steel slag. *Miner. Eng.* **173**, 107232.

Clark D. E., Gunnarsson I., Aradóttir E. S., Þ. Arnarson M., Þorgeirsson Þ. A., Sigurðardóttir S. S., Sigfússon B., Snæbjörnsdóttir S. Ó., Oelkers E. H. and Gíslason S. R. (2018) The chemistry and potential reactivity of the CO_2 -H_2S charged injected waters at the basaltic CarbFix2 site, Iceland. *Energy Procedia* **146**, 121–128.

Clark D. E., Oelkers E. H., Gunnarsson I., Sigfússon B., Snæbjörnsdóttir S., Aradóttir E. S. and Gíslason S. R. (2020) CarbFix2: CO_2 and H_2S mineralization during 3.5 years of continuous injection into basaltic rocks at more than 250 °C. *Geochim. Cosmochim. Acta* **279**, 45–66.

Colbourn G., Ridgwell A. and Lenton T. M. (2015) The time scale of the silicate weathering negative feedback on atmospheric CO_2. *Global Biogeochem. Cycles* **29**, 583–596.

Colman S. M. (1981) Rock-Weathering Rates as Functions of Time. *Quat. Res.* **15**, 250–264.

Courtillot V. E. and Renne P. R. (2003) On the ages of flood basalt events. *Comptes Rendus - Geosci.* **335**, 113–140.

Cox G. M., Halverson G. P., Stevenson R. K., Vokaty M., Poirier A., Kunzmann M., Li Z. X., Denyszyn S. W., Strauss J. V. and Macdonald F. A. (2016) Continental flood basalt weathering as a trigger for Neoproterozoic Snowball Earth. *Earth Planet. Sci. Lett.* **446**, 89–99.

Delerce, S., Bénézeth, P., Schott, J., Oelkers, E.H., 2023. The dissolution rates of naturally altered basalts at pH 3 and 120 °C: Implications for the in-situ mineralization of CO_2 injected into the subsurface. Chem. Geol. **621**, 121353.

Deng K., Yang S. and Guo Y. (2022) A global temperature control of silicate weathering intensity. *Nat. Commun.* **13**, 1–10.

Dessert C., Dupré B., Gaillardet J., François L. M. and Allègre C. J. (2003) Basalt weathering laws and the impact of basalt weathering on the global carbon cycle. *Chem. Geol.* **202**, 257–273.

Eiriksdottir, E.S., Louvat, P., Gislason, S.R., Óskarsson, N., Hardardóttir, J., (2008) Temporal variation of chemical and mechanical weathering in NE Iceland: Evaluation of a steady-state model of erosion. Earth Planet. Sci. Lett. **272**, 78–88.

Eggleton R.A., Foudoulis, C. and Varkevisser, D. (1987) Weathering of basalt: Changes in rock

chemistry and mineralogy. *Clays Clay Min*.. **35,** 161-169.

Falkowski P., Scholes R. J., Boyle E., Canadell J., Canfield D., Elser J., Gruber N., Hibbard K., Hogberg P., Linder S., Mackenzie F. T., Moore B., Pedersen T., Rosental Y., Seitzinger S., Smetacek V. and Steffen W. (2000) The global carbon cycle: A test of our knowledge of earth as a system. *Science* **290**, 291–296.

Fridleifsson I. B., Gibson I. L., Hall J. M., Johnson H. P., Chistensen N. I., Schmincke H.-U. and Schönharting G. (1982) The Iceland Research Drilling Project. *J. Geophys. Res.* **87**, 6359–6361.

Gadikota G. (2021) Carbon mineralization pathways for carbon capture, storage and utilization. *Commun. Chem.* **4**, 1–5.

Gadikota G., Matter J., Kelemen P., Brady P. V. and Park A. H. A. (2020) Elucidating the differences in the carbon mineralization behaviors of calcium and magnesium bearing alumino-silicates and magnesium silicates for CO_2 storage. *Fuel* **277**, 117900.

Galeczka I., Oelkers E. H. and Gislason S. R. (2018) The effect of the 2014-15 Bárðarbunga volcanic eruption on chemical denudation rates and the CO_2 budget. *Energy Procedia* **146**, 53–58.

Gislason S. R., Arnorsson S. and Armannsson H. (1996) Chemical weathering of basalt in Southwest Iceland: effects of runoff, age of rocks and vegetative/glacial cover. *Am. J. Sci.* **296**, 837–907.

Gislason S. R., Oelkers E. H., Eiriksdottir E. S., Kardjilov M. I., Gisladottir G., Sigfusson B., Snorrason A., Elefsen S., Hardardottir J., Torssander P. and Oskarsson N. (2009) Direct evidence of the feedback between climate and weathering. *Earth Planet. Sci. Lett.* **277**, 213–222.

Gudbrandsson S., Wolff-Boenisch D., Gislason S. R. and Oelkers E. H. (2011) An experimental study of crystalline basalt dissolution from 2≤pH≤11 and temperatures from 5 to 75°C. *Geochim. Cosmochim. Acta* **75**, 5496–5509.

Guidry M. W. and Mackenzie F. T. (2003) Experimental study of igneous and sedimentary apatite dissolution: Control of pH, distance from equilibrium, and temperature on dissolution rates. *Geochim. Cosmochim. Acta* **67**, 2949–2963.

Harouiya N., Chaïrat C., Köhler S. J., Gout R. and Oelkers E. H. (2007) The dissolution kinetics and apparent solubility of natural apatite in closed reactors at temperatures from 5 to 50 °C and pH from 1 to 6. **244**, 554–568.

Harrison A. L., Power I. M. and Dipple G. M. (2013) Accelerated carbonation of brucite in mine tailings for carbon sequestration. *Environ. Sci. Technol.* **47**, 126–134.

Heřmanská M., Voigt M. J., Marieni C., Declercq J. and Oelkers E. H. (2022) A comprehensive and internally consistent mineral dissolution rate database: Part I: Primary silicate minerals and glasses. *Chem. Geol.* **597,** 120807.

Hodson M. E. and Langan S. J. (1999) The influence of soil age on calculated mineral weathering rates. *Appl. Geochemistry* **14**, 387–394.

Humphris, S.E. and Thompson, G. Hydrothermal alteration of oceanic basalts by seawater. *Geocheim. Cosmochim. Acta* **42,** 107-125.

Jercinovic M. J., Keil K., Smith M. R. and Schmitt R. A. (1990) Alteration of basaltic glasses from north-central British Columbia, Canada. *Geochim. Cosmochim. Acta* **54**, 2679–2696.

Kelemen P. B., Aines R., Bennett E., Benson S. M., Carter E., Coggon J. A., de Obeso J. C., Evans O., Gadikota G., Dipple G. M., Godard M., Harris M., Higgins J. A., Johnson K. T. M., Kourim F., Lafay

795 R., Lambart S., Manning C. E., Matter J. M., Michibayashi K., Morishita T., Noël J., Okazaki K.,
796 Renforth P., Robinson B., Savage H., Skarbek R., Spiegelman M. W., Takazawa E., Teagle D., Urai
797 J. L. and Wilcox J. (2018) *In situ* carbon mineralization in ultramafic rocks: Natural processes and
798 possible engineered methods. *Energy Procedia* **146**, 92–102.

799 Kelemen P. B., Matter J., Streit E. E., Rudge J. F., Curry W. B. and Blusztajn J. (2011) Rates and
800 Mechanisms of Mineral Carbonation in Peridotite: Natural Processes and Recipes for Enhanced,
801 *in situ* CO_2 Capture and Storage. *Annu. Rev. Earth Planet. Sci.* **39**, 545–576.

802 Kelemen P., Benson S. M., Pilorgé H., Psarras P. and Wilcox J. (2019) An Overview of the Status and
803 Challenges of CO_2 Storage in Minerals and Geological Formations. *Front. Clim.* **1**, 1–20.

804 Kennedy M. J., Chadwick O. A., Vitousek P. M., Derry L. A. and Hendricks D. M. (1998) Changing
805 sources of base cations during ecosystem development, Hawaiian Islands. *Geology* **26**, 1015–
806 1018.

807 Knapp W. J. and Tipper E. T. (2022) The efficacy of enhancing carbonate weathering for carbon
808 dioxide sequestration. *Front. Clim.* **4**, 928215.

809 Kristmannsdottir, H. (1979) Alteration of basaltic rocks by hydrothermal activity at 100 to 300 ^{o}C.
810 *Dev. Sedimentology* **27**, 359-367.

811 Lewis A. L., Sarkar B., Wade P., Kemp S. J., Hodson M. E., Taylor L. L., Yeong K. L., Davies K., Nelson P.
812 N., Bird M. I., Kantola I. B., Masters M. D., DeLucia E., Leake J. R., Banwart S. A. and Beerling D. J.
813 (2021) Effects of mineralogy, chemistry and physical properties of basalts on carbon capture
814 potential and plant-nutrient element release via enhanced weathering. *Appl. Geochemistry* **132**,
815 105023.

816 Li Gaojun, Hartmann J., Derry L. A., West A. J., You C. F., Long X., Zhan T., Li L., Li Gen, Qiu W., Li T., Liu
817 L., Chen Y., Ji J., Zhao L. and Chen J. (2016) Temperature dependence of basalt weathering.
818 *Earth Planet. Sci. Lett.* **443**, 59–69.

819 Liu D., Agarwal R., Li Y. and Yang S. (2019) Reactive transport modeling of mineral carbonation in
820 unaltered and altered basalts during CO_2 sequestration. *Int. J. Greenh. Gas Control* **85**, 109–120.

821 Louvat P. and Allègre C. J. (1997) Present denudation rates on the island of Réunion determined by
822 river geochemistry: Basalt weathering and mass budget between chemical and mechanical
823 erosions. *Geochim. Cosmochim. Acta* **61**, 3645–3669.

824 Louvat P. and Allègre C. J. (1998) Riverine erosion rates on Sao Miguel volcanic island, Azores
825 archipelago. *USDA For. Serv. - Gen. Tech. Rep. RMRS-GTR* **148**, 177–200.

826 Maesano C. N., Campbell J. S., Foteinis S., Furey V., Hawrot O., Pike D., Aeschlimann S., Reginato P. L.,
827 Goodwin D. R., Looger L. L., Boyden E. S. and Renforth P. (2022) Geochemical Negative
828 Emissions Technologies: Part II. Roadmap. *Front. Clim.* **4**, 945332.

829 Malmström M., Banwart S., Lewenhagen J., Duro L. and Bruno J. (1996) The dissolution of biotite and
830 chlorite at 25°C in the near-neutral pH region. *J. Contam. Hydrol.* **21**, 201–213.

831 Marieni C., Matter J. M. and Teagle D. A. H. (2020) Experimental study on mafic rock dissolution rates
832 within CO_2-seawater-rock systems. *Geochim. Cosmochim. Acta* **272**, 259–275.

833 Marieni C. and Oelkers E. (2018) Carbon sequestration potential of altered mafic reservoirs. *Energy*
834 *Procedia* **146**, 68–73.

835 Marieni C., Voigt M. J. and Oelkers E. H. (2021) Experimental study of epidote dissolution rates from
836 pH 2 to 11 and temperatures from 25 to 200 °C. *Geochim. Cosmochim. Acta* **294**, 70–88.

Matter J. M. and Kelemen P. B. (2009) Permanent storage of carbon dioxide in geological reservoirs by mineral carbonation. *Nat. Geosci.* **2**, 837–841.

Matter J. M., Stute M., Snæbjörnsdóttir S. Ó., Oelkers E. H., Gislason S. R., Aradottir E., Sigfusson B., Gunnarsson I., Sigurdardottir H., Gunnlaugsson E., Axelsson G., Alfredsson H. A., Wolff-Boenisch D., Mesfin K., Taya D. F. de la R., Hall J., Dideriksen K. and Broecker W. S. (2016) Rapid carbon mineralization for permanent disposal of anthropogenic carbon dioxide emissions. *Science* **352**, 1312 –1314.

McGrail B. P., Schaef H. T., Ho A. M., Chien Y. J., Dooley J. J. and Davidson C. L. (2006) Potential for carbon dioxide sequestration in flood basalts. *J. Geophys. Res. Solid Earth* **111**, 1–13.

McGrail B. P., Schaef H. T., Spane F. A., Horner J. A., Owen A. T., Cliff J. B., Qafoku O., Thompson C. J. and Sullivan E. C. (2017) Wallula Basalt Pilot Demonstration Project: Post-injection Results and Conclusions. *Energy Procedia* **114**, 5783–5790.

Mehegan J. M., Robinson P. T. and Delaney J. R. (1982) Secondary mineralization and hydrothermal alteration in the Reydarfjordur drill core, eastern Iceland. *J. Geophys. Res.* **87**, 6511–6524.

Morgan, B., Lahav, O., 2007. The effect of pH on the kinetics of spontaneous Fe(II) oxidation by O_2 in aqueous solution - basic principles and a simple heuristic description. *Chemosphere* **68**, 2080–2084.

Murray R. S. and Quirk J. P. (1990) Surface Area of Clays. *Langmuir* **6**, 122–124.

Nesbitt H. W. and Wilson R. E. (1992) Recent chemical weathering of basalts. *Am. J. Sci.* **292**, 740–777.

Oelkers E. H. (2001) General kinetic description of multioxide silicate mineral and glass dissolution. *Geochim. Cosmochim. Acta* **65**, 3703–3719.

Oelkers, E.H., Arkadakskiy, S., Afifi, A.M., Hoteit, H., Richards, M., Fedorik, J., Delaunay, A., Torres, J.E., Ahmed, Z.T., Kunnummal, N., Gislason, S.R., 2022. The subsurface carbonation potential of basaltic rocks from the Jizan region of Southwest Saudi Arabia. *Int. J. Greenh. Gas Control* **120**, 103772.

Oelkers, E.H., Butcher, R., Pogge von Strandmann, P.A.E., Schuessler, J.A., von Blanckenburg, F., Snæbjörnsdóttir, S.Ó., Mesfin, K., Aradóttir, E.S., Gunnarsson, I., Sigfússon, B., Gunnlaugsson, E., Matter, J.M., Stute, M., Gislason, S.R., 2019. Using stable Mg isotope signatures to assess the fate of magnesium during the in situ mineralisation of CO_2 and H_2S at the CarbFix site in SW-Iceland. *Geochim. Cosmochim. Acta* **245**, 542–555.

Oelkers E. H., Golubev S. V., Chairat C., Pokrovsky O. S. and Schott J. (2009) The surface chemistry of multi-oxide silicates. *Geochim. Cosmochim. Acta* **73**, 4617–4634.

Oelkers E. H., Schott J. and Devidal J. L. (1994) The effect of aluminum, pH, and chemical affinity on the rates of aluminosilicate dissolution reactions. *Geochim. Cosmochim. Acta* **58**, 2011–2024.

Olsson J., Stipp S. L. S., Dalby K. N. and Gislason S. R. (2013) Rapid release of metal salts and nutrients from the 2011 Grimsvötn, Iceland volcanic ash. *Geochim. Cosmochim. Acta* **123**, 134–149.

Óskarsson B. V. and Riishuus M. S. (2013) The mode of emplacement of Neogene flood basalts in Eastern Iceland: Facies architecture and structure of the Hólmar and Grjótá olivine basalt groups. *J. Volcanol. Geotherm. Res.* **267**, 92–118.

Parkhurst D. L. and Appelo C. a. J. (2013) Description of Input and Examples for PHREEQC Version 3 — A Computer Program for Speciation , Batch-Reaction , One-Dimensional Transport , and Inverse

879 Geochemical Calculations. In *U.S. Geological Survey Techniques and Methods, book 6, Chapter*
880 *A43* pp. 6-43A.

881 Parnell J., Macleod K. and Hole M. J. (2014) Carbon dioxide drawdown by Devonian lavas. *Earth*
882 *Environ. Sci. Trans. R. Soc. Edinburgh* **105**, 1–8.

883 Parruzot B., Jollivet P., Rébiscoul D. and Gin S. (2015) Long-term alteration of basaltic glass:
884 Mechanisms and rates. *Geochim. Cosmochim. Acta* **154**, 28–48.

885 Penman D. E., Caves Rugenstein J. K., Ibarra D. E. and Winnick M. J. (2020) Silicate weathering as a
886 feedback and forcing in Earth's climate and carbon cycle. *Earth-Science Rev.* **209**, 103298.

887 Peuble S., Andreani M., Gouze P., Pollet-Villard M., Reynard B. and Van de Moortele B. (2018) Multi-
888 scale characterization of the incipient carbonation of peridotite. *Chem. Geol.* **476**, 150–160.

889 Philpotts A.R., Ague J.J. (2009) Principles of igneous and metamorphic petrology. Cambridge
890 University Press.

891 Power I. M., Dipple G. M., Bradshaw P. M. D. and Harrison A. L. (2020) Prospects for CO_2
892 mineralization and enhanced weathering of ultramafic mine tailings from the Baptiste nickel
893 deposit in British Columbia, Canada. *Int. J. Greenh. Gas Control* **94**, 102895.

894 Rad S., Rivé K., Vittecoq B., Cerdan O. and Allègre C. J. (2013) Chemical weathering and erosion rates
895 in the lesser antilles: An overview in guadeloupe, martinique and dominica. *J. South Am. Earth*
896 *Sci.* **45**, 331–344.

897 Ratouis T. M. P., Snæbjörnsdóttir S., Voigt M. J., Sigfússon B., Gunnarsson G., Aradóttir E. S. and
898 Hjörleifsdóttir V. (2022) Carbfix 2: A transport model of long-term CO_2 and H_2S injection into
899 basaltic rocks at Hellisheidi, SW-Iceland. *Int. J. Greenh. Gas Control* **114**.

900 Reeves, D. and Rothman, D.H. (2013) Age dependence of mineral dissolution and precipitation.
901 *Global Biogeochem Cycles* **27**, 906-919.

902 Renforth P., Pogge von Strandmann P. A. E. and Henderson G. M. (2015) The dissolution of olivine
903 added to soil: Implications for enhanced weathering. *Appl. Geochemistry* **61**, 109–118.

904 Rinder T. and von Hagke C. (2021) The influence of particle size on the potential of enhanced basalt
905 weathering for carbon dioxide removal - Insights from a regional assessment. *J. Clean. Prod.*
906 **315**, 128178.

907 Robinson, P.T., Hall, M., Christensen, N.I., Gibson, I.A.N.L., Schmincke, H., (1982a). The Iceland
908 Research Drilling Project: Synthesis of results and implications for the nature of Icelandic and
909 oceanic crust. *J. Geophys. Res.* **87**, 6657–6667.

910 Robinson P. T., Mehegan J., Gibson I. L. and Schmincke H. U. (1982b) Lithology and structure of the
911 volcanic sequence in eastern Iceland. *J. Geophys. Res.* **87**, 6429–6436.

912 Rogers K. L., Neuhoff P. S., Pedersen A. K. and Bird D. K. (2006) CO_2 metasomatism in a basalt-hosted
913 petroleum reservoir, Nuussuaq, West Greenland. *Lithos* **92**, 55–82.

914 Schott J., Pokrovsky O. S. and Oelkers E. H. (2009) The link between mineral dissolution/precipitation
915 kinetics and solution chemistry. *Rev. Mineral. Geochemistry* **70**, 207–258.

916 Seton M., Müller R. D., Zahirovic S., Williams S., Wright N. M., Cannon J., Whittaker J. M., Matthews
917 K. J. and McGirr R. (2020) A Global Data Set of Present-Day Oceanic Crustal Age and Seafloor
918 Spreading Parameters. *Geochemistry, Geophys. Geosystems* **21**, 1–15.

919 Shen J., Yin R., Zhang S., Algeo T. J., Bottjer D. J., Yu J., Xu G., Penman D., Wang Y., Li L., Shi X.,

Planavsky N. J., Feng Q. and Xie S. (2022) Intensified continental chemical weathering and carbon-cycle perturbations linked to volcanism during the Triassic–Jurassic transition. *Nat. Commun.* **13**, 1–10.

Singer, P.C., Stumm, W., 1970. Acidic Mine Drainage: The Rate-Determining Step. *Science* **167**, 1121–1123.

Snæbjörnsdóttir S. Ó., Oelkers E. H., Mesfin K., Aradóttir E. S., Dideriksen K., Gunnarsson I., Gunnlaugsson E., Matter J. M., Stute M. and Gislason S. R. (2017) The chemistry and saturation states of subsurface fluids during the *in situ* mineralisation of CO_2 and H_2S at the CarbFix site in SW-Iceland. *Int. J. Greenh. Gas Control* **58**, 87–102.

Snæbjörnsdóttir, S.Ó., Sigfússon, B., Marieni, C., Goldberg, D., Gislason, S.R., Oelkers, E.H., 2020. Carbon dioxide storage through mineral carbonation. *Nat. Rev. Earth Environ.* **1**, 90–102.

Snæbjörnsdóttir S. Ó., Wiese F., Fridriksson T., Ármansson H., Einarsson G. M. and Gislason S. R. (2014) CO_2 storage potential of basaltic rocks in Iceland and the oceanic Ridges. *Energy Procedia* **63**, 4585–4600.

Stefánsson A. and Gíslason S. R. (2001) Chemical weathering of basalts, southwest Iceland: Effect of rock crystallinity and secondary minerals on chemical fluxes to the ocean. *Am. J. Sci.* **301**, 513–556.

Stroncik N. A. and Schmincke H. U. (2002) Palagonite - A review. *Int. J. Earth Sci.* **91**, 680–697.

Stubbs A. R., Paulo C., Power I. M., Wang B., Zeyen N. and Wilson S. A. (2022) Direct measurement of CO_2 drawdown in mine wastes and rock powders: Implications for enhanced rock weathering. *Int. J. Greenh. Gas Control* **113**, 103554.

Taylor A. and Blum J. D. (1995) Relation between soil age and silicate weathering rates determined from the chemical evolution of a glacial chronosequence. *Geology* **23**, 979–982.

Tester J. W., Worley W. G., Robinson B. A., Grigsby C. O. and Feerer J. L. (1994) Correlating quartz dissolution kinetics in pure water from 25 to 625°C. *Geochim. Cosmochim. Acta* **58**, 2407–2420.

Valdés M. G., Pérez-Cordoves A. I. and Díaz-García M. E. (2006) Zeolites and zeolite-based materials in analytical chemistry. *Trends Anal. Chem.* **25**, 24–30.

Voigt M., Marieni C., Clark D. E., Gíslason S. R. and Oelkers E. H. (2018) Evaluation and refinement of thermodynamic databases for mineral carbonation. *Energy Procedia* **146**, 81–91.

Walker G. P. L. (1958) Geology of the reydarfjördur area, Eastern Iceland. *Q. J. Geol. Soc. London* **114**, 367–391.

Walker G. P. L. (1963) The Breiddalur central volcano, eastern Iceland. *Q. J. Geol. Soc. London* **119**, 29–63.

Walker J. C. G., Hays P. B. and Kasting J. F. (1981) A negative feedback mechanismfor the long-term stabilization of earth's surface temperature. *J. Geophys. Res.* **86**, 9776–9782.

White A. F., Blum A. E., Schulz M. S., Bullen T. D., Harden J. W. and Peterson M. L. (1996) Chemical Weathering of a Soil Chronosequence on Granite Alluvium I. Reaction Rates Based on Changes in Soil Mineralogy. *Geochim. Cosmochim. Acta* **60**, 2533–2550.

White A. F. and Brantley S. L. (2003) The effect of time on the weathering of silicate minerals: Why do weathering rates differ in the laboratory and field? *Chem. Geol.* **202**, 479–506.

White S. K., Spane F. A., Schaef H. T., Miller Q. R. S., White M. D., Horner J. A. and McGrail B. P. (2020)

961 Quantification of CO_2 Mineralization at the Wallula Basalt Pilot Project. *Environ. Sci. Technol.*

962 Xiong W., Wells R. K., Horner J. A., Schaef H. T., Skemer P. A. and Giammar D. E. (2018) CO_2 Mineral
963 Sequestration in Naturally Porous Basalt. *Environ. Sci. Technol. Lett.* **5**, 142–147.

964 Yates D. J. C. (1968) Studies on the surface area of zeolites, as determined by physical adsorption and
965 X-ray crystallography. *Can. J. Chem.* **46**, 1695–1701.

966 Zhang R., Zhang X., Guy B., Hu S., De Ligny D. and Moutte J. (2013) Experimental study of dissolution
967 rates of hedenbergitic clinopyroxene at high temperatures: dissolution in water from 25 °C to
968 374 °C. *Eur. J. Mineral.* **25**, 353–372.

969 Zhen-Wu B. Y., Dideriksen K., Olsson J., Raahauge P. J., Stipp S. L. S. and Oelkers E. H. (2016)
970 Experimental determination of barite dissolution and precipitation rates as a function of
971 temperature and aqueous fluid composition. *Geochim. Cosmochim. Acta* **194**, 193–210.

972 Zhou Z., Fyfe W. S., Tazaki K. and Van Der Gaast S. J. (1992) The structural characteristics of
973 palagonite from DSDP Site 335. *Can. Mineral.* **30**, 75–81.

Experimental determination of the reactivity of basalts as a function of their degree of alteration

Sylvain Delerce[a*], Matylda Heřmanská[a], Pascale Bénézeth[a], Jacques Schott[a], Eric H. Oelkers[b]

[a] *Géosciences Environnement Toulouse, GET – CNRS – CNES – IRD – OMP – Université de Toulouse, 14 Avenue Edouard Belin, 31400 Toulouse, France*

[b] *Institute of Earth Sciences, University of Iceland, Sæmundargata 2, 102 Reykjavík, Iceland*

Abstract

The element release rates from naturally altered basalts were measured in batch experiments at 27 °C, and in mixed-flow experiments at 25 °C in reactive fluids initially consisting of pH 3 or 4 aqueous solutions. The basalts reacted in this study consist of 1) surface weathered basalts ranging in age up to 13 million years, and 2) hydrothermally altered basalts from zeolite to actinolite alteration zones (temperatures of ~ 50 to 300 °C). The *in situ* pH in the batch experiments increased over time with the final pH of the fluids ranging from to 4 to 8. Most experiments exhibited a preferential release of Ca and Mg compared to Si from the dissolving basalts, both initially and over the long-term. This behavior is attributed to the combination of an initial rapid cation-proton exchange reaction and the relatively fast dissolution rates of Ca-bearing minerals. The BET surface area normalized Si release rates for all of the altered basalts are within one order of magnitude of each other, and from one to two orders of magnitude lower than corresponding rates from fresh basaltic glass and fresh crystalline basalts. This is interpreted to stem from 1) the fast removal of reactive basaltic glass and olivine from fresh basalts during the natural alteration of the rocks, 2) the similarity of the dissolution rates of the remaining albitic plagioclase, pyroxenes, epidote, and zeolites, and 3) the high surface areas of some less reactive secondary minerals such as clays. Overall, the results suggest that altered basalts will be effective in consuming CO_2 during both natural and engineered processes, though at a somewhat slower rate than unaltered basalts.

Keywords: basalt, alteration, mineralization, CO_2 storage, weathering

1. Introduction

The weathering of basalts on the Earth's surface and the ocean floor plays a critical role in the global carbon cycle. It proceeds through the dissolution of atmospheric CO_2 into aqueous solutions forming a weak acid. This slightly acidic solution dissolves basalts, which both increases the pH and releases divalent cations, notably Ca^{2+} and Mg^{2+}, to the fluid phase (Walker et al., 1981; Berner, 1999; Dessert et al., 2003). The released divalent metal cations combine with bicarbonate ions to form stable carbonate minerals. The weathering rate of basalts is temperature and runoff dependent (Brady and Carroll, 1994; Stefánsson and Gíslason, 2001; Gislason et al., 2009; Li et al., 2016; Deng et al., 2022). This creates a feedback between atmospheric CO_2, global temperature and the CO_2 drawdown capacity caused by silicate weathering. This feedback has constrained Earth's temperature variations over geologic timescales (Brady, 1991; Falkowski et al., 2000; Colbourn et al., 2015; Penman et al., 2020). Numerous studies have shown that fresh basalts are particularly efficient at lowering atmospheric CO_2 concentrations through Earth surface weathering right after major volcanic events (Louvat and Allègre, 1997, 1998; Rad et al., 2013; Li et al., 2016; Galeczka et al., 2018; Liu et al., 2019). It has also been suggested that the weathering rates of silicate rocks decrease as they are altered (Colman, 1981; Taylor and Blum, 1995; White et al., 1996; Kennedy et al., 1998; Chadwick et al., 1999; Hodson and Langan, 1999; White and Brantley, 2003), lowering their CO_2 drawdown potential over time (Börker et al., 2019).

Similar processes have been observed in the subsurface, notably in geothermal systems where basalt (Alt and Teagle, 1999; Rogers et al., 2006~~; Weise et al., 2008~~) and peridotite dissolution (Kelemen et al., 2011, 2018; Peuble et al., 2018) can provoke the CO_2 mineralization. This process has attracted interest as a means to store CO_2 in the subsurface (Matter and Kelemen, 2009; Matter et al., 2016; McGrail et al., 2017; Kelemen et al., 2019; Snæbjörnsdóttir et al., 2020). Efforts are currently under development to optimize this process, either at Earth surface conditions by enhanced weathering (Harrison et al., 2013; Renforth et al., 2015; Power et al., 2020; Chukwuma et al., 2021; Lewis et al., 2021; Rinder and von Hagke, 2021; ~~Romaniello et al., 2021;~~ Knapp and Tipper, 2022; Stubbs et al., 2022) or in the subsurface (Oelkers et al., 2018, 2022; Xiong et al., 2018; Gadikota et al., 2020; White et al., 2020; Gadikota, 2021; Campbell et al., 2022; Maesano et al., 2022) by injecting

CO_2 captured from either industrial sites or directly from the atmosphere. The results obtained by the CarbFix project in Iceland and the Wallula project in the USA demonstrated that it is possible to fix CO_2 through its mineralization in subsurface reservoirs containing fresh or mildly altered basalts in a matter of years (Matter et al., 2016; McGrail et al., 2017; Clark et al., 2020; Ratouis et al., 2022). The degree to which CO_2 mineralization can be efficient in more altered basaltic rocks is currently unclear. Nevertheless, altered basalts are more available on Earth's surface than fresh basalts or other young mafic rocks, which are primarily limited to active volcanic systems and rift zones (Courtillot and Renne, 2003; Seton et al., 2020). It is therefore necessary to investigate in detail the degree to which mineral carbon storage may be possible and effective in altered basaltic rocks.

To date there has been relatively few studies of the reactivity of altered basaltic rocks and their ability to mineralize CO_2. Marieni and Oelkers (2018) compared the dissolution rates of primary and secondary basaltic minerals and concluded that the carbonation rates of altered basalts are likely 0.5 to 3 orders of magnitude slower than that of fresh basaltic glass. Xiong et al. (2017) exposed fractured cores of Columbia River Basalt and of serpentinized basalt to CO_2 charged water at 100 and 150 °C and found significant differences in the resulting carbonation products after 40 weeks of reaction. Taking account of these results, Liu et al. (2019) suggested that the slower dissolution rates of altered basalts compared to fresh basalts could be advantageous to better maintain fluid circulation in the subsurface reservoirs.

The objective of this study is to quantify the reactivity of altered basalts. Towards this goal we have measured the element release rates of 22 different basalts representing both surface-weathered and hydrothermally altered basalts, as a function of their age and degree of alteration in batch reactors at 27 °C. An additional four mixed-flow experiments were performed to validate the batch experiment results. From the results obtained in this study we can (i) assess the potential for the subsurface carbonation of altered basalts, and (ii) illuminate the degree to which chemical weathering rates slow as basaltic rocks alter over time.

2. Material and methods

2.1. Sample preparation and characterization

Two suites of altered basalts have been collected and studied; one consisting of Earth surface weathered basalts of various ages and the other of hydrothermally altered basalts collected from the subsurface. These samples were selected to span the likely compositions to be targeted for Earth surface and subsurface mineral carbon storage.

2.1.1. Surface weathered basalts as a function of age

Surface basalt samples were collected from Eastern Iceland and have ages ranging from 9 to 13 Myr. The samples were collected from the Grjótá olivine basalt group (GOB), the Vindháls porphyritic group (VP), the Grænavatn porphyritic group (GRVP) and the Heiðarvatn olivine basalt group. The age, formation and composition of these basalts have been previously described by Óskarsson and Riishuus (2013), Walker (1958), Óskarsson et al. (2017), and Walker (1963) respectively. Younger basalt samples were originally collected by Eiriksdottir ~~(2016~~et al. (2008). These latter samples consist of suspended basaltic material collected from Eastern Iceland rivers. The ages of these suspended material samples, estimated from the average age of the bedrock in the river catchment areas, range from 0.2 to 2.1 Myr (Eiriksdottir~~, 2016~~ et al., 2008). Finally, volcanic ash collected during the 2011 Grímsvötn's volcanic eruption was also used to represent youngest basalt (Olsson et al., 2013).

2.1.2. Basalt hydrothermal alteration as a function of depth/temperature

Ten basalt samples were selected from a core originally retrieved in Eastern Iceland during the Iceland Research Drilling Project (IRDP). The two kilometer long core, drilled near Reyðarfjörður during the summer of 1978 (Fridleifsson et al., 1982; Robinson et al., 1982a) crossed a succession of lava flows with their corresponding flow tops and breccias (Mehegan et al., 1982; Robinson et al., 1982b). We selected samples from the brecciated flow tops, where the alteration is more pronounced (McGrail et al., 2006), rather than from the thick dense lava flows. Three additional samples were provided by CarbFix and taken from well HE-65 near the Hellisheiði powerplant (southeast Iceland). A summary of the samples is provided in Table 1 and the sampling locations are shown in Figure 1.

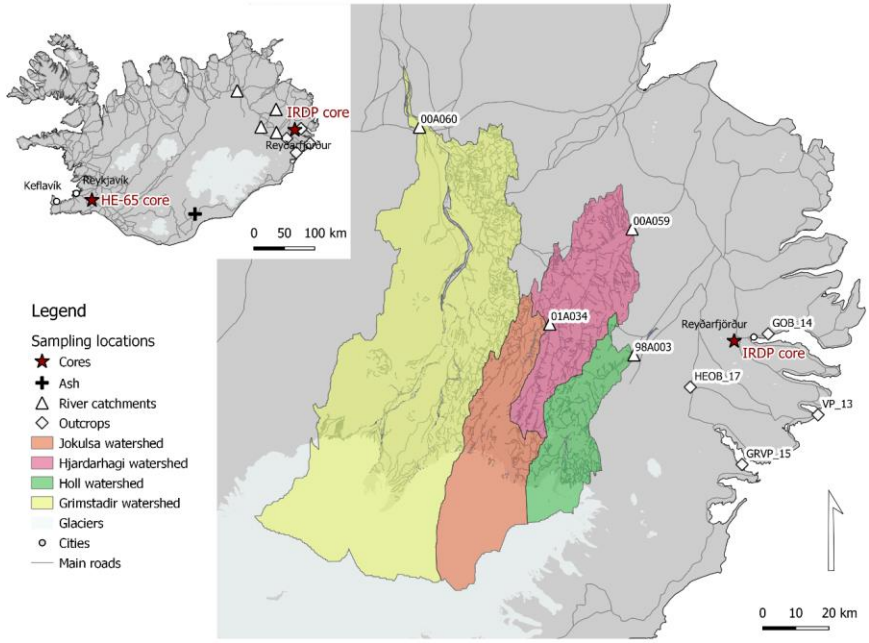

Figure 1 : Map showing the sampling locations of each altered basalt considered in this study. The colored areas represent the catchment area covered by each of the sampling points from which suspended material was collected.

2.2. Preparation of the solids

Core and outcrop samples were first cleaned to remove any evident foreign material. In cases where outer parts of the samples exhibited distinct differences from the bulk rock sample, they were removed using a diamond saw. The samples were cut and a representative part of each rock was selected to prepare 30 µm thick thin sections for microprobe analysis. The remaining rock sample was then crushed by hammer and subsequently ground using an agate vibrating-disc mill. The resulting powders were dry sieved to obtain the 40-150 µm size fraction with the exception of sample HE65_22 for which the 40-125 µm size fraction was collected. This final sample had a slightly different size fraction as it was originally prepared for a different study. To ensure that the results of our experiments are consistent with previously reported rates, the prepared size fractions were first cleaned to remove fine particles by gravitational settling using ultrapure deionized

137 water (DIW) and then further cleaned using an ultrasonic bath with DIW and then ethanol.
138 Depending on the sample, 5 to 20 cleaning cycles using DIW and gravitational setting and 5
139 to 10 cleaning cycles using the ultrasonic bath with DIW and ethanol were required to clean
140 the collected basalt powders. The grains were considered clean when the fluid phase was
141 clear to the eye after an ultrasonic cleaning cycle. The cleaned powders were finally oven
142 dried at 50 °C for two days. The suspended material samples collected from rivers and the
143 volcanic ash were dry sieved to remove particles larger than 630 µm, then used directly in
144 the experiments. SEM images of representative prepared powders before the experiments
145 are depicted in Figure 2a and b. Grains appear clean with no fine particles present. The size
146 of the grains corresponds to the selected size fraction.

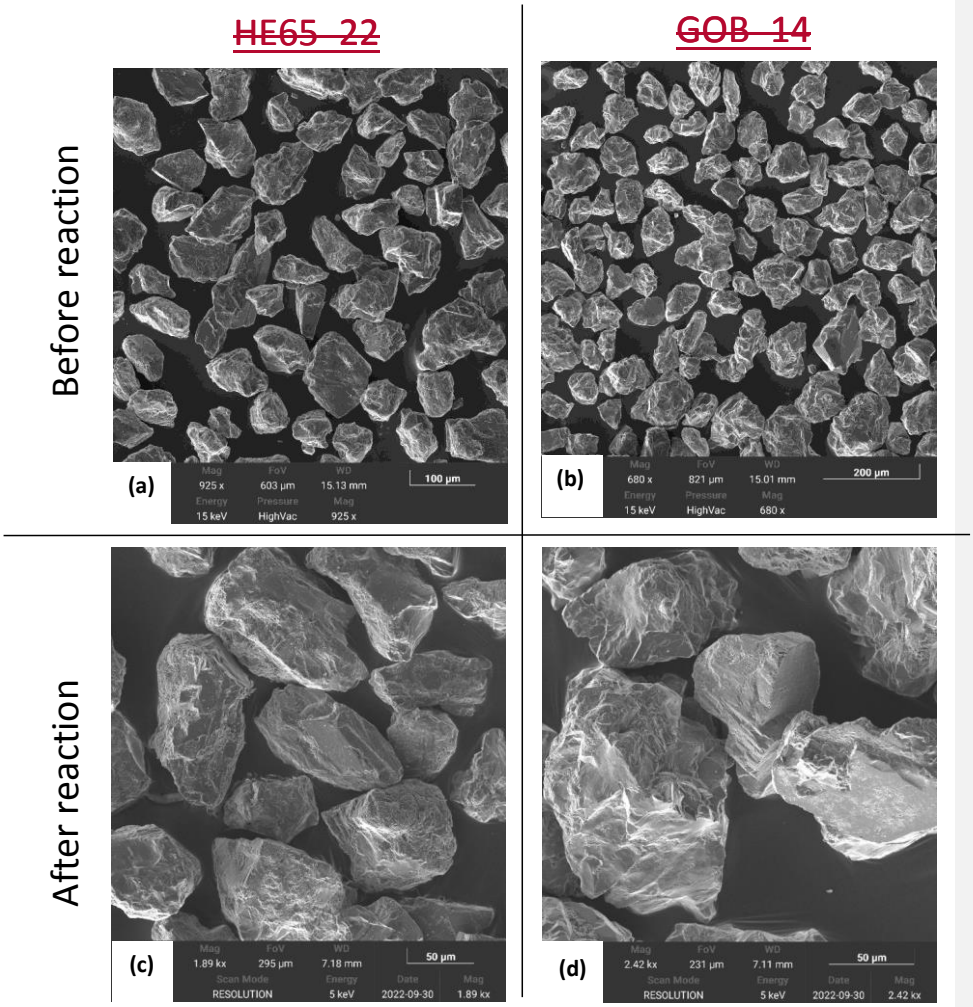

Figure 2 : SEM images of the prepared powders before experiment of (a) sample HE65_22 and (b) GOB_14, and after batch experiments of (c) sample HE65_22 and (d) GOB_14. Images of powders before the experiment are shown at a smaller scale to show the homogeneity of the grains and the quality of the preparation. Images of powders after reactions have a larger scale to make it possible to see potential precipitated phases.

2.3. Characterization of the prepared rock powders

The specific surface areas of the prepared rock powders before their use in the experiments were measured using the Brunauer-Emmet-Teller (BET) method with 11 adsorption points. The measurements were performed using the Quantachrome Autosorb-

1MP gas sorption system at Géosciences Environment Toulouse. The geometric surface areas of the prepared powders were also calculated using:

$$A_{geo} = \frac{6}{\rho * d_{eff}} \quad (1)$$

where ρ refers to the density of the rock and d_{eff} corresponds to the effective particle diameter (Tester et al., 1994). The density of the basalts considered in this study were not measured directly. Instead, we used the average density of basalt of 2.9 g cm^{-3} (Philpotts and Ague, 2009). The variation of sample mineral and elemental composition suggests the density of our solids should vary by no more than 10% from this value. The effective particle diameter, d_{eff} was calculated using (Tester et al., 1994):

$$d_{eff} = \frac{d_{max} - d_{min}}{\ln(\frac{d_{max}}{d_{min}})} \quad (2)$$

where d_{max} and d_{min} refer to the maximum and minimum diameter of the sieves used to prepare the powders. The geometric surface area could not be calculated for the volcanic ash or the river-suspended materials as these samples were naturally ground and the available mass of these samples was too low to measure their grain size distribution.

The bulk chemical compositions of the prepared rock powders were measured using X-Ray Fluorescence spectrometry (XRF) using a S2 Ranger Bruker spectrometer (GET, Toulouse, France). The measured compositions are reported in Table S1. The mineralogy of all solid samples was determined at Activation laboratories (Canada) using a Bruker D8 Endeavour diffractometer equipped with Cu X-ray source measuring at 40 kV and 40 mA on a range of 4 – 70° with a step size of 0.02°. The PDF4/Minerals ICDD database was used for mineral identification. The quantities of the crystalline mineral phases were determined by Rietveld refinement. The amounts of the crystalline minerals were recalculated based on the addition of a known percentage of corundum to the sample. The mass of amorphous and poorly crystalline material was estimated from the difference between the sum of the volume fractions of the identified crystalline phases and 100%. To further characterize the mineralogy of the samples, the composition of selected minerals was determined by microprobe analyses on a CAMECA SXFive electronic microprobe located at the Raimond Castaing micro characterization center in Toulouse.

2.4. Experimental methods

Dissolution experiments with all the prepared rock samples were performed in batch reactors. They were complemented with four mixed-flow experiments at pH 4, as described below.

2.4.1. Batch experiments

Batch dissolution experiments were run in parallel in closed 750 ml High-Density Polyethylene (HDPE) reactors immersed in a GFL 1083 thermoregulated shaking bath (Baker et al., 2009; Zhen-Wu et al., 2016). The temperature of the bath was maintained at 27±1 °C throughout all batch experiments. Before each experiment, three grams of the selected rock powder was placed into the reactor together with 300 ml of the initial reactive fluid. This water to rock ratio was chosen to allow sufficient reaction to characterize rates and sufficient fluid for sampling over two months while ensuring measurable elemental concentrations. The initial reactive fluid was made from Merck reagent grade HCl and NaCl diluted into ultrapure distilled water to obtain a pH 3 solution with an ionic strength of 0.01 mol kg^{-1}. This pH was chosen to be close to that of the CO_2 charged waters that are injected during subsurface mineral carbonation efforts (Gislason et al., 2010). The ionic strength was chosen to mimic the salinity observed in the CarbFix injection site (Snæbjörnsdóttir et al., 2017; Clark et al., 2018), and to facilitate the comparison of the results with previously reported experimental data. A schematic illustration of the experimental reactor system is shown in Figure 3.

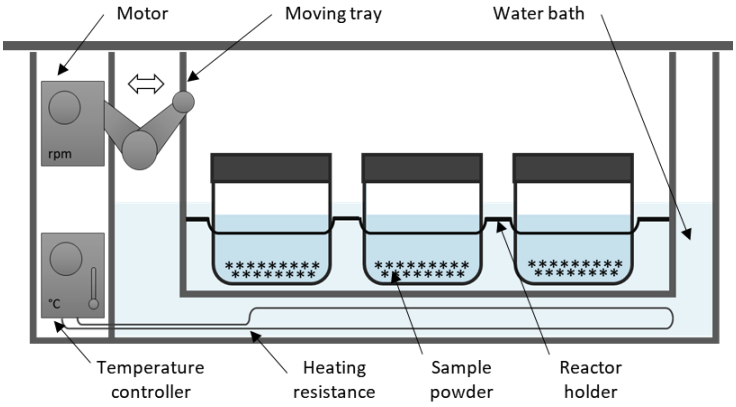

Figure 3 : Schematic illustration of the batch reactor system used in this study

Reactive fluids samples were collected regularly using syringes equipped with 0.45 µm Polytetrafluoroethylene (PTFE) filters to track the temporal evolution of the chemical composition of the fluids. The fluid samples for element concentration analysis were immediately acidified with Suprapur HNO_3 prior to storage in a refrigerator and further analysis.

2.4.2. Mixed flow reactor experiments

Four mixed-flow reactors experiments were run in closed 120 ml Savillex reactors. Each reactor had an inlet and an outlet port. The inlet port injected fluid into the bottom of the reactor, while the outlet port removed fluid from the top. Each reactor was equipped with a Teflon suspended stirring bar, allowing fluid-solid mixing and avoiding rock powder grinding. The reactors were positioned on a multi magnetic stirring plate so that all had identical stirring rates. A Gilson manifold pump was used to inject the inlet fluid into the reactors at approximately 0.15 ml min^{-1}. The inlet fluids were stored in polypropylene compressible bags before their injection into the reactors. The reactor outlets were equipped with 0.45 µm cellulose ester filters to prevent the powder from escaping the reactor. The complete reactor system was placed in a thermoregulated chamber set at 25±1 °C. A schematic illustration of the experimental reactor system is provided in Figure 4.

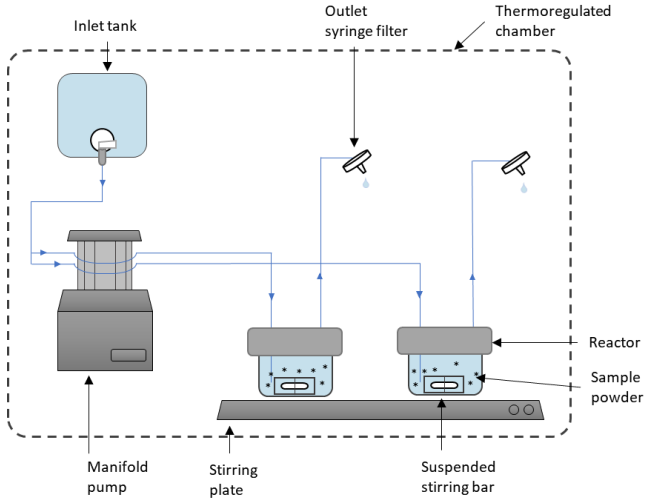

Figure 4 :Schematic illustration of the mixed-flow reactor system used in this study

242 Two to three grams of rock powder were initially placed in the reactors together with
243 sufficient inlet fluid to fill the reactors. This leads to fluid-rock ratio of 40 to 60; the lower
244 fluid to rock ratio was selected for sample B316S3 due to its lower surface area. The inlet
245 fluid was made from Merck reagent grade HCl and NaCl diluted into DIW to obtain a pH 4
246 solution with an ionic strength of 0.01 mol kg^{-1}. This fluid composition was selected to match
247 the conditions of the batch experiments. Once filled, the reactors were sealed and placed in
248 the thermostatically controlled chamber and the experiment started. The outlet fluids were
249 regularly sampled to measure pH and major elements. Some gas bubbles formed in some of
250 the reactors over time. These were removed manually to avoid their potential blocking of
251 the fluid outlet port.

252 At the end of the batch and mixed-flow experiments, the solids were recovered by
253 filtering the reactor's content using a 0.45 µm PTFE filter. The post-experimental powders
254 were air-dried for several days and stored for further analyses.

255 **2.5. Chemical Analyses**

256 The pH evolution of all sampled batch experiment reactive fluids was measured *in situ*
257 using an extended pH probe connected to a MetrOhm pH meter. The pH in the mixed-flow
258 experiments was measured immediately after sampling in non-acidified outlet fluid samples.
259 The electrodes were calibrated using NIST pH 4.01, 7.00 and 10.01 buffer solutions, and
260 replicate analyses of buffers and samples showed analytical accuracy of 0.03 pH units and
261 precision of ±0.02 pH units at room temperature.

262 Fluid samples were analyzed for Al, Ca, Fe, Mg, and Si concentrations using a Horiba
263 Ultima Expert Inductively Coupled Plasma Optical Emission Spectrometer (ICP-OES), with an
264 analytical accuracy of 3% and quantification limits of 10 ppb for Al and Fe, and 20 ppb for Ca,
265 Mg and Si. Potassium was not measured due to its low concentrations in the initial rock
266 samples and Na was not measured since it was present in the initial solution at 0.01 mol kg^{-1}
267 concentration.

268 **2.6. Calculation of fluid saturation index and elemental release rates**

269 Geochemical calculations in the present study were performed using PHREEQC V 3.6.2
270 (Parkhurst and Appelo, 2013) together with the CarbFix.dat V1.1 database (Voigt et al.,

2018). The saturation index of the reactive fluids with respect to primary and potential secondary phases were calculated based on the measured pH and element concentrations.

Element release rates from the batch experiments were calculated using two methods. The first consists of calculating the slope, dn_i/dt, of a least squares fit of the total mass of the i^{th} element released by the rock sample to the fluid as a function of time, as described in Marieni et al. (2021). The mass of each element released was calculated by multiplying the concentration of the element by the reactor fluid mass, taking into account the mass of fluid removed due to sampling over time. Because of large changes in reactive fluid pH and Si release rates, only concentrations measured in fluids collected after 12 days of the start of each experiment were used for calculating dn_i/dt. This allowed retrieval of approximately constant element release rates that were calculated using:

$$r_{i.j} = \frac{(\frac{dn_i}{dt})}{A_j\, m} \quad (3)$$

where (dn_i/dt) refers to the slope of the least square fit of the mass of the i^{th} element released from the rock as a function of time, A_j refers to the initial specific surface area of the solid before the experiment, j represents either BET or geometric surface area, and m designates the initial mass of the solid placed into the reactor. Initial surface areas were used for this calculation to be consistent with previously published rates and to avoid ambiguities associated with the contributions to surface areas of secondary minerals that might have formed during the experiments. The pH was not buffered during the batch experiments. Consequently, the rates obtained using equation (3) correspond to the reactive fluid pH from which the slope was obtained.

A second method used to quantify rates from the batch experiments took account of the change in pH over time following an approach proposed by Blum and Lasaga (1988), Guidry and Mackenzie (2003) Harouiya et al. (2007), and Zhen-Wu et al. (2016). In this approach the pH is first fit using:

$$pH = \alpha\, t^{1/\beta} + \gamma \quad (4)$$

where t designates the elapsed time since the beginning of the experiment and α, β and γ designate fit parameters. The proton activity generated using equation (4) and the measured Si concentrations in each reactor were then fit by numerical integration using:

$$r_{i,j} = dn_i/dt = (k_s/A_j\, m)\ a_{H^+}{}^{\varepsilon} \qquad (5)$$

where k_S refers to a rate constant, a_{H^+} denotes the proton activity and ε represents a reaction order. A_j refers to the initial specific surface area of the solid, j represents either BET or geometric surface area, and m designates the initial mass of the solid placed into the reactor. The parameters k_S and ε were estimated using a numerical solver so that the calculated rates best fit the measured reactor fluid compositions during the experiments. The resulting parameters can then be used together with equation (5) to estimate the element release rates at a chosen constant pH.

Steady-state elemental release rates in mixed-flow experiments were calculated using:

$$r_{i,j} = \frac{C_i\, Q}{A_j\, m} \qquad (6)$$

where $r_{i,j}$ refers to the release rate of the i^{th} element normalized to the surface area A_j, where j represents either BET or geometric surface area. C_i denotes the concentration of the i^{th} element in the outlet fluid, at steady state and Q designates the flow rate.

3. RESULTS

3.1. Mineral and chemical composition of the altered basalts

The mineralogical compositions of the collected surface weathered basalts are summarized in Figure 5 and further details are provided in Table S2. The mineralogy of these samples is dominated by primary phases. More than 88% of the mineral content of each of these rocks consists of plagioclase, pyroxenes, and an amorphous phase.

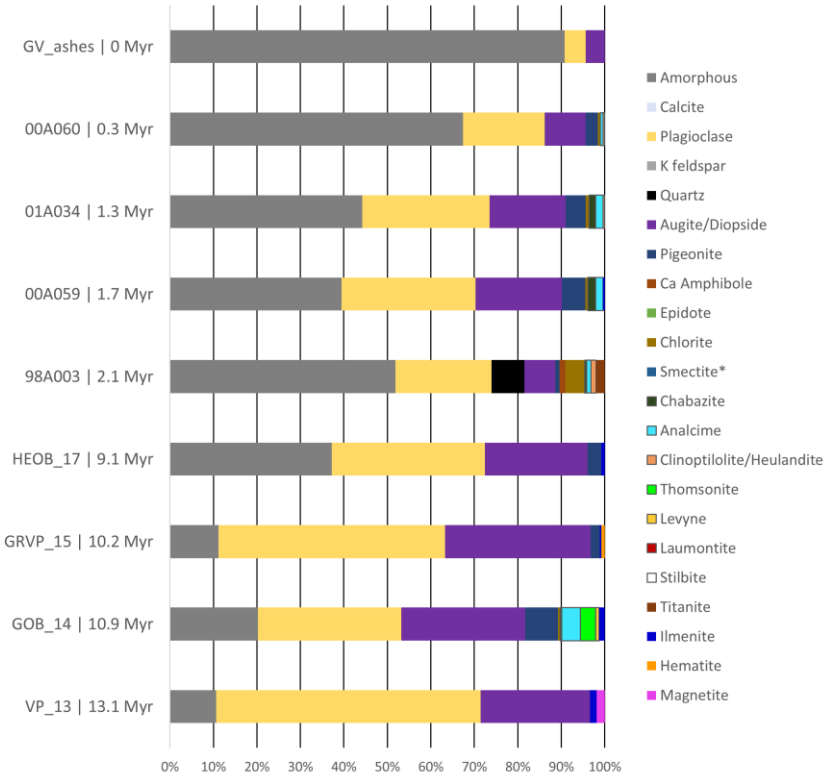

Figure 5 : Mineralogy of the surface samples as determined by XRD Rietveld refinement, in weight percent ordered based on the age of the samples.

Microprobe analyses revealed that the plagioclase in these rocks is mostly labradorite, with minor andesine and bytownite detected, and that the pyroxenes were of augitic composition. The secondary phases observed were primarily minor chlorites and zeolites. These secondary minerals may have been formed during the initial cooling of the molten basalts.

Two notable trends are evident in the composition of these rocks as a function of their age. First, as shown in Figure S1, the amorphous phase content of these rocks decreases substantially with age. The rocks less than 2.2 Myr old have amorphous contents ranging between 40 to 90%, while the older rocks have amorphous contents of less than 40%.

Second, the chemical composition of the amorphous phase contained in these samples exhibits distinct trends with rock age. These compositions, obtained from microprobe analyses, are listed in Table S3. The amorphous phase in the older rocks have lower Ca, Al, Na and K contents, but are relatively enriched in Fe compared to younger rocks and fresh basaltic glass. These observations suggest the continuous alteration of the original glass through palagonitization as described by Stroncik and Schmincke (2002) and Parruzot et al. (2015), where basaltic glass is replaced by a heterogeneous microcrystalline solid composed of different clays, zeolites, and oxides, or mixtures of these (Jercinovic et al., 1990; Zhou et al., 1992).

The mineralogical compositions of the collected hydrothermally altered basalt samples are depicted schematically in Figure 6.

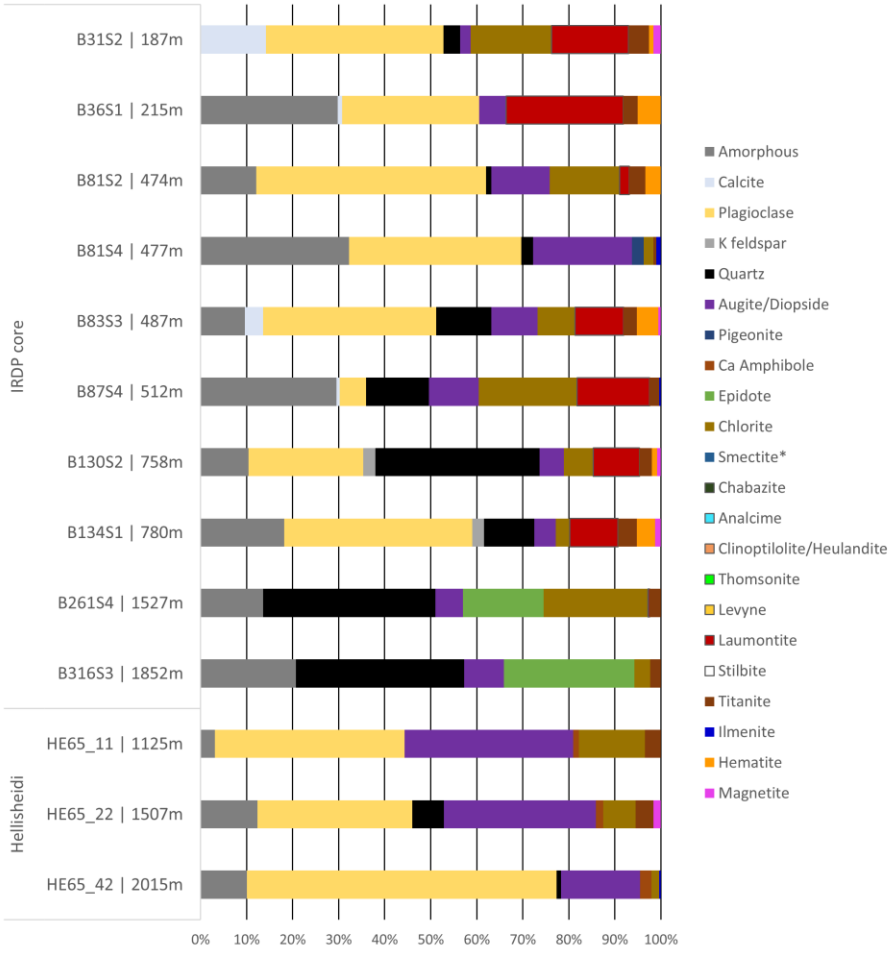

Figure 6: Mineralogy of the hydrothermally altered basalts considered in this study as determined by XRD Rietveld refinement, in weight percent. Samples are ordered by sample origin and increasing depth.

The alteration of samples collected from the IRDP core corresponds to the zeolite's facies with variable amounts of laumontite and chlorite. Only the two deepest samples from this core, B261S4 and B316S3, contain epidote. These deepest samples contain no plagioclase, but a significant amount of quartz. The plagioclases in the IRDP core samples were all of albitic composition and the pyroxenes had an augite composition. The alteration of the rocks sampled from the Hellisheiði core was less extensive, with primary phases better preserved. Plagioclase and pyroxenes are present in significant amounts in the

Hellisheiði samples, where andesine, labradorite, oligoclase, and albite were detected by microprobe. Pyroxenes were of augitic composition and some Ca-amphiboles were also present in small amounts. The amorphous phase content of all of the hydrothermally altered basalts varies between 0 and 30% with no consistent trend. Four samples from the shallower part of the IRDP core contain from 0.7 to 14.2 wt% calcite.

The chemical compositions of the amorphous phase of some of the hydrothermally altered basalts are shown in Table S3. The compositions of these amorphous phases are depleted in Ca, lower in Al and Si, and enriched in Fe compared to basaltic glass, possibly due to the palagonitization of the original basaltic glass (Stroncik and Schmincke, 2002; Parruzot et al., 2015).

The measured BET surface areas of all samples are reported in

Table 1 together with the corresponding calculated geometric surface areas. The BET specific surface areas of the rock powders used in the experiments varied from 0.3 to 28 $m^2 g^{-1}$. Part of this variation can be explained by sample preparation. Most rock samples were prepared at the CNRS laboratory in Toulouse in an identical manner, with the exception of the volcanic ash sample (GV_ash) and the four river suspended material samples (00A060, 01A034, 00A059, 98A003). These natural rock powders exhibited BET surface areas among the highest considered in this study (see

376 Table 1).

377

Table 1: BET and geometric surface areas of all the samples. NA stands for not available

		Sample	*Age (MYr) / **Depth (m)***	*Size fraction (µm)*	*BET surface area (m^2 g^{-1})*	*Geometric surface area (m^2 g^{-1})*
Surface weathered basalts	*Volcanic ash*	GV_ash	0	Raw <630	0.4	NA
	River suspended material	00A060	0.3	Raw <630	7.7	NA
		01A034	1.3	Raw <630	23.6	NA
		00A059	1.7	Raw <630	28.1	NA
		98A003	2.1	Raw <630	11.5	NA
	Surface outcrops	HEOB_17	9.1	40-150	0.4	0.0248
		GRVP_15	10.2	40-150	4.7	0.0248
		GOB_14	10.9	40-150	1.6	0.0248
		VP_13	13.1	40-150	5.0	0.0248
Hydrothermally altered basalts	*IRDP core*	B31S2	**187.3**	40-150	9.0	0.0248
		B36S1	**214.6**	40-150	4.5	0.0248
		B81S2	**473.9**	40-150	3.6	0.0248
		B81S4	**476.8**	40-150	2.7	0.0248
		B83S3	**487.1**	40-150	2.5	0.0248
		B87S4	**512.3**	40-150	4.2	0.0248
		B130S2	**758.4**	40-150	1.7	0.0248
		B134S1	**780.4**	40-150	2.3	0.0248
		B261S4	**1526.6**	40-150	1.5	0.0248
		B316S3	**1851.7**	40-150	0.4	0.0248
	Hellisheiði	HE65_11	**1125.3**	40-150	1.0	0.0248
		HE65_22	**1506.7**	40-125	2.0	0.0277
		HE65_42	**2014.6**	40-150	0.3	0.0248

3.2. Temporal evolution of the reactive fluid pH, elemental concentrations, and mineral saturation states

3.2.1. pH and elemental concentrations

The temporal evolution of the composition of reactive fluids in all batch experiments is provided in Table S4. The reactive fluid pH evolution of three representative experiments is provided in Figure 7.

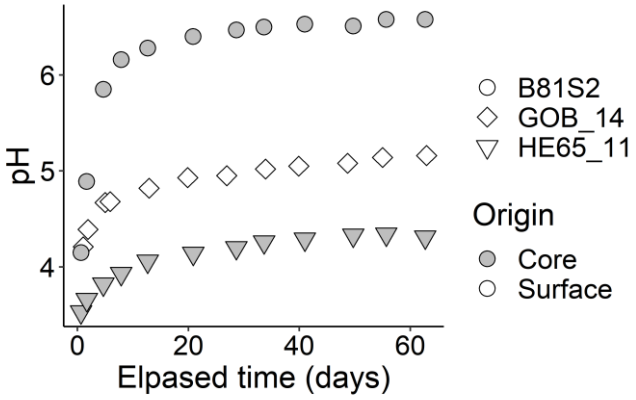

386

387 *Figure 7: Temporal evolution of the reactive fluid pH during three representative batch*
388 *experiments. The size of the uncertainties is smaller than the symbol size.*

389 The reactive fluid pH in all batch reactor experiments increases rapidly during the first
390 10 days. The highest final pH values, close to 8, were observed in experiments performed on
391 samples containing significant amounts of calcite in their original composition (see Table S4).

392 The temporal evolution of the dissolved Si, Ca, Mg, Al, and Fe concentrations during
393 three representative batch experiments are shown in Figure 8. The concentrations of Ca, Mg,
394 and Si increased in the fluids of all batch experiments over time. Al and Fe showed a distinct
395 behavior: Al concentrations decreased over time during most of the experiments and Fe
396 concentrations were below the detection limit in all experiments where the pH exceeded pH
397 5. These observations suggest the precipitation of Al and Fe-rich phases such as Al and Fe
398 oxy-hydroxides during the experiments.

399

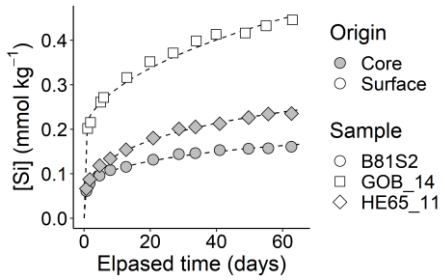

400

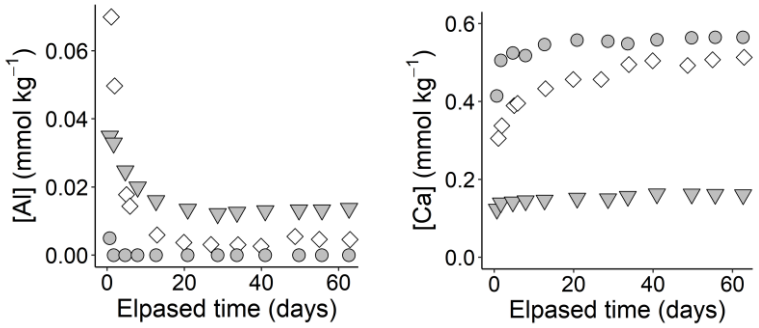

401

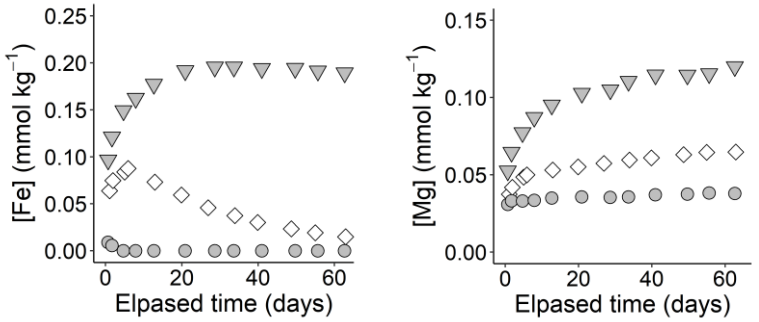

402

403 *Figure 8: Temporal evolution of Si, Al, Ca, Fe, and Mg concentrations of three representative*
404 *batch experiments. The dashed lines in the Si graph represent Si concentrations obtained*
405 *from equation (5) together with the fit parameters corresponding to each experiment. The*
406 *size of the uncertainties is smaller than the symbol size.*

407

3.2.2. Saturation state of the reactive fluids

The saturation indices of the reactive fluids with respect to the phases present in the initial solids and potential secondary phases were estimated using measured fluid chemistry and pH with PHREEQC. A complete list of these saturation indices is provided in Table S5. Numerous phases are found to be supersaturated during the experiments including smectites, aluminum and iron oxyhydroxides, and quartz. None of these phases, however, were identified in post experimental XRD analyses or the SEM observations (Figure 2). The precipitation of Al and Fe oxyhydroxides, however, is likely as the fluid concentrations of these elements decreased over time during most batch experiments. For some samples, scattered nanocrystals were observed on the reacted grains. These nanocrystals were too small to determine their composition with energy dispersive spectrometry.

3.3. Element release rates

3.3.1. Batch reactor experiments

Silicon release rates are often used as a proxy for the dissolution rates of silicate minerals because Si-O bonds maintain the structure of most of these minerals (Oelkers et al., 1994; Oelkers, 2001; Brantley, 2008; Schott et al., 2009). Silicon release rates from all experiments obtained using equation (3), together with the measured slopes of Si mass versus time are shown as a function of the *in situ* pH in Figure 9, and provided in Table S6. Also shown in this figure are Si release rates obtained from the mixed-flow experiments, as described below. Two observations are evident in this plot. First, the measured Si release rates obtained from the temporal evolution of the reactive fluid composition tend to be consistent with the steady-state rates obtained from the mixed flow reactors. Second, the Si release rates appear to plot as a single function of pH. This latter observation suggests that there is little effect of the degree of basalt alteration on these Si release rates.

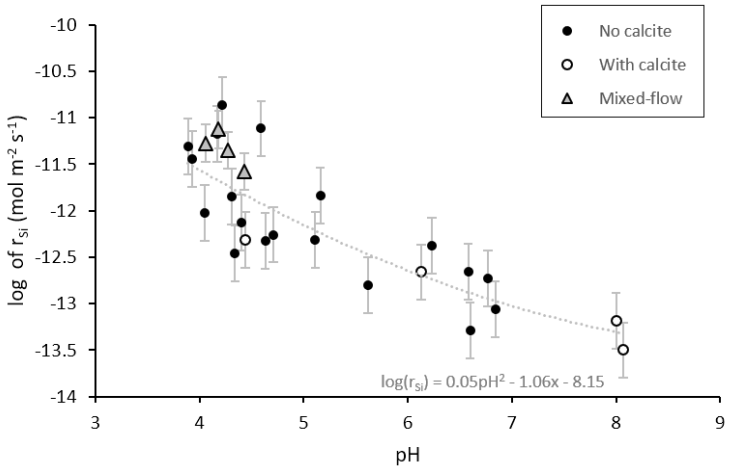

Figure 9: Logarithm of BET surface area normalized Si release rates as a function of the corresponding reactive fluid pH. The grey dashed line shows the result of a polynomial regression of these rates. Error bars indicate a ±0.3 log units uncertainty on the Si release rates. Uncertainties on the measured pH are smaller than the symbol size.

Si release rates generated for pH 4 using equations (4) and (5) are presented together with corresponding rates for individual silicate minerals in Figure Figure 60. All calculated rates are reported in Table S7. Silicon release rates at pH 4 are similar for most of the altered basalts, and many are identical to each other considering the associated uncertainty. Surface area normalized Si release rates range from $10^{-10.6}$ to $10^{-11.8}$ mol m^{-2} s^{-1}, except for sample B261S4, which had a release rate of $10^{-12.4}$ mol m^{-2} s^{-1}. These rates are substantially lower than either those of Ca-rich plagioclase or fresh basaltic glass, but substantially faster than those of common clay minerals. Although the least altered basalts considered in this study (based on the relative volume of primary phases present in the rocks) exhibit rates that are among the fastest rates measured, the Si release rates of surface and core samples are evenly distributed and no clear trends are evident.

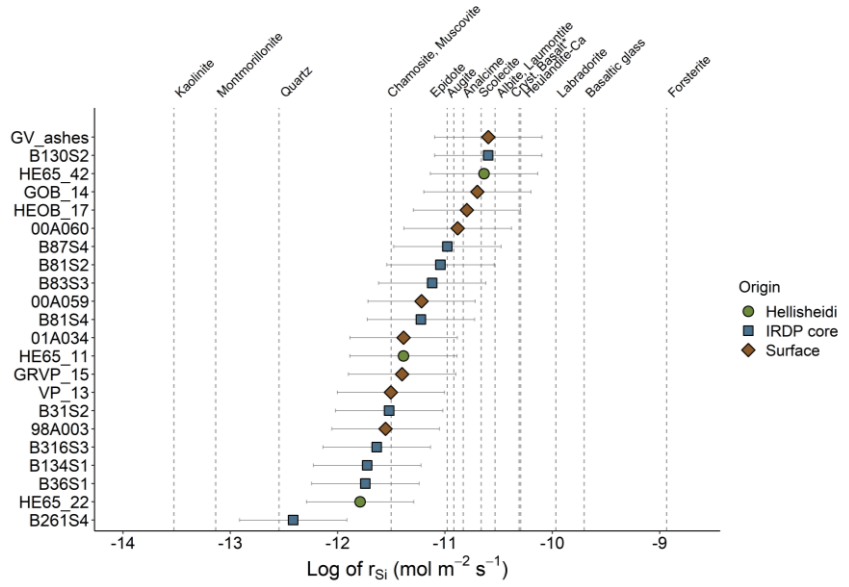

Figure 60: Logarithm of estimated BET surface area normalized Si release rates at pH 4 for all studied rock samples. Rates for individual minerals are represented with dashed lines and were obtained using equations and parameters reported by Heřmanská et al. (2022). The rate for crystalline basalt was taken from Gudbrandsson et al. (2011).

3.3.2. Mixed flow reactor experiments

The rock samples used in the mixed-flow reactor experiments were selected to span a diversity of mineralogy observed in the samples. An example of the temporal fluid evolution of a mixed-flow reactor experiment is shown in Figure 71; a complete table of the temporal fluid concentrations in the samples collected from the mixed-flow experiments is provided in Table S8.

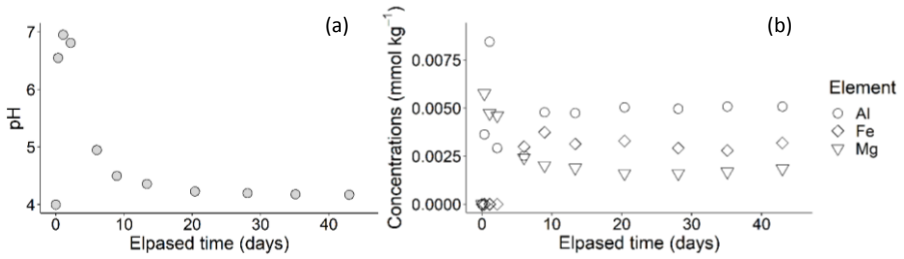

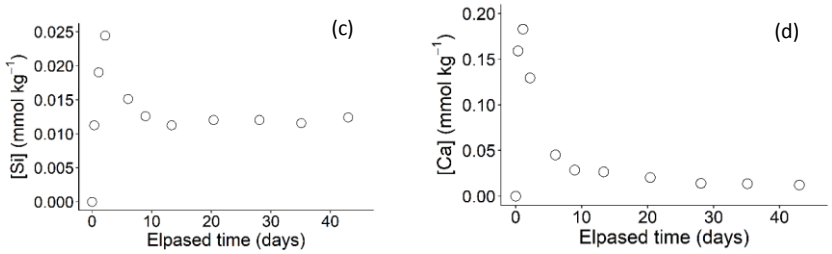

Figure 71: Temporal evolution of the (a) pH, (b) Al, Fe and Mg, (c) Si and (d) Ca concentrations of the outlet fluids for the B130S2 mixed-flow experiment. The size of the uncertainties is smaller than the symbol size.

In all the mixed-flow experiments, the pH, Si, Ca and Mg concentrations peaked during the first few days before decreasing towards a stable steady state value. During the early part of the B130S2 mixed-flow experiment, the pH reached values close to 7 before decreasing to 4. This high initial pH explains why Fe concentrations were below the quantification limit at the beginning of the experiment; likely due to Fe oxidation and precipitation (Singer and Stumm, 1970; Morgan and Lahav, 2007). Concentrations of Al did not exhibit consistent trends across all the experiments. Element release rates were obtained from the steady-state outlet fluid concentrations using equation (6). Resulting steady state reaction rates obtained from these experiments are summarized in Table 2. These rates are also plotted as a function of pH, together with corresponding batch experiment rates in Figure 9. The steady-state rates obtained from the mixed-flow experiments are largely consistent with corresponding rates obtained from batch reactors. One exception is the Si release rate of sample HE65_22, which is close to an order of magnitude faster than that of the corresponding rate estimated from the batch experiments.

Table 2: Summary of the results of the mixed-flow experiments. Steady state element release rates are given as logarithms values in units mol m^{-2} s^{-1}. The Log values of Si release rates from batch experiments were calculated using equation (5) at the final pH value of the corresponding mixed-flow experiment.

Sample	*B83S3*	*B130S2*	*B316S3*	*HE65_22*
Final pH	4.3	4.2	4.1	4.4
final fluid molar Ca/Si ratio	1.91	1.11	1.33	1.71
Molar Ca/Si of the rock sample	0.16	0.09	0.23	0.24
final fluid molar Mg/Si ratio	0.23	0.14	0.82	1.35

Molar Mg/Si ratio of the rock sample	0.12	0.05	0.11	0.17
Log of Ca release rate	-11.1	-11.1	-11.1	-11.3
Log of Mg release rate	-12.0	-12.0	-11.4	-11.4
Log of Si release rate	-11.3	-11.1	-11.3	-11.6
Log of Si release rate from corresponding batch experiment	-11.3	-10.7	-11.7	-12.5

3.4 Experimental uncertainties

The uncertainties associated with the reported surface area normalized Si release rates obtained from the batch experiments were estimated by summing the different sources of uncertainty. These sources include those associated with the BET surface area measurements, the measurement of reactive fluid compositions, and the linear regression of fluid Si masses over time. The combination of these uncertainties suggests that the rates generated using equation (3) and shown in Figure 9 have uncertainties on the order of 0.3 log units. Rates generated at a constant pH of 4 using equation (5) and summarized in Figure 10 have higher uncertainties due to the extrapolation of measured rates to this constant pH. The total uncertainty on these latter rates is estimated to be on the order of 0.5 log units. In contrast, Si release rates obtained from the mixed-flow experiments do not require a linear regression of fluid Si mass nor were extrapolated to a constant pH of 4. This results in lower uncertainty in the Si release rates from these experiments, which is estimated to be 0.2 log units.

4. Discussion

4.1. Surface areas

The BET surface areas of the laboratory prepared basalt powders range from 0.3 to 9 m^2 g^{-1}. The origin of these differences is challenging to determine, but sample mineralogy can have an influence. Minerals including the chlorites (Malmström et al., 1996), zeolites (Yates, 1968; Valdés et al., 2006), and clays (Murray and Quirk, 1990) have been reported to have relatively high BET surface areas. To illuminate the degree to which the presence of these minerals influences the surface areas of the laboratory prepared samples, the BET surface areas of all laboratory-prepared rock powders are plotted as a function of their combined chlorite and zeolite contents in Figure 82.

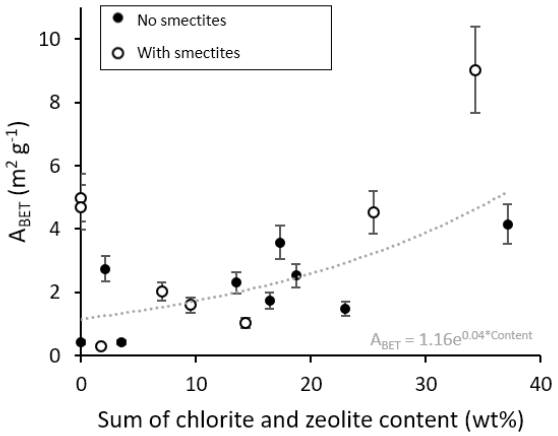

Figure 82: Plot of the BET surface area of the laboratory prepared rock powders used in this study as a function of the sum of their zeolite and chlorite contents. Open circles indicate samples observed to contain clay minerals. Error bars represent the uncertainty on BET measurements. The grey dashed line shows the result of an exponential regression of these surface areas.

Measured BET surface areas are observed to increase with chlorite and zeolite content. Note that the mass of clay minerals, such as smectite, was not quantified by Rietveld analysis. Only their presence or absence was reported. This may likely be the reason for the high surface areas of the two chlorite and zeolite-free samples that plot on the left side of Figure 82 as they do contain clays minerals.

4.2. Reactivity of altered basalts

Several significant observations can be made concerning the measured Si release rates determined in the present study. First the Si release rates from all altered basalts are similar, regardless of their degree of alteration. The differences in rates measured from batch experiments are largely explained by the pH differences, as seen in Figure 9. When these rates are recalculated to pH 4, as in Figure 10, the differences between these Si release rates are low compared to the associated uncertainty. The results from the mixed-flow experiments performed in this study confirm this observation, with rates measured from basalts with contrasting alteration profiles falling within 0.5 log units of one another.

The similarity in these rates likely stems from the mineralogy of these altered basalt samples. The alteration of basalt rapidly removes basaltic glass and olivine due to their low thermodynamic stability and high reactivity. After the removal of these phases the most reactive minerals present in the altered basalts are plagioclase, augite, zeolites and epidote. Collectively these minerals represent from 25 to 85 wt% of the mass of the studied samples. The logarithm of Si release rates for these minerals at pH 4 and 25 °C range over a relatively small range, from $10^{-10.0}$ to $10^{-11.5}$mol m^{-2} s^{-1}. Other minerals in these altered rocks, such as chlorite, quartz and clay minerals are significantly less reactive than these phases (Brantley, 2008), and likely contribute little to the release of Si to the fluids during the experiments performed in this study.

A second significant observation is that the BET surface area normalized Si release rates measured in this study on altered basalts are one to two orders of magnitude slower than that of basaltic glass, and somewhat slower than those of fresh crystalline basalt. This observation confirms the impact of alteration on rock dissolution rates. Alteration preferentially removes most reactive phases decreasing the average dissolution rate of the overall rock. The slowing of weathering rates of rocks over time due to rock alteration has been previously explored in a number of studies (e.g. Colman, 1981; White et al., 1996; White and Brantley, 2003; Reeves and Rothman, 2013).

A third observation is that the measured surface area normalized rates of altered basalts determined in this study tend to be lower than those of the individual minerals, such as plagioclase, present in the altered rock samples. The lower surface area normalized Si release rates determined in this study can be attributed to the formation of high surface area but slowly reacting minerals during the natural alteration process. The formation of clay minerals, chlorite, and nanocrystalline Fe and Al-oxides increases the surface area of altered basalts without changing significantly the rate of Si release. As a consequence, the presence of such phases lowers the measured surface area normalized Si release rates of altered basalts.

4.3. Relative release rates of the elements

The temporal evolution of the Ca/Si molar release ratios normalized to the corresponding ratio of the original rock for some representative experiments is shown in

Figure 93. The reactive fluid Ca concentration was significantly higher than that of Si at the beginning of each batch experiment. The Ca/Si molar ratio of the reactive fluids decreased sharply after the first days of each experiment and tended to stabilize over time. Marieni et al. (2020) observed a similar behavior reacting altered oceanic basalts in batch reactors. The initial rapid Ca release could result either from rapid initial cation for proton exchange reactions (Oelkers et al., 2009; Zhang et al., 2013), consistent with the observation that the intensity of the observed preferential release of divalent cations is correlated to increased surface areas of the altered basalt samples, or from the presence of a rapidly dissolving Ca bearing, Si-free mineral such as calcite, in the original rock samples. Note that although calcite was not observed to be present with XRD analyses in the solids considered in Figure 13, minor quantities of calcite could have gone undetected as the detection limit for XRD is on the order of 1%.

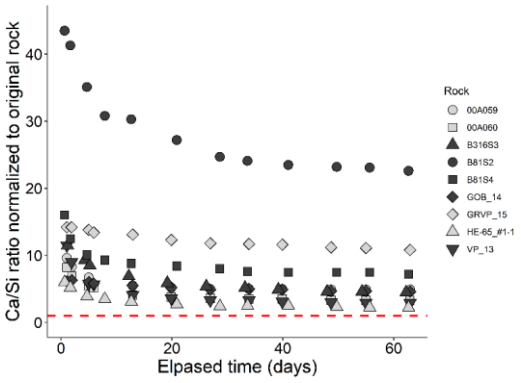

Figure 93: Temporal evolution of the Ca/Si molar ratio of the reactive fluids normalized to that of the original rock for selected representative batch experiments. The red dashed line represents the Ca/Si ratio of stoichiometric dissolution.

In some cases, the preferential release of both Mg and Ca persists until the end of the experiments. To further explore this preferential release, the Ca and Mg to Si release rate ratios were calculated from a linear regression of the fluid masses during the latter part of each batch experiment using equation (3). The resulting release rate ratios are provided in Table 3. Most hydrothermally altered basalt samples exhibited a preferential release of Ca and Mg, relative to Si over the whole experiment, whereas surface altered samples tended to approach stoichiometric element release rates over time. This behavior may stem from

the alteration process itself. The hydrothermal alteration of basalts leads to the formation of minerals such as zeolites and epidote (Humphris and Thompson, 1978; Kristmannsdottir, 1979). These minerals contain abundant Ca and react relatively fast compared to Ca poor alteration phases. The alteration of basalts at the Earth's surface tends to preferentially remove Ca and to a lesser degree Mg, without the precipitation of divalent metal-rich secondary phases (e.g.Eggleton et al., 1987). This process does tend to result in relatively lower quantities of Ca and Mg bearing secondary minerals. The long-term preferential release of Mg can be explained by the faster dissolution rate of augite/diopside relative to the whole rock, or by the exchange of Mg from chlorites and smectites.

Table 3: Ratios of the molar Ca and Mg release rates to Si release rates during the final part of all batch experiments. Values in bold correspond to experiments where the Ca and Mg release rates were significantly higher than the corresponding original altered basalt stoichiometry.

Origin	*Sample*	*Ca/Si release rate*	*Rock Ca/Si*	*Mg/Si Release rate*	*Rock Mg/Si*	*Rock Normalized Ca/Si ratio*	*Rock Normalized Mg/Si ratio*
IRDP core	B31S2*	**9.97**	0.19	**0.34**	0.16	**51.8**	**2.1**
	B36S1*	**0.32**	0.18	0.10	0.16	**1.7**	0.7
	B81S2	**0.41**	0.16	0.08	0.15	**2.6**	0.6
	B81S4	**0.78**	0.22	**0.31**	0.15	**3.6**	**2.1**
	B83S3*	**27.51**	0.16	**0.25**	0.12	**168.9**	**2.2**
	B87S4*	NA	0.14	**0.21**	0.20	**NA**	**1.0**
	B130S2	**1.98**	0.09	0.07	0.05	**21.8**	**1.3**
	B134S1	**0.82**	0.12	**0.24**	0.08	**6.6**	**3.1**
	B261S4	**0.35**	0.21	**0.58**	0.19	**1.7**	**3.0**
	B316S3	**0.44**	0.23	**1.38**	0.11	**1.9**	**13.1**
Hellisheiði	HE65_11	0.21	0.31	**0.29**	0.26	0.7	**1.1**
	HE65_22	0.19	0.24	**0.58**	0.17	0.8	**3.4**
	HE65_42	0.14	0.30	0.15	0.23	0.5	0.7
River suspended material	00A059	**0.55**	0.23	0.16	0.18	**2.4**	0.9
	00A060	0.13	0.22	0.15	0.16	0.6	0.9
	01A034	**0.81**	0.21	**0.35**	0.17	**3.9**	**2.0**
	98A003	0.14	0.15	0.08	0.19	0.9	0.4
Surface outcrops	GOB_14	**0.64**	0.25	0.10	0.22	**2.6**	0.5
	GRVP_15	**0.74**	0.26	**0.29**	0.18	**2.9**	**1.6**
	VP_13	0.15	0.23	**0.24**	0.15	0.6	**1.6**
	HEOB_17	0.14	0.23	**0.22**	0.18	0.6	**1.2**
Volcanic ash	GV_ash	0.21	0.21	0.15	0.17	1.0	0.9

*Sample marked with * contained calcite*

595 The preferential release of Ca and Mg was also observed during the mixed-flow
596 experiments. The measured elemental release ratios of elements are shown in Table 2. All
597 four mixed-flow experiments exhibited a preferential Ca and Mg release at steady state,
598 even after more than 40 days of reaction. In these experiments, an initial maximum of molar
599 Ca/Si and Mg/Si release ratios was also observed, again consistent with a rapid initial metal
600 for proton exchange reaction. Similar results were reported by Marieni et al. (2020), who
601 observed a strong preferential initial and long-term release of Ca compared to Si from
602 altered mid-ocean ridge basalts collected from the Juan de Fuca Plate and the Mid-Atlantic
603 ridge.

604 **4.4 Insight into the slowing of basalt weathering rates as a function of age and**
605 **alteration**

606 The ages of the surface altered samples investigated in this study ranged from 0.3 to 13
607 Myr. All samples were void of olivine, and their original basaltic glass variably altered. The Si
608 release rates from all surface weathered basalt samples are similar considering
609 uncertainties. This suggests that after a rapid palagonitization of basaltic glass and the
610 removal of any olivine present, the reactivity of surface altered basalts becomes largely
611 insensitive to the age or degree of alteration of the rock. Nesbitt and Wilson (1992) came to
612 similar conclusion in their study of the reactivity of altered basalts from Baytown, Australia,
613 and so did Gislason et al. (1996) in their study of the weathering of basalt in Iceland.

614 All the surface altered basalt samples contained a substantial quantity of primary
615 phases, notably plagioclase and pyroxene. These are among the most reactive minerals after
616 basaltic glass and olivine. It is likely, therefore, that the Si release rates of altered basalts are
617 controlled by the presence of plagioclase and pyroxene in these rocks. As these phases
618 persist in all of the studied Earth surface altered samples, their measured Si release rates are
619 similar to each other.

620 Based on such observations, it seems likely that the slowing of basalt weathering rates
621 in nature is a non-linear function of time. Rates decrease rapidly as the reactive olivine and
622 basaltic glass are selectively removed. Once these are depleted from the basalts, a slower
623 longer term but near constant Si release rate is observed due to the persistence of
624 plagioclase and pyroxene in these rocks. Similar results were suggested by Gislason et al.

(1996) and are consistent with observations reported by Kennedy et al. (1998) and Chadwick et al. (1999).

The slowing of element release rates, as a result of the surface alteration of basalts, and the non-linear slowing of these rates has implications for the drawdown of CO_2 following large volcanic events. Although volcanic eruptions emit large masses of CO_2, they also emit large quantities of fresh volcanic rock, which can drawdown CO_2 due to weathering. A number of past studies noted that fresh basalts may have a large contribution to drawing down CO_2 from the atmosphere after major eruptions (Parnell et al., 2014; Cox et al., 2016; Shen et al., 2022). The results of the present study suggest this enhanced drawdown due to the presence of fresh basalts on the Earth's surface is short lived and will persist only as long as fresh basaltic glass and olivine in present in these basalts.

4.5. Application to subsurface carbon mineralization

The experiments in the present study were performed at acidic conditions and at atmospheric CO_2 concentrations. The direct carbonation of the altered basalts at these conditions is not observed. The results presented in this study, nevertheless, suggest that altered basalts could be favorable for subsurface carbon storage by mineralization. The ability of altered basalts to promote CO_2 carbonation is favored by the preferential release of the divalent metal Ca and Mg to the fluid phase and the ability of altered basalt dissolution to increase fluid pH. Both processes, observed in our experiments, favor the formation of carbonate minerals in the presence of water dissolved CO_2.

The surface area normalized Si release rates of the altered basalts considered in this study are one to two orders of magnitude slower than the corresponding fresh basalts. Part of this gap is most probably associated to the increased surface area due to the presence of alteration minerals with high surface area and low reactivity. The lower Si release rates of the altered basalts is somewhat compensated by the preferential release rates of Ca and Mg from these rocks even after the initial phase due to exchange reactions. This was particularly true for hydrothermally altered basalts and related to the presence of reactive secondary phases such as zeolites and epidote.

The observation that altered basalts are less reactive than corresponding fresh basalts agree with the results obtained from mixed-flow reactor experiments at 120 °C in Delerce et

al., (2023). In this previous study, Si release rates from altered basalts were also found to be similar to each other and mostly independent of the extent of basalt alteration. Although basalt alteration slows reactivity, the effect of this slower rate in terms of carbon storage through mineralization can be overcome by increasing temperature. This is confirmed by the comparison of the results obtained in this study with those from Delerce et al., (2023) and by the observations made during the CarbFix project. During CarbFix1, 95% of the CO_2 injected into fresh basalt at ~30 °C and 400 to 800 m depth mineralized in less than two years (Matter et al., 2016). During the CarbFix2 project, more than half of the CO_2 injected into hydrothermally altered basalts at ~250 °C and 750 m depth was mineralized within 4 months (Clark et al., 2020). This illustrates how increased temperature can compensate for the slower reactivity of altered basalts for mineral carbon storage.

5. Conclusions

This study measured and reported the element release rates of a wide variety of altered basalts of various ages. The major conclusions of this study include:

- Alteration of basalt at the Earth's surface tends to rapidly remove reactive basaltic glass and olivine. This alteration slows the BET surface area-normalized Si release rates from the rocks by one to two orders of magnitude. Although some of this decrease in rates can be attributed to the formation of less reactive high-surface-area minerals during alteration, the slowing of these rates is also evident in natural systems (c.f. Gislason et al., 1996).
- Once the rapidly reactive phases are removed from the fresh basalt, surface area normalized Si release rates remain close to constant.
- A preferential release of Ca and Mg is observed during the first days of reaction for all the altered basalts. A long-term preferential release of these elements is observed for the studied hydrothermally altered basalts containing secondary phases such as zeolites and epidote. This preferential release of divalent cations, and the associated increase in fluid pH could favor the carbonation of altered basaltic rocks.

6. Acknowledgments

The authors are particularly grateful to Iwona Galeczka for her help in sampling during COVID lockdowns with the valuable advice of Birgir Vilhelm Óskarsson. They also thank Sigurdur R. Gislason for coordinating access to the IRDP core. The authors acknowledge the valuable insights and support from Chiara Marieni, Giuseppe Saldi, Carole Causserand, Alain Castillo, and Pascal Gisquet. This work has been carried out within the European projects CarbFix2 and GECO that have received funding from the European Union's Horizon 2020 research and innovation program under grant agreements # 764760 and # 818169, respectively.

7. Appendix A: Supplementary material

The supplementary material to this article contains:

- ~~Chemical~~ the chemical composition of all the rock samples used in this study
- ~~Mineralogy~~, the mineralogy of all the samples used in the study
- ~~Chemical~~, the chemical composition of the amorphous phase in selected samples
- ~~Temporal~~, the temporal evolution of the pH, the fluid volume present in the reactor, the elemental concentrations for Al, Ca, Fe, Mg, and Si in batch experiments
- ~~Calculated~~, the calculated saturation indices for all possible mineral phases based on fluid chemistry at the end of the experiment
- , the BET and geometric surface areas normalized release rates calculated using equation (3~~)~~
- ~~Calculated~~), the calculated Si release rates at ~~pH4~~pH 4 using the fitting method
- ~~Temporal~~, the temporal evolution of the pH, the elemental concentrations for Al, Ca, Fe, Mg, and Si in mixed flow experiments~~.~~
- ~~Last~~, the last measured Ca/Si and Mg/Si values for all the rocks, compared to the initial Ca/Si and Mg/Si ratios of the rocks, and the evolution of the amorphous phase content of the surface basalt samples as a function of age.
- ~~Evolution of the amorphous phase content of the surface basalt samples as a function of age~~

8. References

Alt J. C. and Teagle D. A. H. (1999) The uptake of carbon during alteration of ocean crust. *Geochim. Cosmochim. Acta* **63**, 1527–1535.

Formatted: Font: 12 pt

Formatted: Font: 12 pt

Formatted: Font: 12 pt

Formatted: Font: 12 pt

Formatted: Font: 12 pt

Formatted: Font: 12 pt

Formatted: Font: 12 pt

Formatted: Font: 12 pt

Formatted: Font: 12 pt

Formatted: Justified, Indent: First line: 0.49", Line spacing: 1.5 lines, No bullets or numbering

Formatted: Font: 12 pt

Formatted: Font: 12 pt

Baker H. M., Massadeh A. M. and Younes H. A. (2009) Natural Jordanian zeolite: Removal of heavy metal ions from water samples using column and batch methods. *Environ. Monit. Assess.* **157**, 319–330.

Berner, R.A., (1999.) A new look at the long-term carbon cycle, *GSA Today* **9**, 11, 1-6.

Blum A. and Lasaga A. (1988) Role of surface speciation in the low-temperature dissolution of minerals. *Nature* **331**, 431–433.

Börker J., Hartmann J., Romero-Mujalli G. and Li G. (2019) Aging of basalt volcanic systems and decreasing CO_2 consumption by weathering. *Earth Surf. Dyn.* **7**, 191–197.

Brady P. V. (1991) The effect of silicate weathering on global temperature and atmospheric CO_2. *J. Geophys. Res.* **96**, 18,101-18,106.

Brady P. V. and Carroll S. A. (1994) Direct effects of CO_2 and temperature on silicate weathering: Possible implications for climate control. *Geochim. Cosmochim. Acta* **58**, 1853–1856.

Brantley S. L. (2008) Kinetics of Mineral Dissolution. In *Kinetics of Water-Rock Interaction* Springer New York, New York, NY. pp. 151–210.

Campbell J. S., Foteinis S., Furey V., Hawrot O., Pike D., Aeschlimann S., Maesano C. N., Reginato P. L., Goodwin D. R., Looger L. L., Boyden E. S. and Renforth P. (2022) Geochemical Negative Emissions Technologies : Part I . Front Clim. **4**:879133.

Chadwick O. A., Derry L. A., Vitousek P. M., Huebert B. J. and Hedin L. O. (1999) Changing sources of nutrients during four million years of ecosystem development. *Nature* **397**, 491–497.

Chukwuma J. S., Pullin H. and Renforth P. (2021) Assessing the carbon capture capacity of South Wales' legacy iron and steel slag. *Miner. Eng.* **173**, 107232.

Clark D. E., Gunnarsson I., Aradóttir E. S., Þ. Arnarson M., Þorgeirsson Þ. A., Sigurðardóttir S. S., Sigfússon B., Snæbjörnsdóttir S. Ó., Oelkers E. H. and Gíslason S. R. (2018) The chemistry and potential reactivity of the CO_2 -H_2S charged injected waters at the basaltic CarbFix2 site, Iceland. *Energy Procedia* **146**, 121–128.

Clark D. E., Oelkers E. H., Gunnarsson I., Sigfússon B., Snæbjörnsdóttir S., Aradóttir E. S. and Gíslason S. R. (2020) CarbFix2: CO_2 and H_2S mineralization during 3.5 years of continuous injection into basaltic rocks at more than 250 °C. *Geochim. Cosmochim. Acta* **279**, 45–66.

Colbourn G., Ridgwell A. and Lenton T. M. (2015) The time scale of the silicate weathering negative feedback on atmospheric CO_2. *Global Biogeochem. Cycles* **29**, 583–596.

Colman S. M. (1981) Rock-Weathering Rates as Functions of Time. *Quat. Res.* **15**, 250–264.

Courtillot V. E. and Renne P. R. (2003) On the ages of flood basalt events. *Comptes Rendus - Geosci.* **335**, 113–140.

Cox G. M., Halverson G. P., Stevenson R. K., Vokaty M., Poirier A., Kunzmann M., Li Z. X., Denyszyn S. W., Strauss J. V. and Macdonald F. A. (2016) Continental flood basalt weathering as a trigger for Neoproterozoic Snowball Earth. *Earth Planet. Sci. Lett.* **446**, 89–99.

Delerce, S., Bénézeth, P., Schott, J., Oelkers, E.H., 2023. The dissolution rates of naturally altered basalts at pH 3 and 120 °C: Implications for the in-situ mineralization of CO_2 injected into the subsurface. Chem. Geol. **621**, 121353.

Deng K., Yang S. and Guo Y. (2022) A global temperature control of silicate weathering intensity. *Nat. Commun.* **13**, 1–10.

Formatted: Font: Italic

Formatted: Subscript

Formatted: Subscript

Formatted: Font: Bold

Dessert C., Dupré B., Gaillardet J., François L. M. and Allègre C. J. (2003) Basalt weathering laws and the impact of basalt weathering on the global carbon cycle. *Chem. Geol.* **202**, 257–273.

~~Eiriksdottir E. S. (2016) Weathering and riverine fluxes in pristine and controlled river catchments in Iceland. University of Iceland.~~

Eiriksdottir, E.S., Louvat, P., Gislason, S.R., Óskarsson, N., Hardardóttir, J., (2008) Temporal variation of chemical and mechanical weathering in NE Iceland: Evaluation of a steady-state model of erosion. Earth Planet. Sci. Lett. **272**, 78–88.

Eggleton R.A., Foudoulis, C. and Varkevisser, D. (1987) Weathering of basalt: ~~Chemges~~Changes in rock ~~chemistru~~chemistry and ~~mineraligy~~mineralogy. *Clays Clay Min*.. **35,** 161-169.

Falkowski P., Scholes R. J., Boyle E., Canadell J., Canfield D., Elser J., Gruber N., Hibbard K., Hogberg P., Linder S., Mackenzie F. T., Moore B., Pedersen T., Rosental Y., Seitzinger S., Smetacek V. and Steffen W. (2000) The global carbon cycle: A test of our knowledge of earth as a system. *Science* **290**, 291–296.

Fridleifsson I. B., Gibson I. L., Hall J. M., Johnson H. P., Chistensen N. I., Schmincke H.-U. and Schönharting G. (1982) The Iceland Research Drilling Project. *J. Geophys. Res.* **87**, 6359–6361.

Gadikota G. (2021) Carbon mineralization pathways for carbon capture, storage and utilization. *Commun. Chem.* **4**, 1–5.

Gadikota G., Matter J., Kelemen P., Brady P. V. and Park A. H. A. (2020) Elucidating the differences in the carbon mineralization behaviors of calcium and magnesium bearing alumino-silicates and magnesium silicates for CO_2 storage. *Fuel* **277**, 117900.

Galeczka I., Oelkers E. H. and Gislason S. R. (2018) The effect of the 2014-15 Bárðarbunga volcanic eruption on chemical denudation rates and the CO_2 budget. *Energy Procedia* **146**, 53–58.

Gislason S. R., Arnorsson S. and Armannsson H. (1996) Chemical weathering of basalt in Southwest Iceland~~:~~; effects of runoff, age of rocks and vegetative/glacial cover. *Am. J. Sci.* **296**, 837–907.

Gislason S. R., Oelkers E. H., Eiriksdottir E. S., Kardjilov M. I., Gisladottir G., Sigfusson B., Snorrason A., Elefsen S., Hardardottir J., Torssander P. and Oskarsson N. (2009) Direct evidence of the feedback between climate and weathering. *Earth Planet. Sci. Lett.* **277**, 213–222.

Gudbrandsson S., Wolff-Boenisch D., Gislason S. R. and Oelkers E. H. (2011) An experimental study of crystalline basalt dissolution from 2≤pH≤11 and temperatures from 5 to 75°C. *Geochim. Cosmochim. Acta* **75**, 5496–5509.

Guidry M. W. and Mackenzie F. T. (2003) Experimental study of igneous and sedimentary apatite dissolution: Control of pH, distance from equilibrium, and temperature on dissolution rates. *Geochim. Cosmochim. Acta* **67**, 2949–2963.

Harouiya N., Chaïrat C., Köhler S. J., Gout R. and Oelkers E. H. (2007) The dissolution kinetics and apparent solubility of natural apatite in closed reactors at temperatures from 5 to 50 °C and pH from 1 to 6. **244**, 554–568.

Harrison A. L., Power I. M. and Dipple G. M. (2013) Accelerated carbonation of brucite in mine tailings for carbon sequestration. *Environ. Sci. Technol.* **47**, 126–134.

Heřmanská M., Voigt M. J., Marieni C., Declercq J. and Oelkers E. H. (2022) A comprehensive and internally consistent mineral dissolution rate database: Part I: Primary silicate minerals and glasses. *Chem. Geol.* **597,** 120807.

Hodson M. E. and Langan S. J. (1999) The influence of soil age on calculated mineral weathering rates. *Appl. Geochemistry* **14**, 387–394.

Humphris, S.E. and Thompson, G. ~~Hydrothrmal~~Hydrothermal alteration of oceanic basalts by seawater. *Geocheim. Cosmochim. Acta* **42,** 107-125.

Jercinovic M. J., Keil K., Smith M. R. and Schmitt R. A. (1990) Alteration of basaltic glasses from north-central British Columbia, Canada. *Geochim. Cosmochim. Acta* **54**, 2679–2696.

Kelemen P. B., Aines R., Bennett E., Benson S. M., Carter E., Coggon J. A., de Obeso J. C., Evans O., Gadikota G., Dipple G. M., Godard M., Harris M., Higgins J. A., Johnson K. T. M., Kourim F., Lafay R., Lambart S., Manning C. E., Matter J. M., Michibayashi K., Morishita T., Noël J., Okazaki K., Renforth P., Robinson B., Savage H., Skarbek R., Spiegelman M. W., Takazawa E., Teagle D., Urai J. L. and Wilcox J. (2018) *In situ* carbon mineralization in ultramafic rocks: Natural processes and possible engineered methods. *Energy Procedia* **146**, 92–102.

Kelemen P. B., Matter J., Streit E. E., Rudge J. F., Curry W. B. and Blusztajn J. (2011) Rates and Mechanisms of Mineral Carbonation in Peridotite: Natural Processes and Recipes for Enhanced, *in situ* CO_2 Capture and Storage. *Annu. Rev. Earth Planet. Sci.* **39**, 545–576.

Kelemen P., Benson S. M., Pilorgé H., Psarras P. and Wilcox J. (2019) An Overview of the Status and Challenges of CO_2 Storage in Minerals and Geological Formations. *Front. Clim.* **1**, 1–20.

Kennedy M. J., Chadwick O. A., Vitousek P. M., Derry L. A. and Hendricks D. M. (1998) Changing sources of base cations during ecosystem development, Hawaiian Islands. *Geology* **26**, 1015–1018.

Knapp W. J. and Tipper E. T. (2022) The efficacy of enhancing carbonate weathering for carbon dioxide sequestration. *Front. Clim.* **4**, 928215.

Kristmannsdottir, H. (1979) Alteration of basaltic rocks by hydrothermal activity at 100 to 300 °C. *Dev. Sedimentology* **27**, 359-367.

Lewis A. L., Sarkar B., Wade P., Kemp S. J., Hodson M. E., Taylor L. L., Yeong K. L., Davies K., Nelson P. N., Bird M. I., Kantola I. B., Masters M. D., DeLucia E., Leake J. R., Banwart S. A. and Beerling D. J. (2021) Effects of mineralogy, chemistry and physical properties of basalts on carbon capture potential and plant-nutrient element release via enhanced weathering. *Appl. Geochemistry* **132**, 105023.

Li Gaojun, Hartmann J., Derry L. A., West A. J., You C. F., Long X., Zhan T., Li L., Li Gen, Qiu W., Li T., Liu L., Chen Y., Ji J., Zhao L. and Chen J. (2016) Temperature dependence of basalt weathering. *Earth Planet. Sci. Lett.* **443**, 59–69.

Liu D., Agarwal R., Li Y. and Yang S. (2019) Reactive transport modeling of mineral carbonation in unaltered and altered basalts during CO_2 sequestration. *Int. J. Greenh. Gas Control* **85**, 109–120.

Louvat P. and Allègre C. J. (1997) Present denudation rates on the island of Réunion determined by river geochemistry: Basalt weathering and mass budget between chemical and mechanical erosions. *Geochim. Cosmochim. Acta* **61**, 3645–3669.

Louvat P. and Allègre C. J. (1998) Riverine erosion rates on Sao Miguel volcanic island, Azores archipelago. *USDA For. Serv. - Gen. Tech. Rep. RMRS-GTR* **148**, 177–200.

Maesano C. N., Campbell J. S., Foteinis S., Furey V., Hawrot O., Pike D., Aeschlimann S., Reginato P. L., Goodwin D. R., Looger L. L., Boyden E. S. and Renforth P. (2022) Geochemical Negative Emissions Technologies: Part II. Roadmap. *Front. Clim.* **4**, 945332.

Formatted: French (France)

Malmström M., Banwart S., Lewenhagen J., Duro L. and Bruno J. (1996) The dissolution of biotite and chlorite at 25°C in the near-neutral pH region. *J. Contam. Hydrol.* **21**, 201–213.

Marieni C., Matter J. M. and Teagle D. A. H. (2020) Experimental study on mafic rock dissolution rates within CO_2-seawater-rock systems. *Geochim. Cosmochim. Acta* **272**, 259–275.

Marieni C. and Oelkers E. (2018) Carbon sequestration potential of altered mafic reservoirs. *Energy Procedia* **146**, 68–73.

Marieni C., Voigt M. J. and Oelkers E. H. (2021) Experimental study of epidote dissolution rates from pH 2 to 11 and temperatures from 25 to 200 °C. *Geochim. Cosmochim. Acta* **294**, 70–88.

Matter J. M. and Kelemen P. B. (2009) Permanent storage of carbon dioxide in geological reservoirs by mineral carbonation. *Nat. Geosci.* **2**, 837–841.

Matter J. M., Stute M., Snæbjörnsdóttir S. Ó., Oelkers E. H., Gislason S. R., Aradottir E., Sigfusson B., Gunnarsson I., Sigurdardottir H., Gunnlaugsson E., Axelsson G., Alfredsson H. A., Wolff-Boenisch D., Mesfin K., Taya D. F. de la R., Hall J., Dideriksen K. and Broecker W. S. (2016) Rapid carbon mineralization for permanent disposal of anthropogenic carbon dioxide emissions. *Science* **352**, 1312 –1314.

McGrail B. P., Schaef H. T., Ho A. M., Chien Y. J., Dooley J. J. and Davidson C. L. (2006) Potential for carbon dioxide sequestration in flood basalts. *J. Geophys. Res. Solid Earth* **111**, 1–13.

McGrail B. P., Schaef H. T., Spane F. A., Horner J. A., Owen A. T., Cliff J. B., Qafoku O., Thompson C. J. and Sullivan E. C. (2017) Wallula Basalt Pilot Demonstration Project: Post-injection Results and Conclusions. *Energy Procedia* **114**, 5783–5790.

Mehegan J. M., Robinson P. T. and Delaney J. R. (1982) Secondary mineralization and hydrothermal alteration in the Reydarfjordur drill core, eastern Iceland. *J. Geophys. Res.* **87**, 6511–6524.

Morgan, B., Lahav, O., 2007. The effect of pH on the kinetics of spontaneous Fe(II) oxidation by O_2 in aqueous solution - basic principles and a simple heuristic description. *Chemosphere* **68**, 2080–2084. ~~https://doi.org/10.1016/j.chemosphere.2007.02.015~~Murray R.

Murray R. S. and Quirk J. P. (1990) Surface Area of Clays. *Langmuir* **6**, 122–124.

Nesbitt H. W. and Wilson R. E. (1992) Recent chemical weathering of basalts. *Am. J. Sci.* **292**, 740–777.

Oelkers E. H. (2001) General kinetic description of multioxide silicate mineral and glass dissolution. *Geochim. Cosmochim. Acta* **65**, 3703–3719.

Oelkers, E.-H., Arkadakskiy, S., Afifi, A.-M., Hoteit, H., Richards, M., Fedorik, J., Delaunay, A., Torres, J. E~~. and~~., Ahmed, Z.–T~~.~~ (., Kunnummal, N., Gislason, S.R., 2022~~)~~. The subsurface carbonation potential of basaltic rocks from the Jizan region of Southwest Saudi Arabia. ~~*Hal Environ. Sci.*~~*Int. J. Greenh. Gas Control* **120**, ~~1–37.~~103772.

Oelkers, E.-H., Butcher, R., Pogge von Strandmann, P.-A.-E., Schuessler, J.-A., ~~Von Blankenburg~~von Blanckenburg, F., Snæbjörnsdóttir, S.–Ó., Mesfin~~–F~~, K., Aradóttir, E.–S., Gunnarsson, I., ~~Sigfusson~~Sigfússon, B., Gunnlaugsson, E., Matter, J.-M., Stute, M~~. and~~., Gislason, S.-R~~. (2018)~~., 2019. Using stable Mg isotope signatures to assess the fate of magnesium during the in situ mineralisation of CO_2 and H_2S at the CarbFix site in SW-Iceland. *Geochim. Cosmochim. Acta*~~.~~ **245**, 542–555.

Oelkers E. H., Golubev S. V., Chairat C., Pokrovsky O. S. and Schott J. (2009) The surface chemistry of multi-oxide silicates. *Geochim. Cosmochim. Acta* **73**, 4617–4634.

Formatted: Subscript

Formatted: Font: Italic

Formatted: Font: Bold

Formatted: Font: Not Italic

878 Oelkers E. H., Schott J. and Devidal J. L. (1994) The effect of aluminum, pH, and chemical affinity on
879 the rates of aluminosilicate dissolution reactions. *Geochim. Cosmochim. Acta* **58**, 2011–2024.

880 Olsson J., Stipp S. L. S., Dalby K. N. and Gislason S. R. (2013) Rapid release of metal salts and nutrients
881 from the 2011 Grimsvötn, Iceland volcanic ash. *Geochim. Cosmochim. Acta* **123**, 134–149.

882 Óskarsson B. V. and Riishuus M. S. (2013) The mode of emplacement of Neogene flood basalts in
883 Eastern Iceland: Facies architecture and structure of the Hólmar and Grjótá olivine basalt
884 groups. *J. Volcanol. Geotherm. Res.* **267**, 92–118.

885 Parkhurst D. L. and Appelo C. a. J. (2013) Description of Input and Examples for PHREEQC Version 3 —
886 A Computer Program for Speciation , Batch-Reaction , One-Dimensional Transport , and Inverse
887 Geochemical Calculations. In *U.S. Geological Survey Techniques and Methods, book 6, Chapter*
888 *A43* pp. 6-43A.

889 Parnell J., Macleod K. and Hole M. J. (2014) Carbon dioxide drawdown by Devonian lavas. *Earth*
890 *Environ. Sci. Trans. R. Soc. Edinburgh* **105**, 1–8.

891 Parruzot B., Jollivet P., Rébiscoul D. and Gin S. (2015) Long-term alteration of basaltic glass:
892 Mechanisms and rates. *Geochim. Cosmochim. Acta* **154**, 28–48.

893 Penman D. E., Caves Rugenstein J. K., Ibarra D. E. and Winnick M. J. (2020) Silicate weathering as a
894 feedback and forcing in Earth's climate and carbon cycle. *Earth-Science Rev.* **209**, 103298.

895 Peuble S., Andreani M., Gouze P., Pollet-Villard M., Reynard B. and Van de Moortele B. (2018) Multi-
896 scale characterization of the incipient carbonation of peridotite. *Chem. Geol.* **476**, 150–160.

897 Philpotts A.R., Ague J.J. (2009) Principles of igneous and metamorphic petrology. Cambridge
898 University Press.

899 Power I. M., Dipple G. M., Bradshaw P. M. D. and Harrison A. L. (2020) Prospects for CO_2
900 mineralization and enhanced weathering of ultramafic mine tailings from the Baptiste nickel
901 deposit in British Columbia, Canada. *Int. J. Greenh. Gas Control* **94**, 102895.

902 Rad S., Rivé K., Vittecoq B., Cerdan O. and Allègre C. J. (2013) Chemical weathering and erosion rates
903 in the lesser antilles: An overview in guadeloupe, martinique and dominica. *J. South Am. Earth*
904 *Sci.* **45**, 331–344.

905 Ratouis T. M. P., Snæbjörnsdóttir S., Voigt M. J., Sigfússon B., Gunnarsson G., Aradóttir E. S. and
906 Hjörleifsdóttir V. (2022) Carbfix 2: A transport model of long-term CO_2 and H_2S injection into
907 basaltic rocks at Hellisheidi, SW-Iceland. *Int. J. Greenh. Gas Control* **114**.

908 Reeves, D. and Rothman, D.H. (2013) Age dependence of ~~mienral~~mineral dissolution and
909 precipitation. *Global Biogeochem Cycles* **27**, 906-919.

910 Renforth P., Pogge von Strandmann P. A. E. and Henderson G. M. (2015) The dissolution of olivine
911 added to soil: Implications for enhanced weathering. *Appl. Geochemistry* **61**, 109–118.

912 Rinder T. and von Hagke C. (2021) The influence of particle size on the potential of enhanced basalt
913 weathering for carbon dioxide removal - Insights from a regional assessment. *J. Clean. Prod.*
914 **315**, 128178.

915 Robinson, P.–T., Hall, M., Christensen, N.–I., Gibson, I.–A.–N.–L.~~ and~~., Schmincke, H.., (1982a~~)~~). The
916 Iceland Research Drilling Project: Synthesis of results and implications for the nature of
917 Icelandic and oceanic crust. *J. Geophys. Res.* **87**, 6657–6667.

918 Robinson P. T., Mehegan J., Gibson I. L. and Schmincke H. U. (1982b) Lithology and structure of the
919 volcanic sequence in eastern Iceland. *J. Geophys. Res.* **87**, 6429–6436.

Formatted: Font: Italic

Rogers K. L., Neuhoff P. S., Pedersen A. K. and Bird D. K. (2006) CO_2 metasomatism in a basalt-hosted petroleum reservoir, Nuussuaq, West Greenland. *Lithos* **92**, 55–82.

~~Romaniello S., Stopnitzky S., Green T., Montserrat F., Matzner E., Moreau C., Syverson D., Lopez P., Hayden M., Sulpis O. and Ley B. (2021) Progress toward small scale field trials of coastal enhanced weathering of olivine. In *EGU General Assembly 2021* European Association of Geochemistry, France.~~

Schott J., Pokrovsky O. S. and Oelkers E. H. (2009) The link between mineral dissolution/precipitation kinetics and solution chemistry. *Rev. Mineral. Geochemistry* **70**, 207–258.

Seton M., Müller R. D., Zahirovic S., Williams S., Wright N. M., Cannon J., Whittaker J. M., Matthews K. J. and McGirr R. (2020) A Global Data Set of Present-Day Oceanic Crustal Age and Seafloor Spreading Parameters. *Geochemistry, Geophys. Geosystems* **21**, 1–15.

Shen J., Yin R., Zhang S., Algeo T. J., Bottjer D. J., Yu J., Xu G., Penman D., Wang Y., Li L., Shi X., Planavsky N. J., Feng Q. and Xie S. (2022) Intensified continental chemical weathering and carbon-cycle perturbations linked to volcanism during the Triassic–Jurassic transition. *Nat. Commun.* **13**, 1–10.

Singer, P.C., Stumm, W., 1970. Acidic Mine Drainage: The Rate-Determining Step. *Science* **167**, 1121–1123. ~~https://doi.org/10.1126/science.167.3921.1121~~

Snæbjörnsdóttir S. Ó., Oelkers E. H., Mesfin K., Aradóttir E. S., Dideriksen K., Gunnarsson I., Gunnlaugsson E., Matter J. M., Stute M. and Gislason S. R. (2017) The chemistry and saturation states of subsurface fluids during the *in situ* mineralisation of CO_2 and H_2S at the CarbFix site in SW-Iceland. *Int. J. Greenh. Gas Control* **58**, 87–102.

Snæbjörnsdóttir, S.~~-~~Ó., Sigfússon, B., Marieni, C., Goldberg, D., Gislason, S.~~-~~R~~. and .~~ Oelkers, E.~~-~~H~~. (.~~ 2020~~).~~ Carbon dioxide storage through mineral carbonation. *Nat. Rev. Earth Environ.* **1**, 90–102.

Snæbjörnsdóttir S. Ó., Wiese F., Fridriksson T., Ármansson H., Einarsson G. M. and Gislason S. R. (2014) CO_2 storage potential of basaltic rocks in Iceland and the oceanic Ridges. *Energy Procedia* **63**, 4585–4600.

Stefánsson A. and Gíslason S. R. (2001) Chemical weathering of basalts, southwest Iceland: Effect of rock crystallinity and secondary minerals on chemical fluxes to the ocean. *Am. J. Sci.* **301**, 513–556.

Stroncik N. A. and Schmincke H. U. (2002) Palagonite - A review. *Int. J. Earth Sci.* **91**, 680–697.

Stubbs A. R., Paulo C., Power I. M., Wang B., Zeyen N. and Wilson S. A. (2022) Direct measurement of CO_2 drawdown in mine wastes and rock powders: Implications for enhanced rock weathering. *Int. J. Greenh. Gas Control* **113**, 103554.

Taylor A. and Blum J. D. (1995) Relation between soil age and silicate weathering rates determined from the chemical evolution of a glacial chronosequence. *Geology* **23**, 979–982.

Tester J. W., Worley W. G., Robinson B. A., Grigsby C. O. and Feerer J. L. (1994) Correlating quartz dissolution kinetics in pure water from 25 to 625°C. *Geochim. Cosmochim. Acta* **58**, 2407–2420.

Valdés M. G., Pérez-Cordoves A. I. and Díaz-García M. E. (2006) Zeolites and zeolite-based materials in analytical chemistry. ~~*TrAC* –~~*Trends Anal. Chem.* **25**, 24–30.

Voigt M., Marieni C., Clark D. E., Gíslason S. R. and Oelkers E. H. (2018) Evaluation and refinement of thermodynamic databases for mineral carbonation. *Energy Procedia* **146**, 81–91.

Walker G. P. L. (1958) Geology of the reydarfjördur area, Eastern Iceland. *Q. J. Geol. Soc. London* **114**,

Formatted: Font: Italic

Formatted: Font: Bold

962 367–391.

963 Walker G. P. L. (1963) The Breiddalur central volcano, eastern Iceland. *Q. J. Geol. Soc. London* **119**,
964 29–63.

965 Walker J. C. G., Hays P. B. and Kasting J. F. (1981) A negative feedback mechanismfor the long-term
966 stabilization of earth's surface temperature. *J. Geophys. Res.* **86**, 9776–9782.

967 ~~Weise F., Fridriksson T. and Ármannsson H. (2008) CO_2 fixation by calcite in high temperature~~
968 ~~geothermal systems in Iceland ed. ISOR.~~ **~~ISOR–2008/~~**.

969 White A. F., Blum A. E., Schulz M. S., Bullen T. D., Harden J. W. and Peterson M. L. (1996) Chemical
970 Weathering of a Soil Chronosequence on Granite Alluvium I. Reaction Rates Based on Changes
971 in Soil Mineralogy. *Geochim. Cosmochim. Acta* **60**, 2533–2550.

972 White A. F. and Brantley S. L. (2003) The effect of time on the weathering of silicate minerals: Why do
973 weathering rates differ in the laboratory and field? *Chem. Geol.* **202**, 479–506.

974 White S. K., Spane F. A., Schaef H. T., Miller Q. R. S., White M. D., Horner J. A. and McGrail B. P. (2020)
975 Quantification of CO_2 Mineralization at the Wallula Basalt Pilot Project. *Environ. Sci. Technol.*

976 Xiong W., Wells R. K., Horner J. A., Schaef H. T., Skemer P. A. and Giammar D. E. (2018) CO_2 Mineral
977 Sequestration in Naturally Porous Basalt. *Environ. Sci. Technol. Lett.* **5**, 142–147.

978 Yates D. J. C. (1968) Studies on the surface area of zeolites, as determined by physical adsorption and
979 X-ray crystallography. *Can. J. Chem.* **46**, 1695–1701.

980 Zhang R., Zhang X., Guy B., Hu S., De Ligny D. and Moutte J. (2013) Experimental study of dissolution
981 rates of hedenbergitic clinopyroxene at high temperatures: dissolution in water from 25 °C to
982 374 °C. *Eur. J. Mineral.* **25**, 353–372.

983 Zhen-Wu B. Y., Dideriksen K., Olsson J., Raahauge P. J., Stipp S. L. S. and Oelkers E. H. (2016)
984 Experimental determination of barite dissolution and precipitation rates as a function of
985 temperature and aqueous fluid composition. *Geochim. Cosmochim. Acta* **194**, 193–210.

986 Zhou Z., Fyfe W. S., Tazaki K. and Van Der Gaast S. J. (1992) The structural characteristics of
987 palagonite from DSDP Site 335. *Can. Mineral.* **30**, 75–81.

988

989

Formatted: Indent: Left: 0", Hanging: 0.33"

Declaration of interests

☒ The authors declare that they have no known competing financial interests or personal relationships that could have appeared to influence the work reported in this paper.

☐The authors declare the following financial interests/personal relationships which may be considered as potential competing interests:
